Analysis and improvement of a process-based model of fruit growth and composition to explore genetic variability of fruit growth mechanisms, : design ideotypes and analyze the effects of water transfers and solutes concentrations on fruit growth

Dario Constantinescu

UNIVERSITE D'AVIGNON

ED 536 – AGROSCIENCES ET SCIENCES

INRA – INSTUT NATIONAL DE LA RECHERCHE AGRONOMIQUE
UNITE PSH – PLANTES ET SYSTEMES DE CULTURE HORTICOLE

Thèse présentée pour obtenir le grade universitaire de docteur

Dario CONSTANTINESCU

Analyse et amélioration d'un modèle mécaniste de croissance et composition du fruit

Etude de la variabilité génétique des mécanismes de croissance du fruit, conception d'idéotypes et analyse des effets des transferts d'eau et de la concentration des solutés sur la croissance du fruit.

Soutenue le 19/12/2019 devant le jury :

Thierry SIMONNEAU	INRA Montpellier	Rapporteur
Delphine LUQUET	CIRAD Montpellier	Rapporteur
Laurent URBAN	Université d'Avignon	Examinateur
Yves GIBON	INRA Bordeaux	Examinateur
Marion CARRIER	Cybeletech	Examinateur
Michel GENARD	INRA Avignon	Directeur de thèse
Gilles VERCAMBRE	INRA Avignon	Co-directeur de thèse

Encadrement de la thèse : Michel GENARD, Gilles VERCAMBRE, Nadia BERTIN

Title

Analysis and improvement of a process-based model of fruit growth and composition to explore genetic variability of fruit growth mechanisms, design ideotypes and analyze the effects of water transfers and solutes concentrations on fruit growth.

Résumé

Développer la connaissance des réponses du développement des fruits aux pratiques agricoles et aux conditions environnementales est important, depuis les sélectionneurs jusqu'aux producteurs. Cela soutiendrait la conception de pratiques agricoles permettant d'augmenter le rendement et la qualité des fruits et d'adapter la production fruitière au changement climatique, afin de satisfaire la croissance de la demande alimentaire. Le but de cette thèse était d'utiliser et d'améliorer un modèle mécaniste de croissance du fruit pour explorer la variabilité génétique de la tomate, concevoir des idéotypes de tomate plus résistants à la sécheresse, mettre en évidence des modes de circulation de l'eau et des sucres dans le système pédicel-fruit au cours de la journée, et étudier les effets des variations des concentrations en solutés dans la pulpe des fruits sur la croissance, qui détermine la qualité des fruits à la récolte. Les modèles développés ont permis de décrire de manière adéquate les processus biophysiques et métaboliques déterminant la croissance des fruits et la composition des solutés. Les résultats de simulation du modèle obtenus suggèrent que la conductivité pédiculaire et l'absorption active des sucres pourraient être des mécanismes clés pour déterminer la variabilité génétique des fruits et devraient être maximisés dans la recherche d'idéotypes. De plus, les résultats obtenus suggèrent que la régulation des flux d'eau peut générer une régulation de l'absorption diurne de sucre par le fruit et pourrait prévenir la perte d'eau au travers de la recirculation entre le xylème et le phloème et entre le phloème et l'apoplasme. Enfin, les résultats obtenus à partir d'un modèle intégré incluant la description de la croissance des fruits et du métabolisme des solutés de fruits ont mis en évidence que la variation des concentrations en acides et en minéraux due aux processus d'accumulation et de dilution pourrait avoir un impact non négligeable sur la croissance des fruits. Les études présentées dans cette thèse ont mis en évidence que l'estimation des paramètres physiologiques de la croissance des fruits et les techniques de conception et de calibration des modèles devraient être améliorées pour les rendre plus adaptés à la conception de meilleurs pratiques agricoles.

Abstract

Developing knowledge on fruit development responses to agricultural practices and environmental conditions is important from breeders to growers. Indeed, this would support the design of agricultural practices that could increase fruit yield and quality and adapt fruit production to climate change, for satisfying the increasing food demand. The aim of this thesis was to use and improve a mechanistic model of fruit growth for exploring the genetic variability of tomato growth in fresh and dry mass, designing drought-resistant tomato ideotypes, underlining patterns of diurnal water and sugars flows in the pedicel-fruit system, and studying the effects on fruit growth of the variations of fruit pulp solutes concentrations that determine fruit quality at harvest. The models developed allowed to describe in an adequate way biophysical and metabolic processes determining fruit growth and solutes composition. The obtained model simulation results suggested that pedicel conductivity and sugars active uptake could be key mechanisms in determining the fruit genetic variability and should be maximized in the research of ideotypes. In addition, the obtained results suggested that water flows regulation may generate a diurnally regulated fruit sugar uptake and could prevent water loss through water recirculation between xylem and phloem and between phloem and apoplast. Finally, the results obtained from an integrating model approach including the description of fruit growth and fruit solutes metabolism highlighted that acids and minerals concentrations variation due to both accumulation and dilution processes could have a non-negligible impact on fruit growth. The works presented in this thesis have highlighted that the estimation of the fruit growth physiological parameters and the techniques of models conception and calibration should be improved to make them increasingly suitable for the design of better-suited agricultural practices.

Acknowledgements

This work was conducted within the project MAGESTAN (PS2A no2016-0244) and was funded by the FranceAgriMer through the “Programme d’investissements d’avenir PIA”. I warmly thank members of the project “MAGESTAN”

Remerciements

Je tiens à remercier mes encadrants de thèse pour leur soutien constant pendant ces années de thèse. Je remercie Michel Génard pour l'échange continu d'idées scientifiques et pour m'avoir encouragé dans ma recherche de nouvelles idées et de nouveaux concepts pour ce travail. Je remercie Gilles Vercambre de m'avoir transmis le sens de la rigueur et de la logique dans le travail scientifique. Je remercie Nadia Bertin d'avoir été un guide important, surtout au cours de la première année de mon expérience de chercheur. Je tiens également à remercier les permanents et les thésards du laboratoire PSH, car ils ont toujours été prêts à m'aider lorsque j'ai rencontré des difficultés dans ce travail. Je remercie les membres de mon comité de suivi de thèse : Marion Carrier, Florent Pantin, Benoit Pallas, Zhanwu Dai, Mohamed Memmah, d'être toujours prêts à me donner des suggestions et de nouvelles orientations pour poursuivre ce travail de thèse. Enfin, je remercie Philippe Lobit et Gabriella Leonardi. Grâce à leur aide et à leurs conseils précieux, le travail final a été de qualité.

Summary

Introduction

Background

Fruits are a fundamental food in human diet (Slavin and Lloyd, 2012) and fruit production will be crucial for fighting malnutrition worldwide (Amine *et al.*, 2003). World fruits and vegetables average productions in the period 1994-2017 were estimated to be 673.2 Mt and 802.8 Mt respectively constituting then an important fraction of the total world crop production (Fig. 1.). The production of the main commercialized fleshy fruits has been increasing in the period 1994-2017 (Fig. 2), tomato being the most produced fleshy fruit in the world (FAOSTAT). This positive trend must be maintained, in order to satisfy the food demand, which is estimated to double from 2005 to 2050 (Tilman *et al.*, 2011).

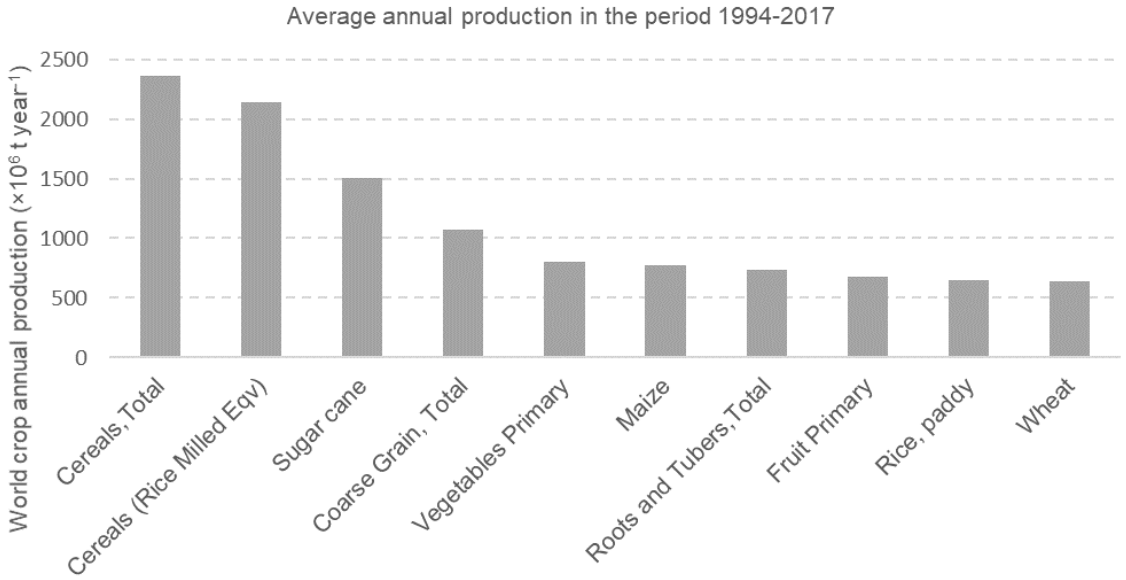

Fig. 1. Average annual world crops production in the period 1994-2017 (source: FAOSTAT)

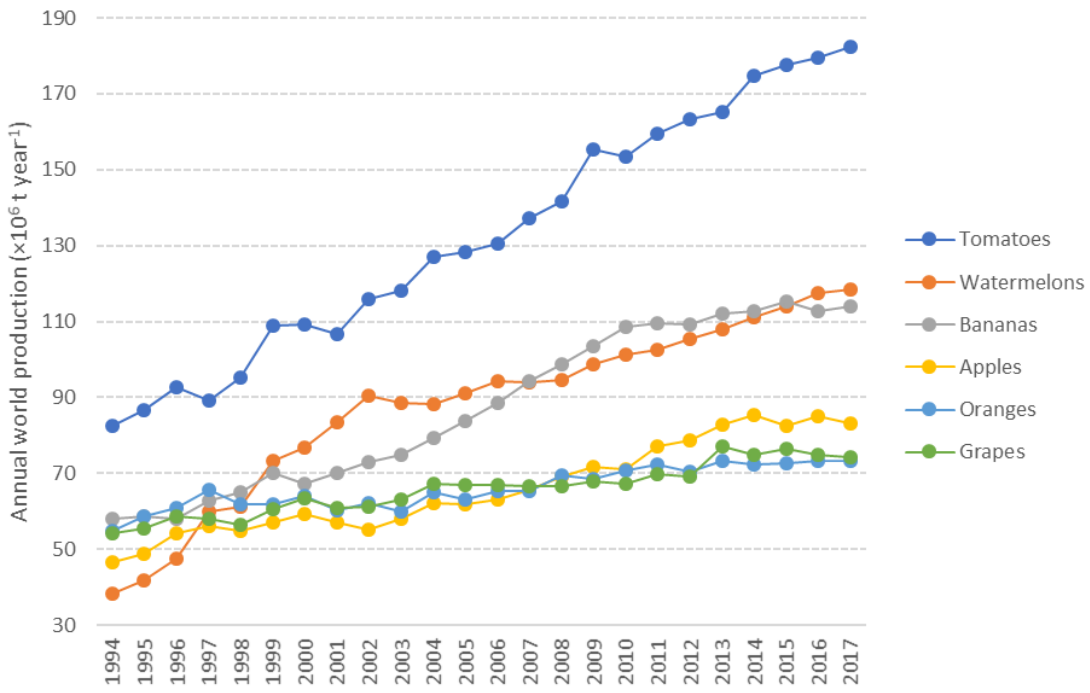

Fig. 2. Annual world production of the most produced fleshy fruits crops (six higher average annual production in the period 1994-2017)

Increasing fruit crop yield is a challenge: not only it constitute an economic advantage for growers, but it is also crucial to meet the increasing food demand (Glazebrook and Kola-Olusanya, 2019). As well as maintaining an increasing fruit yield, assuring a high standard of fruit quality is important for growers (Guichard *et al.*, 2001). Consumers are sensitive to fruit texture and rather prefer fruit with higher dry matter content (i.e. the ratio between the fruit dry and fresh mass) (Nardozza *et al.*, 2011). Dry matter content is then an index of fruit quality that needs to be maintained at a high value in fruit production. Moreover, fruit quality depends on the fruit organoleptic properties (Saliba-Colombani *et al.*, 2001) and the evaluation of fruit quality is made using quality indexes, most of which are defined by mean of the concentrations of solutes in the fruit pulp, e.g. the sugar/acid ratio (Malundo, Shewfelt and Scott, 1995). Therefore, fruit quality depends by the fruit pulp composition.

Fruit yield and quality at harvest depend on how the environmental conditions and the agricultural practices have affected fruit growth. Indeed, environmental conditions and agricultural practices determine modifications of the biophysical phenomena

occurring in the whole plant system and, by consequence, in the fruit along all the growing season (Bertin, Buret and Gary, 2001; Guichard *et al.*, 2001). Understanding responses of the fruit development to different agricultural practices is important for designing practices that are sustainable from an economic point of view. Moreover, in a context of a global climate change, it is becoming crucial to understand the whole plant responses to different environments and to design crop systems that allow maintaining fruit yield and quality minimizing water use (Bodner, Nakhforoosh and Kaul, 2015). Drought determines severe yield losses worldwide. However, in the case of fleshy fruits, moderate drought has been suggested to improve fruit quality (Ripoll *et al.*, 2014).The possible trade-off between crop strategies under water deficit further increases the interest of studying fruit growth responses to changes in crop conditions.

Fruit yield and quality improvement can be reached not only by designing better agricultural practices combination but also by breeding processes that allow the creation of new varieties (Doebley, Gaut and Smith, 2006). As well as improving fruit size and quality by breeding, there is large interest in selecting varieties which are resistant to pest and diseases as well as to certain environmental conditions, with an interest on drought. In this direction, the design of ideotypes, consisting in designing plants model that can perform in a predictable manner within a defined environment (Ripoll *et al.*, 2014), is a promising field.

Understanding the fruit growth biophysical processes can help fruit producers to improve fruit yield and quality

Fruit size and quality at harvest depend on fruit growth. Fruit growth results from a complex interaction between biological and physiological processes that determine the accumulation of water and dry matter (Lee, 1989). Fruit water inflows are determined by fruit water transports occurring between the bearing shoot and the pedicel vascular system (Guichard *et al.*, 2005; Morandi and Corelli Grappadelli, 2009). Fruit water loss occur through transpiration. Effluxes from the fruit could also consist of water backflows, which happen in the xylem and are driven by higher water potential in the fruit than in the plant xylem (Zhang and Keller, 2017). Backflows were observed in many fruit species (Lang and Thorpe, 1989; Huguet *et al.*, 1998; Keller, Smith and Bondada, 2006; Carlomagno *et al.*, 2018). Fruit dry matter mainly results from the

sugar transport processes. According to the Munch's theory, sugars flow from the source's plant to the fruit through the pedicel by a mass flow in the phloem pathway. The mass flow is determined by higher pressure turgor in the plant than in the fruit (Thompson and Holbrook, 2003a). The sugar transfer from the sieve elements to the fruit cells can follow two pathways: symplastic and apoplastic. Symplastic transport consists in a mass flow from the sieve element to the cell cytoplasm across plasmodesmata channels. Apoplastic transport happens in two steps: sugars are transported into the cell apoplast from the sieve element by both diffusion and active uptake, and are then actively transported from the apoplast to the fruit cell cytoplasm (Patrick and Offler, 1996; Manning *et al.*, 2001; Lalonde *et al.*, 2003; Zhang *et al.*, 2004; Lemoine *et al.*, 2013). Sugars that are not used for metabolism remain dissolved in the fruit cell cytoplasm mainly under the form of hexoses and sucrose (Dai *et al.*, 2016). The concentrations of sugars in the fruit cells contribute to changes of the fruit osmotic potential. Sugars accumulation has then a feedback on water transport. Moreover, changes in sugars concentrations in the fruit cells could be driven by their accumulation and by their dilution due to water import. Changes of sugar concentrations due to dilution during fruit growth have been shown to be non-negligible confronted to the changes due to sugars imports and metabolism (Dai *et al.*, 2016). There is then a large interconnection between water flows and sugars accumulation that determine fruit growth. Moreover, acids and minerals fruit pulp concentrations can affect water and dry matter transports by their contributions to the fruit osmotic potential. Therefore, acids and minerals as well are involved in the interplay between water and solutes accumulation. The fruit pulp solutes composition is directly related to fruit quality. By consequence, as well as fruit size, fruit quality depends on the interconnection between biophysical processes that determine fruit growth and fruit pulp solutes formation. Understanding how biophysical and metabolic processes interact to determine fruit composition at harvest is then fundamental to determine how different environmental conditions could modify the fruit characteristics at harvest and, then, to design appropriate agricultural practices.

Process-based models can help to analyze genetic variability of fruit growth-related traits and fruit growth processes responses under different environmental conditions

A process-based (or mechanistic) model is a mathematical tool that predicts the behavior of a complex system through the quantitative representation of the processes underlying it, under given external conditions. In biology, the system is mathematically defined as the link of the physical, chemical, and biological processes that compose it (Jones *et al.*, 2017). Process based models are then useful tools to analyze the biophysical processes that determine a complex phenomenon such as fruit growth. A biophysical model of fruit growth was proposed by Fishman and Génard (1998). This model describes the hourly water and dry matter accumulation rates in fleshy fruits combining mathematical representations of water and sugar transport processes occurring between the plant and the fruit. This model has been shown to be robust and generic in describing fruit growth under contrasted environmental conditions and of different fruit species: peach (Quilot *et al.*, 2005), mango (Lechaudel *et al.*, 2007), kiwifruit (Hall *et al.*, 2013), and tomato (Liu *et al.*, 2007). With respect to its first version, this model has been improved including the description of the mechanisms of water and sugar transport occurring across the fruit pedicel (Hall *et al.*, 2013) and the description of the elasticity of the fruit cells expansion (Lechaudel *et al.*, 2007). Moreover, Hall *et al.* (2017) have proposed a description of the differentiation between the apoplastic and symplastic pathways of sugar uptake by the fruit cells.

The fruit growth model can be used to understand the processes that determine fruit growth, with the objective of the fruit yield and quality improvement.

A biophysical representation of fruit growth processes as the one given by the fruit growth model can be used for improving studies on Quantitative Trait Loci (QTL) and the research of ideotypes. Indeed, each model parameter is related to a set of interconnected processes. We can assume that these are controlled by a group of genes (Tardieu, 2003). Under the hypothesis that a subset of the model parameters is independent on the environment and management but depend on the genotype and that these parameters have an impact on the model behavior, we can consider these genotype-dependent parameters as a phenotypic fingerprint of the genotype and use

them in a QTL analysis (Reymond *et al.*, 2003; Quilot *et al.*, 2005; Bertin *et al.*, 2010). Furthermore, information about the variability of parameter estimations among genotype can be used to search parameters combinations that define fruit ideotypes, i.e. ideal fruits that could maintain good characteristics under certain environment conditions.

Fruit water transports occurring between the plant and the fruit have been characterized at both hourly and diurnal scales in many species (Guichard *et al.*, 2005; Matthews and Shackel, 2005; Morandi and Corelli Grappadelli, 2009). However, the methods used for determining water flows are indirect and can lead to systematic errors (Fishman, Génard and Huguet, 2001). Recently, non-invasive methods such as positron emission tomography (PET) and magnetic resonance imaging (MRI) have been used to determine water transports in the fruit pedicel and to explain relationships between anatomical changes and water flows, such as the observed decline of xylem funtionality in grape and tomato in the late growth stage (Windt, Gerkema and van As, 2009; Knipfer *et al.*, 2015; Van de Wal *et al.*, 2017). Indeed, various and detailed studies have been conducted on water translocations in the plant fruit system. With such indirect destructive and non-destructive methods, we can characterize either the global water balance or the behavior of the water transport happening in a single compartment. However, as discussed in the previous section, it is important to describe the interplay between dry matter accumulation and water transport processes to understand how these transports are related to fruit growth. The mathematical description of water and sugar flows in the fruit model can help identifying patterns of such transports in the different compartments in the whole plant-fruit system and how their behavior responds to given environmental conditions.

The advantage of having a mechanistic description of fruit growth is that we can link the fruit growth model to other mechanistic models to deepen our knowledge of more specific biochemical mechanisms and of the interactions occurring between them. For example, Lescourret and Génard (2005) linked the growth model and a sugar model, showing how with this integrated approach could be identified the main mechanisms that determine peach quality and their responses to environmental conditions. An integrated approach could be useful to understand how solutes in the fruit pulp determine fruit growth processes, by investigating their contribution to the fruit osmotic potential variation. For doing such integration, we need models to describe the

accumulations of these solutes in the fruit pulp. Indeed, mechanistic models of sugars and acids accumulation in the fruit pulp have been developed. Génard and Souty (1996) described the repartition of the carbon entering the fruit growth between different compartments in the fruit pulp: soluble sugars, starch, and other compounds different than sugars that result from the carbon biosynthesis, including those that are necessary to build the cell walls; moreover, Etienne *et al.* (2015) described citric acid accumulation in the fruit pulp with a model that simply describes the TCA cycle, following the approach of Lobit *et al.* (2003); finally, Lobit *et al.* (2006) modeled the malic acid accumulation in the vacuole, linking the mathematical representation of the malic acid transport across the tonoplast and the acid-base equilibrium in the vacuole solution determining the vacuolar pH. These models take as inputs variables related to fruit growth, such as fruit respiration, fruit structural dry weight, fruit dry weight and fresh weight, as well as air temperature. Moreover, their outputs can be used to compute the fruit osmotic potential. Therefore, these models can be linked to the fruit growth model to better understand the interplay between the water and sugars flows, and the solutes accumulation in the fruit.

Objectives and structure of the thesis

Starting from the model of fruit growth of Fishman and Génard (1998), in this thesis I will use and improve this mechanistic model for achieving the following four objectives, each of them representing an aspect of the analysis of the fruit growth among the ones presented in this introduction:

1. Explore the genetic variability of a recombinant inbred line of tomato, highlighting processes that determine water deficit resistance in tomato.
2. Design ideotypes that can resist to water deficit based on the estimated genetic variability.
3. Underline patterns of diurnal water and sugar flows occurring in the pedicel-fruit system.
4. Evaluate the variations of fruit solutes that determine fruit quality, and assess how these variations affect fruit growth.

The thesis will be divided in three chapters, corresponding to two articles and a chapter written with the same structure as that of an article.

In the first chapter, I will address the first and the second objective. I will show how the fruit growth model parameters estimates related to different recombinant inbred lines of tomatoes could be used as a representation of the genetic variability of tomato genotypes. Then, I will use the fruit growth model as a tool for searching parameters combinations that correspond to tomato water deficit resistant ideotypes.

In the second chapter, I will address the third objective. I will present a description of water and sugar flows of the pedicel-fruit system made through a simple mathematical model that includes the pedicel and the distinction between apoplast and symplast. Such a distinction should help to understand water and sugar translocations within fruit cells compartment and, then, permits to identify patterns of water and sugar translocations.

In the third chapter, I will address the fourth objective. In this chapter, I will build an integrated “virtual fruit” model, connecting the fruit growth model with models describing sugars, citric acid, and malic acid accumulations. I will then show how this tool could help to evaluate the roles of solutes on the fruit growth giving us information about the dynamics of the solutes accumulation during the fruit development stage.

Published or submitted chapters

Chapter 1: paper published the 09 December 2016 in *Frontiers In Plant Science*

Title: Model-assisted estimation of the genetic variability in physiological parameters related to tomato fruit growth under contrasted water conditions.

Chapter 2: paper submitted to the review *Journal Of Experimental Botany*, accepted in major revision. The second revision response has been sent to the journal.

Chapter 3: chapter written with the structure of a research paper

1 Model-assisted estimation of the genetic variability in physiological parameters related to tomato fruit growth under contrasted water conditions

Résumé

Le déficit hydrique est un stress abiotique important qui menace la productivité des plantes et des cultures. Dans le cas des fruits charnus, il apparaît essentiel de comprendre les mécanismes qui déterminent l'accumulation d'eau et de carbone, et d'identifier les gènes, les QTL et les phénotypes qui permettront de faire des compromis entre la croissance et la qualité des fruits en situation de déficit hydrique. Ce défi est crucial pour les sélectionneurs et les producteurs. Dans le présent travail, 117 lignées d'une population de Solanum lycopersicum ont été phénotypées sous irrigation optimale et en conditions de déficit hydrique. L'état hydrique, la croissance et la composition des fruits ont été mesurés et les données ont été utilisées pour calibrer un modèle de croissance du fruit basé sur les processus décrivant les flux d'eau et de carbone en fonction de la plante et de son environnement. Huit paramètres du modèle dépendant du génotype ont été estimés à l'aide d'un algorithme évolutif multiobjectif afin de minimiser les erreurs de prédiction de la masse sèche et fraîche des fruits tout au long de leur développement. Le déficit en eau a augmenté la teneur en matière sèche des fruits (jusqu'à 85 % d'augmentation) et diminué leur poids frais (jusqu'à 60 % de réduction), les plus gros génotypes de fruits étant les plus sensibles. Les erreurs quadratiques moyennes normalisées des prédictions se situaient entre 16 et 18 % dans la population. La variabilité des paramètres génotypiques du modèle nous a permis d'explorer diverses stratégies génétiques en réponse au déficit en eau. Un groupe intéressant de génotypes a pu être distingué dans lequel i) la faible perte de

masse fraîche sous déficit en eau était associée à une absorption active élevée de sucres et à une faible valeur de l'extensibilité maximale de la paroi cellulaire, et ii) la forte teneur en matière sèche dans le traitement témoin était associée à une faible diminution pour le flux de masse. En utilisant 501 marqueurs SNP génotypés sur l'ensemble du génome, une analyse QTL des paramètres du modèle a permis de détecter trois QTLs principaux liés aux conductivités du xylème et du phloème, sur les chromosomes 2, 4 et 8. Le modèle a ensuite été appliqué à la conception d'idéotypes à forte teneur en matière sèche en condition contrôlée et à faible perte de masse fraîche en condition de déficit en eau. Les idéotypes construit se sont mieux comportés que les RILs surtout pour les génotypes de grande et moyenne taille, en combinant une conductivité pédiculaire élevée et une absorption active élevée de sucre. Il est intéressant de noter que cinq RILs de petite taille se rapprochaient des idéotypes sélectionnés et présentaient probablement des caractéristiques et des allèles intéressants à adapter au déficit en eau.

frontiers in Plant Science

ORIGINAL RESEARCH
published: 09 December 2016
doi: 10.3389/fpls.2016.01841

Model-Assisted Estimation of the Genetic Variability in Physiological Parameters Related to Tomato Fruit Growth under Contrasted Water Conditions

*Dario Constantinescu[1], Mohamed-Mahmoud Memmah[1], Gilles Vercambre[1], Michel Génard[1], Valentina Baldazzi[1], Mathilde Causse[2], Elise Albert[2], Béatrice Brunel[1], Pierre Valsesia[1] and Nadia Bertin[1]**

[1] Plantes et Systèmes de Culture Horticoles, Institut National de la Recherche Agronomique - Centre PACA, Avignon, France, [2] Unité Génétique et Amélioration des Fruits et Légumes, Institut National de la Recherche Agronomique – Centre PACA, Montfavet, France

Drought stress is a major abiotic stress threatening plant and crop productivity. In case of fleshy fruits, understanding mechanisms governing water and carbon accumulations and identifying genes, QTLs and phenotypes, that will enable trade-offs between fruit growth and quality under Water Deficit (WD) condition is a crucial challenge for breeders and growers. In the present work, 117 recombinant inbred lines of a population of *Solanum lycopersicum* were phenotyped under control and WD conditions. Plant water status, fruit growth and composition were measured and data were used to calibrate a process-based model describing water and carbon fluxes in a growing fruit as a function of plant and environment. Eight genotype-dependent model parameters were estimated using a multiobjective evolutionary algorithm in order to minimize the prediction errors of fruit dry and fresh mass throughout fruit development. WD increased the fruit dry matter content (up to 85%) and decreased its fresh weight (up to 60%), big fruit size genotypes being the most sensitive. The mean normalized root mean squared errors of the predictions ranged between 16–18% in the population. Variability in model genotypic parameters allowed us to explore diverse genetic strategies in response to WD. An interesting group of genotypes could be discriminated in which (i) the low loss of fresh mass under WD was associated with high active uptake of sugars and low value of the maximum cell wall extensibility, and (ii) the high dry matter content in control treatment (C) was associated with a slow decrease of mass flow. Using 501 SNP markers genotyped across the genome, a QTL analysis of model parameters allowed to detect three main QTLs related to xylem and phloem conductivities, on chromosomes 2, 4, and 8. The model was then applied to design ideotypes with high dry matter content in C condition and low fresh mass loss in WD condition. The ideotypes outperformed the RILs especially for large and medium fruit-size genotypes, by combining high pedicel conductance and high active uptake of sugars. Interestingly, five small fruit-size RILs were close to the selected ideotypes, and likely bear interesting traits and alleles for adaptation to WD.

Keywords: fleshy fruit, quality, ideotype, *Solanum lycopersicum*, virtual fruit model, water stress, multiobjective optimization

OPEN ACCESS

Edited by:
Lifeng Xu,
Zhejiang University of Technology, China

Reviewed by:
Teemu Hölttä,
University of Helsinki, Finland
Tsu-Wei Chen,
Leibniz University of Hanover, Germany

****Correspondence:***
Nadia Bertin
nadia.bertin@inra.fr

Specialty section:
This article was submitted to Plant Biophysics and Modeling, a section of the journal Frontiers in Plant Science

Received: *26 August 2016*
Accepted: *22 November 2016*
Published: *09 December 2016*

Citation:
Constantinescu D, Memmah M-M, Vercambre G, Génard M, Baldazzi V, Causse M, Albert E, Brunel B, Valsesia P and Bertin N (2016) Model-Assisted Estimation of the Genetic Variability in Physiological Parameters Related to Tomato Fruit Growth under Contrasted Water Conditions. Front. Plant Sci. 7:1841. doi: 10.3389/fpls.2016.01841

INTRODUCTION

Drought stress is one of the major abiotic stresses, which represents the primary cause of crop loss worldwide, and the development of more water efficient cropping systems is becoming critical (Bodner et al., 2015). Nonetheless, in the case of fleshy fruits, moderate drought has been suggested to improve both organoleptic quality and nutritive value (Ripoll et al., 2014). Trade-offs between quality and yield seem realistic, but depend strongly on stress intensity and genotypes (Ripoll et al., 2016). Indeed, recent studies on tomato revealed a strong genetic variability in the response to drought from negative to nil to positive impact on fruit size and quality (Ripoll et al., 2015). A large number of genes and molecular mechanisms involved in survival under drought have been identified, in particular in *Arabidopsis thaliana* (L.) Heynh. (Blum, 2011). These genes are involved in the control of many physiological processes, but they do not necessarily confer a stress resistance and they may entail detrimental effects on yield and quality in crop plants facing long periods of drought combined with high temperature (Gong et al., 2010; Tardieu, 2012). In tomato, only a few QTLs/genes involved in the response to water deficit are known (Labate et al., 2009). In a recent study (Albert et al., 2016), a RIL population of 117 F7 recombinant inbred tomato lines has been genotyped for 501 SNP markers and phenotyped under control (C) and water deficit (WD). This study revealed a total of 56 QTLs of plant and fruit traits, among which 11 depended on watering regime. Interestingly, these authors observed a large genetic diversity in plant and fruit responses to WD and significant genotype by watering regime interactions, suggesting the possibility to develop tomato genotypes adapted to grow under water limitation. The diversity present in genetic resources of tomato species is a vital source of traits and alleles for crops, many of which may have been inadvertently lost during selection. Thus, identifying main mechanisms governing fruit adaptation to water deficit and pinpointing genes, QTLs and phenotypes that will enable a fruit to maintain growth and improve quality under conditions of limited water supply is a crucial challenge for breeders and growers in the light of current issues related to climate change.

Crop models are adequate tools for analyzing genotype by environment interactions, since they integrate environmental and genetic effects on individual physiological processes and are able to predict interactions among processes during fruit development (Bertin et al., 2010). The Virtual Fruit Model (Fishman and Génard, 1998), an eco-physiological process-based model which describes both water and dry matter accumulation rates in fleshy fruits, has already proven its robustness and genericity under contrasted environmental conditions and for different fruit species: peach (Quilot et al., 2005), mango (Lechaudel et al., 2007), kiwifruit (Hall et al., 2013), and tomato (Liu et al., 2007). Notably, this model has been used to assess water deficit impacts on fruit growth (Lescourret and Génard, 2005; Baldazzi et al., 2013). In such mechanistic models, the parameters are linked to physiological traits or processes which can be linked to loci or genes. Each parameter is in fact related to a set of interconnected processes controlled by a group of genes, which was defined by Tardieu (2003) as "meta-mechanism." Though plant traits generally depend on genotype, environment and cultural practices, model parameters should be, ideally, independent of the environment and management. Some of these parameters,—called genotypic parameters,—are genotype dependent while others are generic and independent of the genotype (Boote et al., 2001). The set of genotypic parameters related to a particular genotype represents a phenotypic fingerprint of this genotype and it is amenable to QTL analysis (Bertin et al., 2010). Several attempts have been made to include genetic information into process-based models and to link model parameters to genes or QTLs (White and Hoogenboom, 1996; Chapman et al., 2003; Reymond et al., 2003; Quilot et al., 2005; Xu et al., 2012; Rebolledo et al., 2015). The main difficulty is that the model should capture sufficient physiological functionalities, to simulate the expression of single genes or a gene network.

An ultimate goal is then to use these enriched process-based models for the design of ideotypes adapted to biotic and abiotic stress environments. Here, an ideotype designates a "plant model which is expected to perform or behave in a predictable manner within a defined environment." However, the fitness landscape (objectives space) to be explored to design ideotypes is often very complex and a large number of parameter combinations must be evaluated in order to identify the best-adapted genotypes. This difficulty comes from the nonlinear and non-convex nature of antagonist criteria and the complex nature of the process-based models, such as the "Virtual Fruit." Consequently, the model-based design of ideotypes is a difficult nonlinear multi-objective optimization problem that resists to the classical simulation and optimization methods. To deal with such multi-objective optimization problems, nature-inspired optimization algorithms (e.g., genetic algorithms and particle swarm optimization algorithms) are suitable and increasingly used. Multi-Objective Evolutionary Algorithms (MOEAs) are amongst the best-known and most effective nature inspired optimization algorithms. They allow exploring high dimensional solution spaces and they do not require any derivative information. MOEAs generate many feasible and non-dominated solutions, i.e., elements of the Pareto optimal set (best tradeoffs between conflicting objectives). Many papers have been published on the use of evolutionary algorithms for ideotype model-based design. For the sake of conciseness, we mention only the works of Letort et al. (2008) on beech trees, of Qi et al. (2010) on maize, of Lu et al. (2012) on wheat, of Quilot-Turion et al. (2012) and Sidi et al. (2014) on peach, and of Ding et al. (2016) on rice.

In the present study our objectives were to use the Virtual Fruit Model (i) to phenotype a RIL population of tomatoes at the process level; (ii) to better understand the fruit growth mechanisms (water and dry matter accumulation) involved in the response to water deficit; (iii) to look for optimized sets of genotypic parameters/genotypes which could reduce the loss of fruit fresh weight under WD and at the same time maintain/improve high fruit dry matter content. The RIL population is the one previously genotyped by Albert et al. (2016). The genetic variability in fruit traits and model parameters was analyzed by Principal Component Analysis (PCA) and through QTL analysis. This step helped to explore diverse genetic

strategies in response to water deficit and to discuss potential processes/genes involved in this response. Then the model was applied to design ideotypes in terms of fruit size and quality.

MATERIALS AND METHODS

RIL Population and Experimental Design

The RIL population, including 117 F7 recombinant inbred lines, was developed from an intraspecific cross between two inbred lines, Cervil and Levovil (described in Saliba-Colombani et al., 2001). Cervil is a cherry type tomato (*S. lycopersicum* var. *cerasiforme*, 6–10 g), whereas Levovil (*S. lycopersicum*) is a large fruited accession (90–160 g). The 117 RILs, the F1 hybrid and the two parents were grown in a heated glasshouse in INRA Avignon (France) from March to July 2013. Based on previous data, eight genotypes were selected in the population in order to have a good representation of the ranges in fruit size and dry matter content. These eight genotypes included the two parents and the F1 hybrid (CxL). Some input parameters of the Virtual Fruit Model (initial fresh and dry weights, fruit surface conductance to water, stem water potential) were accurately measured on these eight representative genotypes and then the same values were applied to all genotypes of the group (see below and **Figure 1**).

Plants were grown in 4 l plastic pots filled with peat (Klasmann 165) and watered with nutritive solution (2, 4, 6 mmol l−1, N, P, and K, respectively). All trusses were pollinated with an electrical bee. The number of flowers per truss was regulated to get homogeneous fruit load and comparable source:sink ratios among plants of a given genotype. The first two trusses of the small fruit genotypes (final fruit size < 30g) were pruned to 8 fruits and the following trusses to 12 fruits. Regarding the medium and large fruit genotypes (final fruit size > 30g), the first two trusses were pruned to 4 fruits and the following trusses to 6 fruits. Climate conditions (temperature, humidity and light intensity) in the glasshouse were recorded every minute and data were averaged hourly throughout the experiment.

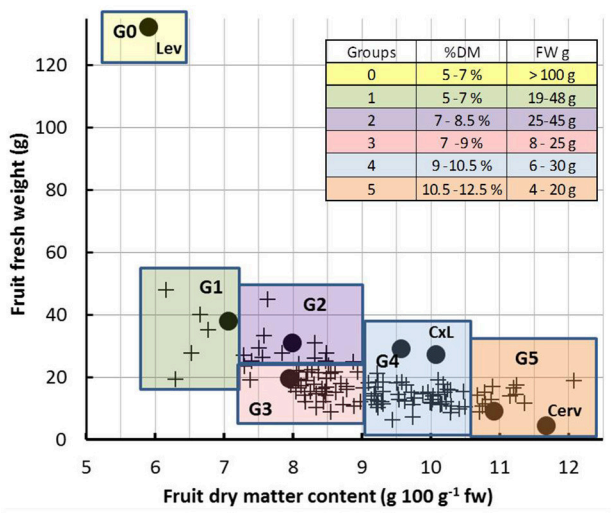

FIGURE 1 | Relationship between fruit fresh weight and dry matter content of ripe fruits under control condition. Each symbol represents one genotype (means of 15 to 20 fruits). Black dots indicate the five representative genotypes, the two parents (Lev and Cerv) and the F1 hybrid (CxL). The colored squares represent the six groups of genotypes (G1 to G6) which were considered for model inputs. The insert gives the ranges of fresh weight (FW) and dry matter content (%dm) of ripe fruits in each group.

From anthesis of the second truss of Cervil (considered as a reference early genotype), two irrigation treatments were applied: control (C) and water deficit (WD). Control plants were irrigated in order to get drainage around 25%. In the WD treatment, water supply was reduced by 64% compared to the control, corresponding to 49% of the potential evapotranspiration on average over the experimental period. The peat substrate humidity was assessed continuously with 12 small soil moisture sensors (EC-5 Decagon devices, USA) inserted in the substrate and randomly distributed in the glasshouse, and twice a week with a water content sensor (WCM-control, Grodan, Roermond, The Netherlands). Peat substrate humidity averaged 60–65% in control plants and 25–30% in WD plants (no drainage). Within the glasshouse, irrigation treatments were applied by row, and the genotypes were randomized within rows. Two plants of each genotype (10 for the parent lines and for the six representative genotypes) were grown under each treatment. The trial plants were surrounded with one row of border tomato plants.

Phenotypic Measurements

Stem water potential was measured using a pressure chamber (SAM Précis 2000 Gradignan, France) at predawn and at solar noon. Measurements were performed twice during the stress period on five plants of the eight representative genotypes under both conditions. The fruit conductance was measured on three ripe fruits of the eight genotypes in both treatments, according to the weight loss method described in Lescourret et al. (2001). Flower anthesis was recorded on four successive trusses on all plants (excluding the first two trusses). The fruit fresh and dry masses were measured from 8 days after anthesis (daa) until fruit ripening (from beginning of June to beginning of July) on the whole population. About 4–5 fruits were sampled every 7 days for the 8 representative genotypes. For all other genotypes, three fruits were sampled at 8–10 daa, 12–15 daa, and 20–25 daa. At ripening about 15 to 20 fruits were sampled on all genotypes. For a given developmental stage, fruits were sampled on trusses which developed during the same time window. Within a truss, the first proximal and last distal fruits were not sampled, in order to avoid fruit position effects. The fruit fresh mass was measured after harvest and the fruit dry mass was measured after drying in a ventilated oven for 72 h. All sampled fruits from the WD treatment were grown after water deficit onset, which means that cell division, cell expansion and ripening processes were all affected by WD.

Virtual Fruit Model Description

Fishman and Génard (1998) developed a biophysical model which simulates water and dry matter accumulation rates in the fruit, using as inputs two climatic variables (fruit temperature and air humidity) and two variables describing the plant status (stem water potential, and phloem sap concentration in sugars). This model describes the biophysical processes involved in fruit

growth, with appropriate equations computing uptakes from the xylem and phloem across composite membranes, and losses of dry matter and water due to respiration and transpiration, respectively. Hall et al. (2013) extended the model formulation by adding a pedicel, which contributes to the major hydraulic resistance of the pathway to the fruit (Mazzeo, 2008). The extended version of Hall et al. (2013) was used in our study. Water and sugar flow from the stem through the pedicel into an intermediate compartment, that we called the fruit vasculature, and then through composite membranes into the fruit. The equations describing flows from the fruit vasculature into the fruit (U_p = mass flow from phloem, U_x = mass flow from xylem, U_s = sugar flow) and those describing fruit respiration (R_f) and transpiration (T_f) are the same as those given by Fishman and Génard (1998). The model simulates two state variables (w = mass of water in fruit, s = dry mass of fruit), whose rates of change are:

$$\frac{dw}{dt} = U_x + U_p + r_w R_f - T_f \quad (1)$$

$$\frac{ds}{dt} = U_s - R_f \quad (2)$$

where r_w is the proportion of dry mass converted to water during respiration ($r_w = 9/16$ according to Hall et al., 2013).

Three parallel mechanisms involved in sugar uptake (U_s) from the phloem were considered: active uptake (using Michaelis-Menten kinetics), mass flow, and diffusion (equations are described in Liu et al., 2007).

The rate of fruit volume (V) increase is given by:

$$\frac{dV}{dt} = \begin{cases} V\phi\left(P_f - Y\right) & P_f > Y \\ 0 & \text{otherwise} \end{cases} \quad (3)$$

where ϕ and Y are respectively, the cell wall extensibility and yield threshold parameters of the Lockhart equation. When this is equated to the rate of volume increase calculated from the mass balance, we get an algebraic equation for P_f (fruit turgor pressure).

The water and carbon fluxes through the pedicel xylem (which primarily carries water) and phloem (which carries water and sugar) were considered, as in the model developed by Hall et al. (2013).

To identify the main genotypic parameters that affect the model outputs, we performed a sensitivity analysis of the "Virtual Fruit" model, which includes 30 parameters. Three sensitivity analysis methods were used for this purpose: one elementary effects method, i.e., Morris method, and two methods based on the variance decomposition, i.e., the Fourier Amplitude Sensitivity Test (FAST) and the Sobol's methods (Saltelli et al., 2008). Based on the conclusions of those methods, a cross selection of the most important parameters was performed. Accordingly, six genotypic parameters involved in different processes had significant impacts on model outputs (**Table 1**). Two additional parameters were chosen because of their impact on carbon and water transports, which are main processes on which this study focusses. The first one (tauS) drives the mass flow, whereas the second one (lp1) is related to the pedicel conductivity which is strongly involved in water uptake from the phloem. These eight genotypic parameters are described in **Table 1**.

Model Calibration

As mentioned above, the model genotypic parameters were assumed to be genotype dependent and environment independent, i.e., they do not depend on the irrigation conditions. Thus, each set of parameters is a footprint of one of the 117 tomato RILs. To account for the different plant and fruit status under C and WD conditions, some of the model inputs were measured experimentally under each treatment: the stem water potential, the fruit surface conductivity to water vapor, the initial dry and fresh masses, and the fruit osmotic pressure related to soluble compounds other than sugars.

The model calibration aims at estimating the values of the eight selected genotypic parameters in order to minimize the fitting errors (observed vs. simulated fruit fresh and dry weights) for each genotype. The performance index used in the model calibration was the Normalized Root Mean Squared Error (NRMSE), a dimensionless indicator that takes into account the time steps in which more observations were available along with fewer observations at other time steps. This index is suggested in Wallach et al. (2013):

$$NRMSE\ [\%] = 100^* \frac{\sqrt{\frac{1}{n}^* \sum_{i=1}^{n} (O_i - S_i)^2}}{\frac{1}{n}^* \sum_{i=1}^{n} O_i} \quad (4)$$

where Oi and Si are respectively, the observed and simulated values of fruit fresh and dry masses, and n is the number of observations.

The four objectives corresponding to the four NRMSE values, related to the fruit dry and fresh masses under C and WD conditions, were aggregated into two objectives. For this purpose the mean NRMSE value calculated under each irrigation condition was considered in order to have a balanced fitting error between the fruit weight components:

$$f_1(\boldsymbol{X}) = NRMSE_{aggr\,C} = \frac{NRMSE_{f\,C} + NRMSE_{d\,C}}{2} \quad (5)$$

$$f_2(\boldsymbol{X}) = NRMSE_{aggr\,WD} = \frac{NRMSE_{f\,WD} + NRMSE_{d\,WD}}{2} \quad (6)$$

where $\boldsymbol{X} = (x_1, x_2, x_3, \ldots, x_8)^T$ is the vector of parameters generating the (f_1,f_2) objective values. $NRMSE_{fC}$ and $NRMSE_{dC}$ are related to respectively, the fruit fresh weight and fruit dry weight predictions in the control (C) condition. $NRMSE_{fWD}$ and $NRMSE_{dWD}$ are related to respectively, the fruit fresh weight and fruit dry weight predictions in the water deficit (WD) condition.

The model calibration was therefore formulated as a multi-objective problem as follows:

$$\min_{X \in D} \left\{ f_1(\boldsymbol{X}), f_2(\boldsymbol{X}) \right\} \quad (7)$$

where D is the search space defined by boundaries of the considered parameters. The problem solutions $\boldsymbol{X}^*$ are all the

TABLE 1 | Description of the eight genotypic parameters used in the calibration step and of the three additional parameters used for designing ideotypes.

Parameter name	Description	Boundaries			
		Calibration		Ideotypes design	
		Lower	Upper	Lower	Upper
phiMax [bar^{-1} h^{-1}]	Maximum cell wall extensibility. Involved in cell expansion rate	1.0E-04	0.01	0.002	0.02
Lp [g cm^{-2} bar^{-1} h^{-1}]	Conductivity of the composite membrane for water transport from phloem to fruit cells	5.0E-04	0.4	0.02	0.6
nuM [gs h^{-1}]	Maximum sugar active uptake rate. Involved in the sugar active uptake calculus (Ua)	0.002	0.15	0.002	0.2
tstar [h]	Involved in the sugar active uptake calculus. The higher is tstar, later the active uptake begins to decrease	10	900	10	900
tauA [h]	Involved in the sugar active uptake calculus. The higher is tauA, the slower is the active uptake decreasing rate in the growth stage	5	900	72	900
tauS [h^{-2}]	Involved in the calculus of the reflection coefficient of the composite membrane (sigmaP) which increases with tauS. sigmaP is involved in phloem mass flow	5.0E-06	1.5E-05	1.5E-06	2E-05
lp1 [g bar^{-1} h^{-1}]	Pedicel conductivity for the water transport in phloem	5.0E-05	0.1	0.002	0.2
rxp [dimensionless]	Rxp=Lx/Lp=Lx1/Lp1. Lx and Lx1 have the same meaning as Lp and Lp1 but they refer to the xylem	0.1	0.6	0.1	0.8
s0 [g][1]	Initial fruit dry weight			0.019	0.086
w0 [g][1]	Initial fruit water weight			0.126	1.0
bssrat [dimensionless][1]	Involved in the soluble sugar concentration calculus. Ssrat = assrat*t/24 + bssrat Ssrat is the ratio between soluble sugars mass and the total dry mass			0.043	0.22

1 = irrigation dependent parameter, optimized only for the ideotype design.
The parameter ranges used in the calibration step are based on literature data. The lower boundaries of phiMax, lp, and lp1 are set near to 0 for computational stability reasons; tauA, tstar, and tauS are based on experimental information on fruit development.

parameter sets belonging to the Pareto front, i.e., the set of solutions that consists in the best tradeoffs between the two conflicting objectives.

Design of Ideotypes

In this step, we aimed to design ideotypes of tomato adapted to WD conditions. The term ideotype designates a combination of genotypic parameters that represent virtual tomato genotypes with optimized tolerance to water deficit. For this purpose, we considered a set of 11 genotypic parameters, adding three new genotype dependent parameters to the search space (**Table 1**). In this study, the ideotype design aimed at (i) maximizing the ratio between dry weight and fresh weight at the ripe stage (dry matter content *dm*) until a maximal value of 10% under C condition, and (ii) minimizing the fresh weight loss associated with water deficit. Thus the ideotype design was formulated as a multi-objective problem as follows:

$$f_1(\boldsymbol{X}_{id}) = dm_C\,[\%] = 100^* \frac{dry_{weight_C}}{fresh_{weight_C}} \tag{8}$$

$$f_2(\boldsymbol{X}_{id}) = loss\,[\%] = 100^* \sqrt{\left(\frac{\left(fresh_{weight_C} - fresh_{weight_{WD}}\right)}{fresh_{weight_C}}\right)^2} \tag{9}$$

The problem formulation becomes:

$$\min_{X_{id} \in D_{id}} \left\{-f_1(\boldsymbol{X}_{id}), f_2(\boldsymbol{X}_{id})\right\}, \text{ Subject to } dm_{C,WD}\,[\%] < 10\% \tag{10}$$

where $\boldsymbol{X}_{id}$ is the parameter vector belonging to the set $D_{\mathbf{id}}$, which represents the ideotypes search space. The negative sign of $f_1(\boldsymbol{X})$ objective is introduced to transform the minimization into maximization.

Because the sensitivity to WD depends on fruit size, we considered three groups of tomatoes differing by their final fresh weight in control conditions: large size (100–300 g), medium size (20–80 g) and small size (5–15 g).

Optimization Algorithm for Model Calibration and Design of Ideotypes

The NSGA-II developed by Deb et al. (2002) has proven to be one of the most efficient algorithms for solving multi-objective problems. Therefore, we used this algorithm both for the "Virtual Fruit" model calibration and for the tomato ideotype design. For sake of simplicity, we do not give a full description of this algorithm. The interested readers can refer to the above cited. The NSGA-II algorithm was applied through the Java package *jMetal*. As the NSGA-II algorithm depends on random variables, the optimization process was repeated 10 times in the calibration phase and 20 times for the ideotype design. At the end of the process, we could have high number of similar solutions. Therefore, the choice of the best compromise solution for the

calibration step was based on the *min-max* decision criterion, to avoid high mean fitting errors in each condition. Therefore, among the solutions $\boldsymbol{X}_i^*$ belonging to the Pareto-optimal solution set P, we chose the solution $\overline{\boldsymbol{X}}$ that satisfied the following condition:

$$\min\left\{\max_{\boldsymbol{X}^*\in P}\left\{f_1\left(\boldsymbol{X}^*\right), f_2\left(\boldsymbol{X}^*\right)\right\}\right\} \quad (11)$$

where P is the set of Pareto-optimal solutions. We also checked that among the best sets of parameters estimated for one genotype (solutions that all have similar objective values), parameters were not correlated (data not shown).

For the design of ideotypes, we performed a Principal Component Analysis on the parameter sets, whose corresponding objective values matched the following decision criteria:

$$dm_C\,[\%] \geq 8\%\ and\ loss\ [\%] \leq 15\% \quad (12)$$

Principal Component Analysis and Hierarchical Clustering on PCA Individuals Score

A Principal Component Analysis (*ade4* package developed for the *R* software) (Dray and Dufour, 2007) was performed on the parameter values estimated for each recombinant line. This analysis was also applied to study the ideotype features. Genotypic parameters obtained for both calibration and ideotype design, were set as active variables. The dry and fresh weights under C and WD conditions and the dry matter content and fresh mass reduction under WD conditions were added as supplementary variables for the first PCA (model calibration step), while for the second (ideotype design) the initial dry weight, the initial fresh weight, and the *bssrat* parameter (contributing to the soluble sugar concentration calculus) were added. Data were previously normalized and centered (subtracting the mean value and dividing by the standard deviation). Among the 120 calibrated individuals, we excluded one outlier individual.

The PCA individual scores of the model calibration were subjected to hierarchical cluster analysis, using the *complete-linkage* clustering method with the *hclust* R function. The cluster number was chosen according to a visual criterion based on the cluster dendogram. For the ideotype analysis, the three groups of fruit size (large, medium and small size) were used to group the individual scores.

QTL Analysis of Model Genotypic Parameters

The best estimations of the eight genotypic parameters for the 120 genotypes and the coordinates of the RILs on the three first axis of the PCA were used as phenotypic traits in the QTL detection. When distributions were skewed, the best corrections for normality were applied: LOG10(nuM); $\sqrt{tstar}$; LOG10(lp1); LOG10(lx); LOG10(lx1); 1/rxp. The QTL detection was performed as presented in Albert et al. (2016) using the genetic map developed by Pascual et al. (2016) which included 501 SNP markers covering 80% of the tomato genome. Briefly, the simple interval parametric mapping model (Lander and Botstein, 1989) based on the EM algorithm method implemented in the R/QTL package (Broman et al., 2003) was used. A 1000-permutation test was performed to estimate the significant thresholds. Firstly, a LOD threshold equal to 3.13 and corresponding to a genome wide significance level of $\alpha = 0.05$ was considered. Then, we also considered lower significance levels to detect more QTLs: $\alpha = 0.10$ (LOD threshold = 2.76), $\alpha = 0.20$ (LOD threshold = 2.42) and $\alpha = 0.30$ (LOD threshold = 2.20). For each detected QTL, position, LOD score, marker at the LOD score peak, confidence interval (CI, LOD decrease of one unit), average phenotypic values of the two parental alleles and percentage of phenotypic variation explained (PVE) were displayed. The CIs were expressed both in cM Haldane (genetic distance) and in Mbp onto the tomato genome (assembly v2.5) (physical distance). The number of genes within each interval was identified from the tomato genome annotation (2.4). We reported the locations between the detected QTLs and the QTLs identified on phenotypic traits (plant and fruit traits) measured on the same plants (see Albert et al., 2016).

RESULTS

Water Deficit Effects on the Observed Dry Matter Content and Fresh Weight

The observed values of fresh weight and dry matter content measured at the ripe stage under control and WD conditions are shown on **Figures 1**, **2**. WD generally increased the dry matter content (up to 85%) and decreased the fruit fresh weight (up to 60%). This was directly connected to the lower influx of water to the fruit under WD conditions. Cervil—characterized by a low fresh weight—was the less sensitive to WD. The dry matter content of the F1 hybrid (CxL) increased substantially, while its fresh weight decreased slightly. On the contrary, Levovil was the most sensitive to WD, since it lost more than half of its fresh weight and it doubled its dry matter content under WD. In the population, the relative decrease in fruit fresh weight under WD was negatively correlated to the fresh weight under control conditions, indicating that large fruit genotypes were the most sensitive to WD, as mentioned in Albert et al. (2016). On the contrary, the increase in dry matter content under WD was rather independent of the dry matter content observed under control condition. Interestingly a few genotypes were close to the bisector and thus, get comparable fresh weight or dry matter content under both conditions. For these genotypes (Cervil, SSD12, SSD17, SSD49, SSD61, SSD65, SSD140, and SSD154), the differences between C and WD conditions was less than 5 g fresh mass and 1% dry matter content (**Figure 2**).

Model Calibration and Genetic Variability in Model Genotypic Parameters in the RIL Population

Eight genotypic parameters of the model (**Table 1**) were estimated for the RILs and for the two parent lines, in order to predict the dry and fresh masses (output variables) during fruit growth. The fittings were fairly good. **Table 2** shows the

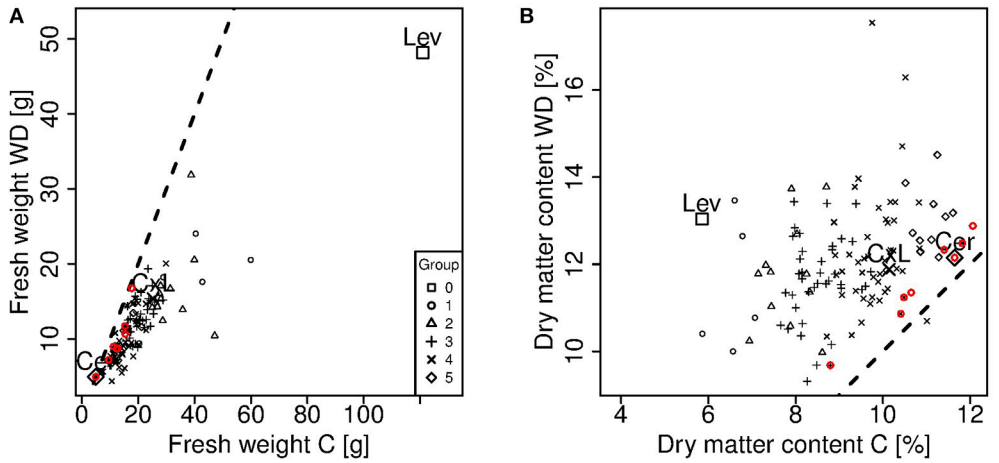

FIGURE 2 | Comparison of fresh weight (A) and dry matter content **(B)** measured on ripe fruits under control (C) and water deficit (WD) conditions. Each point represents one genotype (means of 15 to 20 fruits) and crosses indicate the parental lines (Cervil and Levovil) and the F1 hybrid (CxL). The different symbols represent the six groups of genotypes shown in **Figure 1**. The dashed lines represent the condition in which the plotted variables are equal. The red points represent the genotypes that are near to both dashed lines. These genotypes are the same in **A** and **B**.

TABLE 2 | Statistical summary of the Normalized Relative Mean Squared Errors (NRMSE) obtained with the model calibration under control (C) and water deficit (WD) conditions.

NRMSE	Mean [%]	Standard deviation [%]	Minimum [%]	Maximum [%]	Parents and F1 [%]	
Fresh weight in C condition	17.41	5.35	7.88	34.00	Cer	8.65
					CxL	16.36
					Lev	34.00
Dry weight in C condition	16.48	4.03	8.61	28.18	Cer	9.08
					CxL	8.72
					Lev	15.78
Fresh weight in WD condition	17.76	4.10	9.34	34.20	Cer	9.42
					CxL	12.88
					Lev	24.11
Dry weight in WD condition	17.65	4.19	8.29	27.46	Cer	8.29
					CxL	12.70
					Lev	25.19

The dry and fresh weight increases were fitted from 8 daa until fruit maturation and NRMSE were calculated over this developmental period for each genotype and condition. Mean and standard deviations were calculated for the whole RIL population (including the parent lines). Minimum and maximum refer to the lower and upper values of NRMSE obtained in the population. On the last column, the parents and the F1 hybrid values are shown.

NRMSE values obtained under C and WD conditions that were obtained for the whole population, for the parental lines and for the F1 hybrid. Considering the dry and fresh mass increases over the developmental period (from 8 daa to maturity), the mean NRMSE of the population ranged between 16 and 18% (standard deviation ∼ 4–5%) whatever the condition and output variables (**Table 2**). The total variation of NRMSE values in the population was in the range of 5–34%. NRMSE values obtained for Cervil were close to the minimum for all objectives. The dry mass increase of Levovil fruits was better simulated in C than in WD condition, while the prediction of their fresh mass increase was the worst under C condition.

Considering the ripe stage, the final fruit dry mass was more accurately predicted by the model than the final fresh mass (**Figure 3**), and predictions were better under WD than C condition. Indeed, the model underestimated the fresh mass of the largest fruit-size genotypes in C condition, in particular for Levovil (−34 g). For this genotype, the prediction errors of fresh mass in C conditions were high over the whole development period, as indicated by the NRMSE value in **Table 2**. On the contrary, the model predictions were more accurate for Cervil and the CxL hybrid under both conditions. As a consequence, the final dry matter content was mostly overestimated (differences from −1.73 to 6.17%) and underestimated (differences from −3.16 to 1.37%) in C and WD conditions, respectively (**Figure 4**).

The frequency distributions of the eight genotypic parameters were widely spread over the parameter search spaces, except for lp1 (pedicel conductivity for water transport in the phloem), which varied in a narrow range in the population (**Figure 5**). A principal component analysis was performed on the estimated parameter values. The first three components explained 24, 22, and 16% of the variance, respectively (62% in total). On the first principal component (**Figure 6B**), we observed negative loadings of lx and lp—which are the parameters related to the membrane permeability—and lx1 and lp1—related to the pedicel hydraulic conductance (**Table 1**). So the first axis was mainly associated with parameters controlling water inflow to the fruit from the xylem and phloem tissues. PhiMax which impacts the cell wall plasticity, as well as tauA, nuM, and tauS, which tunes the active sugar uptake and the sugar mass flow intensities, respectively, had a high loading on the second principal component. Parameter phiMax had the highest impact with a negative value, opposite

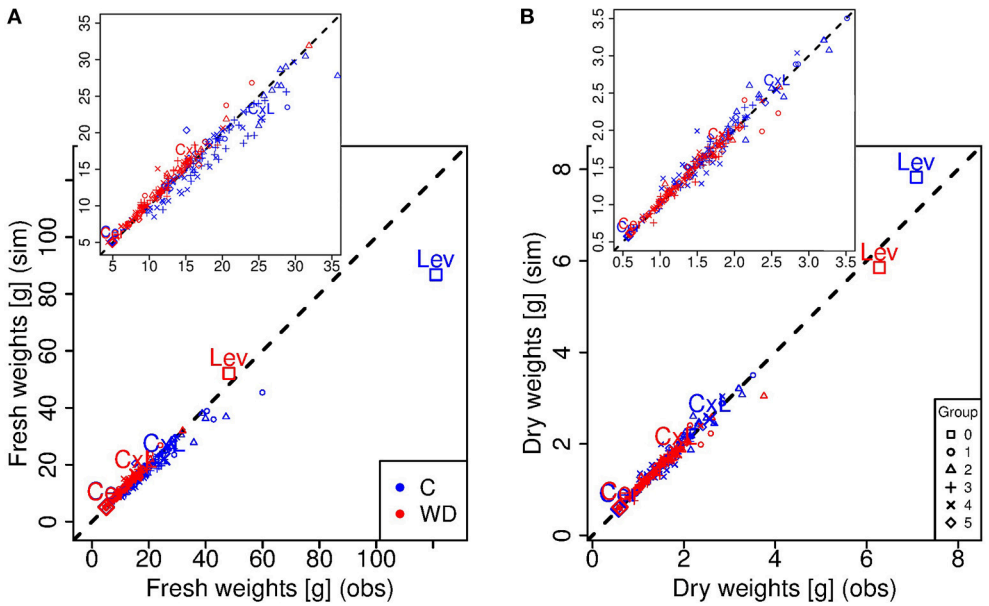

FIGURE 3 | Simulated (y-axis) *versus* observed (x-axis) fresh (A) and dry **(B)** weight values at the red ripe stage for each genotype in control (C, blue) and water deficit (WD, red) conditions. Each point represents one genotype (means of 15 to 20 fruits) and crosses indicate the parental lines (Cervil and Levovil) and the F1 hybrid (CxL). The different symbols represent the six groups of genotypes shown in **Figure 1**. The dashed line represents the points in which the simulated values are equal to the observed one.

with respect to nuM. So the second axis was mainly associated to turgor-driven cell expansion and active sugar uptake.

The fruit dry and fresh masses, the dry matter content under C and WD conditions, and the fresh mass reduction under WD were projected as inactive variables on the correlation circle (**Figure 6C**). Dry matter content in C condition and fresh mass reduction in WD condition correlated negatively. High dry matter content in C condition was associated with high value of tauS (parameter referring to mass flow process). The fresh mass reduction was associated with low values of nuM (maximum active uptake of sugar) and tauS, while it was associated with high values of phiMax (cell wall extensibility) and tauA (whose high values mean a slower decrease of active uptake rate of sugar during fruit development). Five clusters were selected through hierarchical cluster analysis (**Figure 6D**). The two parental lines and the F1 hybrid belonged to different groups. Levovil constituted a single cluster characterized by high fresh weight (fw) and dry weight (dw) under both conditions (first axis) and high reduction in fresh mass (second axis), with high values of lp (on the first component), phiMax and tauA (on the second component). Cluster 1 (including Cervil) and cluster 5 were characterized by high dm content under C conditions and low loss of fresh mass under WD, despite the fact they were associated with different active variables. Cluster 1 was associated with high membrane-permeability and high pedicel-conductance, whereas cluster 5 was associated with high values of nuM and low values of phiMax and tauA. Clusters 2 and 4 overlapped near to the origin of the first two components plan and were characterized by a high loss of fresh mass under WD and low dry matter content under control conditions. The CxL F1 hybrid belonged to cluster 2 and was positioned far from the cluster center.

QTL of Model Genotypic Parameters in the Population

A QTL analysis of the eight model parameters (**Table 1**, best estimation for each RIL line) and the coordinates of the RIL on the PCA axes, was performed independently of the irrigation level. Results are presented in **Table 3**. Two QTLs were detected with a genome wide significance level of $\alpha = 0.05$, on chromosome 2 and 8. These QTLs were associated with lp1 (pedicel conductivity) and lp (composite membrane conductivity) and explained 14 and 13% of the trait variations, respectively (**Table 3**). When considering less stringent significance levels, six supplementary QTLs became significant which explained between 9 and 11% of the parameter variations. Three of them were related to conductivity (lx1, rxp and lx, α between 0.10 and 0.30), one was related to sugar active uptake (nuM, α between 0.20 and 0.30), and two QTLs were associated with the second and third axes of the PCA (α between 0.10 and 0.20). No significant QTL was detected for phiMax, a parameter associated with cell wall extensibility, even when considering lowered significance thresholds.

Among the eight identified QTLs, two colocalized on top of chromosome 8 (for lp and lx), two in the centromeric region of chromosome 4 (for rxp and lx1) and two on top of chromosome 7 (for nuM and axis 2), which may correspond to three unique QTLs. Except for the QTL for rxp on chromosome 4 which included 192 genes over 0.18 Mbp, the QTL intervals were rather large (from 3.6 to 54.95 Mbp, including between 480 and 1180 genes). QTLs for fruit and plant traits detected in the same regions in the same population grown under control and WD conditions (Albert et al., 2016) are indicated in the last column of **Table 3**.

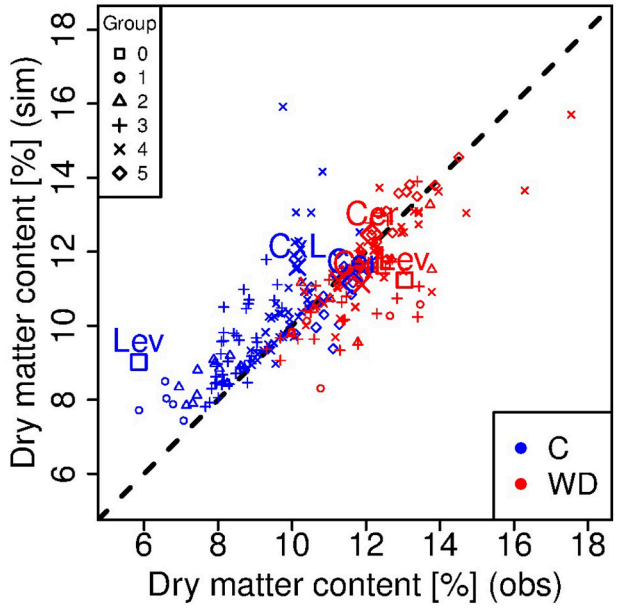

FIGURE 4 | Observed *vs.* simulated dry matter contents at the red ripe stage for each genotype in control (C, blue) and water deficit (WD, red) conditions. Each point represents one genotype (means of 15 to 20 fruits) and crosses indicate the parental lines (Cervil and Levovil) and the F1 hybrid (CxL). The different symbols represent the six groups of genotypes shown in **Figure 1**. The dashed line represents the points in which the simulated values are equal to the observed one.

Design of Tomato Ideotypes to Minimize the Reduction of Fruit Fresh Mass under WD Conditions and Optimize Fruit Dry Matter Content under C Conditions

The design of ideotypes consisted in finding sets of model parameters to match one or more objectives under a given condition (C or WD). Because we observed significant decrease in fruit fw under WD conditions and because fruit dm content is associated with high sugar and acid contents, our objectives were to maximize the dry matter content in C conditions and to minimize the fresh weight loss under the water deficit modality. Moreover, since the sensitivity to WD depends on the fruit fw (**Figure 2**), three classes of fruit grades were considered: large size (100–300 g), medium size (20–80 g) and small size (5–15 g).

In this step, 11 genotypic parameters were considered (**Table 1**), the eight parameters estimated in the calibration step, the initial fresh and dry mass of fruit and one parameter related to sugar content. The threshold between the two objectives is highlighted on **Figure 7**. For the group of large fruits (**Figure 7A**), the objectives were largely improved (dm content around 9% under C conditions and fresh mass loss around 15% under WD) with respect to Levovil (5.5% dm content under C condition and 60% fresh mass loss under WD), the only genotype belonging to the 100–300 g interval. The median fresh weight of the ideotypes in this group was 113 g in C conditions. In the medium-size group (**Figure 7B**) and in the small-size group (**Figure 7C**) of fruits, we obtained a large improvement too, since our selected ideotypes contained between 8 and 10% dm, which was comparable to the RIL population; however, they lost less than 15% fresh mass under WD conditions, which was two to three times less than the RIL population. In these two groups, the median fresh weight in C condition was 21 and 7 g, respectively. Interestingly in the small-size group of fruits, five RILs were in the scatter plot of selected ideotypes, and likely bear interesting traits and alleles for adaptation to WD. These are Cervil, SSD84, SSD107, SSD121, and SSD154.

A PCA was performed on the ideotype parameters obtained through the optimization problem resolution in order to understand the mechanisms of water stress resistance that could be combined in "ideal" fruits. In order to compare the ideotypes and the RILs, the eight genotypic parameters calibrated on the RILs were used as active variables (**Figure 8B**). The three additional parameters estimated for the ideotypes (bssrat, s0, w0) as well as the calculated fresh mass loss under WD, the fresh and dry mass and the dm content under non limiting water supply were projected as inactive variables (**Figure 8C**). The first two principal components explained 49.4 and 14.9% of the variation, respectively (**Figure 8A**). On the first component, lx and lp (composite membrane conductivity) had a positive loading and lx1 and lp1 (pedicel conductivities) had a negative loading. nuM (maximum rate of active sugar uptake) and tauA (negatively linked to the decrease in active sugar uptake rate during the fruit development) showed a negative and a positive loading, respectively, on this first component. The three groups of fruit grades were well-separated in the PC space especially for the big-size fruits (**Figure 8D**, cluster 1 blue colored). The big fruit-size ideotypes (100–300 g) were associated with high value of nuM, high pedicel conductivity and low fruit composite membrane conductivity, suggesting that sugar transport and pedicel conductivity may be interesting issues for improving adaptation of large-fruited genotypes to WD. They were also associated with high fresh mass loss (considered as inactive variable; **Figure 8C**). On the contrary, the cell wall extensibility (phiMax) and the mass flow characteristics (tauS) did not strongly discriminate the ideotype population.

The active variables were correlated in a different way with respect to the calibration situation (**Figure 6A**). In the ideotype principal component space, tstar and tauS correlated to each other, whereas in the calibration parameters space they were uncorrelated. Parameters regarding conductivities were highly correlated in both spaces; however, in the ideotype situation, the pedicel conductivities lp1 and lx1 were negatively correlated with the composite membrane ones (lp and lx). nuM did not show any positive correlation in the calibration case, whereas it correlated positively with the pedicel conductivities in the ideotype case. Most of the RILs, when projected as inactive individuals (**Figure 8A**), lied for in the positive values of the first principal component and in the negative values of the second principal component. Most of the RILs have medium to small-sized fruits (**Figure 2**), but, in the ideotype principal component plan, their positions did not completely overlap the corresponding group of ideotypes (n°2). Levovil is the only large fruited line and it did not belong to ideotype group 1. Cervil

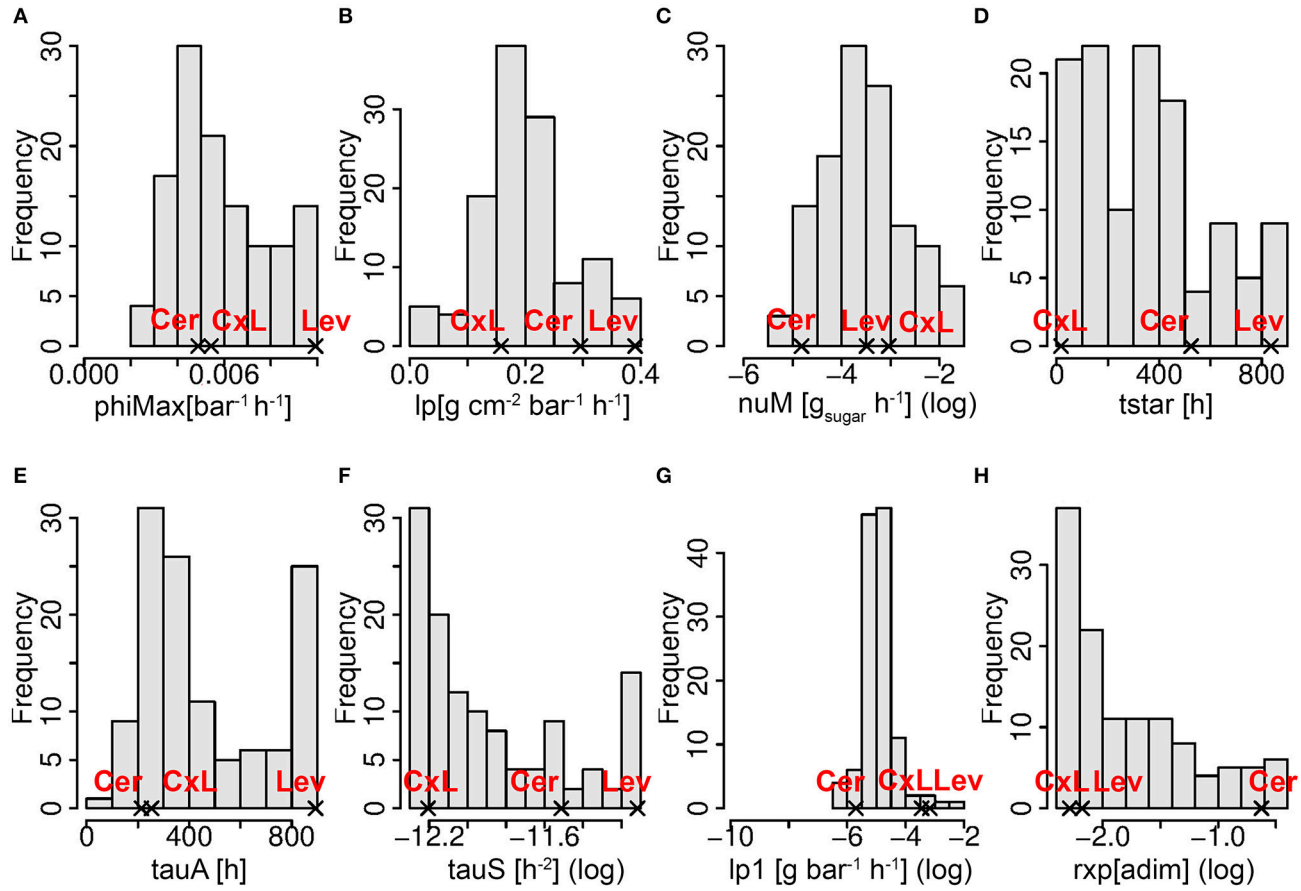

FIGURE 5 | Frequency distributions of the best estimated parameter sets in the RIL population including the two parental lines (Cer: cervil and Lev: levovil), the F1 hybrid (CxL), and the 117 RILs. Panels **(A–H)** represent the frequency distributions of the eight genotypic parameters as indicated in the x-axes title. The x-axes range corresponds to the parameter search space (see **Table 1**). The log in brackets indicates that a natural logarithmic transformation was applied on the variable, for a better legibility.

belonged to its size group. CxL belonged to a region that is the farthest one to group 2.

DISCUSSION

Model-Based Analysis of the Processes Involved in Genetic Variability of Fruit Response to Water Deficit

In this study, we applied a long and severe WD, which caused significant decrease in fruit fresh mass and increase in dm content for most of the RILs. Large fruits were the most sensitive in terms of fresh mass reduction, in agreement with previous studies (Ripoll et al., 2015; Albert et al., 2016). The model was able to reproduce fairly well the genetic variabilities observed in the population and the WD effects, after the calibration of eight genotypic parameters, which are related to cell expansion, water transport, and sugar uptake. These three processes were strongly discriminant in the RIL population (**Figure 6**), and appeared as main traits to be considered in the future for breeding tomato adapted to WD conditions. Interestingly in the population, a few genotypes (among which Cervil) reached comparable fresh and dry masses under C and WD conditions. All these genotypes are in the range 5–20 g FW and 9–12% dm (**Figure 2**), but they clustered in groups 2, 4, and 5, whereas Cervil was in group 1 (**Figure 6**). Thus, the low sensitivity to WD could not be related to one single parameter/process, and a more detailed phenotyping of these RILs at the plant and fruit levels could be useful to identify the main discriminating traits. According to the PCA on the calibrated genotypic parameters, conductivities merit special attention since high conductivities were associated with high dry matter content and heavy fruit weights. The sugar active uptake seemed to play an important role as well: the higher the maximum uptake rate was (nuM), the lower the decrease in fresh mass, which was probably associated with osmotic regulations.

The mean NRMSE value of the population was around 17%, which is quite performing (**Table 2**). The worst value was obtained for Levovil, but the fitting were largely improved when predictions were done independently under C or WD conditions (not shown), suggesting that some WD effects were poorly taken into account in this case. During the calibration step, the WD treatment was taken into account through several

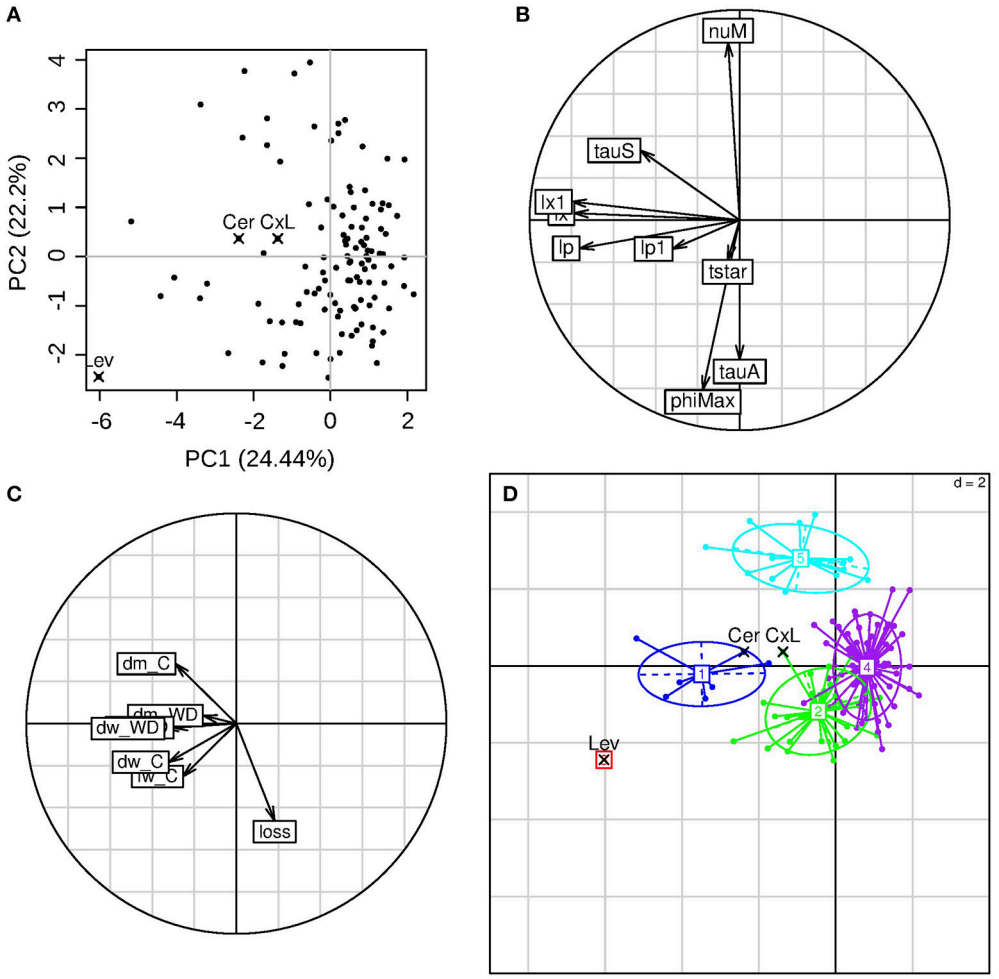

FIGURE 6 | PCA of the calibration parameter results. (A) Individual's positions in the first two principal components plane, with highlighted values for the parental lines (Cervil and Levovil) and F1 hybrid (CxL); each component explained variance is showed in parenthesis. **(B)** Variable coordinates normed to the square root of the eigenvalue represented in the correlation circle. **(C)** Inactive variables coordinates in the correlation circle: *dm* indicates the dry matter content, *dw* and *fw* state for dry and fresh weights of ripe fruits, respectively, *loss* indicates the fresh mass loss index as computed in Equation (11); **(D)** Output clusters from the hierarchical cluster analysis.

plant and fruit variables, i.e., the stem water potential, the initial dry and fresh masses, the sugar concentration of the dry matter, the fruit conductance involved in transpiration and the fruit osmotic pressure related to soluble components other than sugars. These variables were measured experimentally. On the contrary, other parameters were fixed since they cannot be easily measured. In the future, these parameters could be more deeply investigated. For instance, the impact of drought on phloem transport has been nicely illustrated through current model hypotheses (Sevanto, 2014). Accordingly, in the Virtual fruit model, the assumptions of impermeable conduit walls in the fruit pedicel and semipermeable walls in the fruit cells, implicitly involve that phloem transport in the pedicel is vulnerable to the increase of viscosity and to the geometry (number and size) of the conducting vessels. Sevanto (2014) demonstrated that wider or more numerous conduits are required to compensate for the increase in sap viscosity in order to maintain phloem transport under drought. In the present study, WD effects on these two parameters were overlooked. Indeed, in the absence of experimental value, the sugar concentration in phloem sap (Cp) was supposed to be constant over fruit development and the surface (cm2) of exchange of the vascular networks entering the fruit, was assumed to be proportional to the fruit surface area (Af), according to a non-dimensional constant coefficient, leading to smaller exchange area in case of the WD treatment. Thus, the conductivity of the phloem and xylem in the pedicel (lp1 and lx1) or in the fruit (lp and lx), which were estimated, likely integrated several properties of the conducting tissues. Both in the calibrating step (**Figure 6**) and the ideotype design (**Figure 8**), these parameters were highly discriminant and undoubtedly involved in the reduction of fresh weight loss under WD. So sugar concentration in

TABLE 3 | QTLs detected on eight genotypic parameters of the model and on the first three axes of the PCA estimated on the RIL population.

Trait	Sign.	LOD	Chr	Pos	Marker	CI cM (Mpb)	Nb genes	Mean Cer (sd)	Mean Lev (sd)	PVE	Coloc. (Albert et al., 2016)**
lp1*	0.05	3.85	2	95.60	TG167_Y02_52393366	89.73–107.19 (51.19 –54.79)	480	0.01 (0.00)	0.01 (0.00)	13.75	Nbfruits.C&WD fw.C&WD FIR.WD FIR.WD dw.C SSC.Int
rxp*	0.20	2.68	4	36.73	Y04_03230589	33.63–52.44 (0.30–0.48)	192	0.17 (0.12) (0.12)	0.22 (0.13)	10.22	Ø
lx1*	0.10	2.81	4	61.27	Y04_53862540	2.06–63.34 (0.42–55.37)	1604	0.001 (0.00)	0.002 (0.00)	10.7	FIR.C and WD
Axis3	0.20	2.46	4	86.96	Y04_61146494	61.27–95.70 (53.86–62.08)	589 589	−0.36 (0.12)	0.26 (0.13)	9.37	Flw.C Flw.WD Diam.C fw.C FIR.C&WD dw.C VitCFM.C&WD Yield.C
nuM	0.30	2.30	7	93.31	Y07_67908188	82.11–93.31 (65.13–67.90)	408	0.05 (0.01)	0.03 (0.00)	8.80	Ø
Axis2	0.20	2.49	7	88.00	Y07_64327204	73.63–93.31 (63.64–67.90)	575	0.51 (0.20)	−0.44 (0.19)	9.15	Ø
lp	0.05	3.31	8	42.12	Y08_57208257	31.67–58.97 (54.32–59.92)	479	0.22(0.08)	0.16 (0.06)	12.64	pH.WD VitCFM.WD VitCDM.C&WD
lx*	0.30	2.24	8	42.12	Y08_57208257	31.67–101.95 (54.32–65.60)	1180	0.51(0.05)	0.03 (0.01)	8.71	Flw.WD pH.WD VitCFM.WD VitCDM.C&WD Yield.Int

Traits transformed to ensure a normal distribution, LOG10(lp1); 1/rxp; LOG10(lx1); LOG10(lx).

***Nbfruits, plant fruit number; fw, fruit fresh weight; FIR, fruit firmness; dw, fruit dry matter weight; SSC, solid soluble content; Flw, flowering time; Diam, stem diameter; pH, fruit pH; VitCFM, vitamin C content in fruit on a fresh weight basis; VitCDM, vitamin C content in fruit on a dry weight basis; Yield, fruit fresh weight per plant; C, control; WD, water deficit; Int, interactive between watering regimes.*

"Sign." indicates the significance threshold at which the QTL was detected. LOD is the log-likelihood at that marker. The chromosome is indicated under "Chr" and the position of the QTL is expressed in Haldane cM under "Pos." The most closely associated marker is indicated. CI indicates the genetic confidence interval in Haldane cM calculated by LOD decrease of one unit, and its physical equivalent (Mpb) on genome assembly 2.5 between brackets. The number of genes in the QTL interval (genome annotation 2.4) is indicated. The average value of the two parental alleles (Cer and Lev, with the standard deviation between brackets) and the percentage of phenotypic variation explained by the QTL (PVE) are displayed. Colocalizations with phenotypic QTLs detected in Albert et al. (2016) in the same RIL population are indicated. C, QTL specific to the control condition; D, QTL specific to the water deficit condition; C&WD, QTL detected under both condition; Int, QTL with effect changing intensity or direction according to the watering conditions.

the phloem and geometry of conducts appeared as important components of the water deficit adaptation strategies, which have to be more deeply investigated as well as their genetic variability.

The maximum cell wall extensibility (phiMax) also appeared as a discriminant parameter in the population. Despite the growing number of studies and methods to investigate cell wall extensibility and elasticity (Cosgrove, 2016), data are currently missing to parameterize fruit models. In the present model, cell wall extensibility decreases exponentially with time from phiMax, which was considered to be genotype dependent, whereas the rate of decrease was constant and taken from Liu et al. (2007). In the RIL population, phiMax was negatively correlated with the maximum rate of sugar active uptake (nuM) and was associated with high loss of fresh mass under WD, likely because the large fruit-size genotypes (mainly Lev) combined both traits in this population.

QTL Analysis of Model Genotypic Parameters

The added value of QTLs for model parameters lies in their expected stability, on the contrary to other QTLs for phenotypic

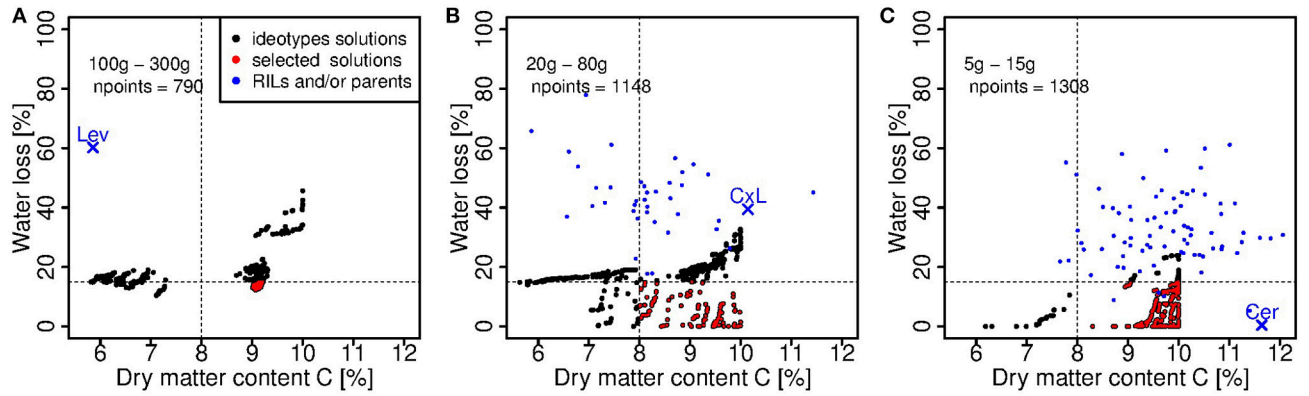

FIGURE 7 | Ideotype solutions considering a fruit fresh weight interval of (A): 100–300 g, **(B)**: 20–80 g, **(C)**: 5–15 g. The black and red points represent the dry matter content of ripe fruits in C conditions and the fresh mass loss value of all the ideotype solutions obtained solving the multi-objective problem for each interval of fruit fresh weight. The red points are the ideotype solutions satisfying simultaneously a high dry matter content in C condition (>8%) and a low loss of fresh mass under WD (<15%), according to Equation (13). npoints is the number of solutions. The blue points represent the dry matter content of ripe fruits in C conditions and the fresh mass loss values computed for the observed individuals in the RIL population, in the respective weight class. The parental lines (Cervil and Levovil) and F1 hybrid (CxL) are highlighted.

traits, which fluctuate with environmental conditions. We detected QTLs for six of the 10 genotypic parameters and two PCA axes, four of them (for Lp1, Lx1, and Lp) with a significance level below 0.1. The QTLs were located in four chromosomic regions. The QTL for lp1 on chromosome 2 colocalized with QTLs detected in Albert et al. (2016) for plant fruit number (constitutive effect under control and WD conditions), fruit firmness (constitutive effect under control and WD conditions), dm (specific to control condition) and soluble solid content (SSC, with changing effect according to the watering regime). Besides, this QTL was present in the genomic region carrying the cloned tomato fresh weight QTL FW2.2 (Frary et al., 2000). Close to this QTL, several QTLs for sugar content were fine mapped (Lecomte et al., 2004) The QTLs for rxp, lx1 and axis3 in the centromeric region of chromosome 4 colocalized with a QTL for fruit firmness (FIR, specific to the WD condition) detected in Albert et al. (2016); this connection between conductivity and firmness under WD may result from the effect of turgor regulation on fruit firmness (Shackel et al., 1991). QTLs detected for nuM and axis 2 (related to sugar active uptake) did not colocalize with any QTL identified in Albert et al. (2016). However, QTL for soluble solid content were identified in this genomic region in other tomato populations (Pascual et al., 2016). Finally, the QTLs for lp and lx on top of chromosome 8 colocalized with QTLs for flowering time (Flw, specific to WD condition), fruit pH (specific to WD condition), vitamin C content in fruit on a fresh weight and on a dry weight basis (WD specific and constitutive, respectively) and yield (with changing effect according to the watering regime). Unfortunately the confidence intervals were too large to check for candidate genes, but future studies should more deeply investigate these regions, in particular regarding the pedicel and fruit conductivities.

Interestingly, the seven genotypes belonging to group 1 in the PCA (**Figure 6**) all carried the Cervil allele for the lp and lx QTLs on chromosome 8. Besides, these genotypes also carried the Cervil allele for a yield QTL detected by (Albert et al., 2016) on chromosome 4, close to the QTLs identified for rxp and lx1 (3.16 Mbp upper on the chromosome). No specific allele at the QTL was identified for the other groups of the PCA. We detected only one QTL for one of the four genotypic parameters related to sugar uptake, hypothetically due to their skewed distribution and to the estimation error. In the Fruit model, sugars may be allocated to fruit through passive diffusion, mass flow or active transport, the last being the most discriminant in our population. Different transporters are required for efficient phloem unloading in fruit pericarp at the rapid expansion phase (Ruan and Patrick, 1995), operating with different energetic and kinetic constraints (reviewed by Osorio et al., 2014). In the model, all these transporters are compiled into one single Michaelis-Menten function, which might explain that no specific QTL was detected.

Ideotypes of Tomato Adapted to WD Depending on Trade-Offs between Fresh Weight and Dry Matter Content

In the light of experimental data, one challenge for producing tomatoes under WD conditions will be to avoid the reduction of fresh mass of large fruited genotypes, while maintaining or increasing the fruit dm content, which correlates with the accumulation of sugars and acids, both involved in fruit taste. In confront to previous works (Semenov et al., 2014; Rötter et al., 2015), the problem was complex, first, because the process-based model used in this study was relatively sophisticated, second, because we aimed at maintaining quality and increasing yield under WD conditions. We were able to design large-fruited ideotypes rich in dm (9% dm content) and with reasonable fresh mass loss under WD (<20%) which outperformed Levovil

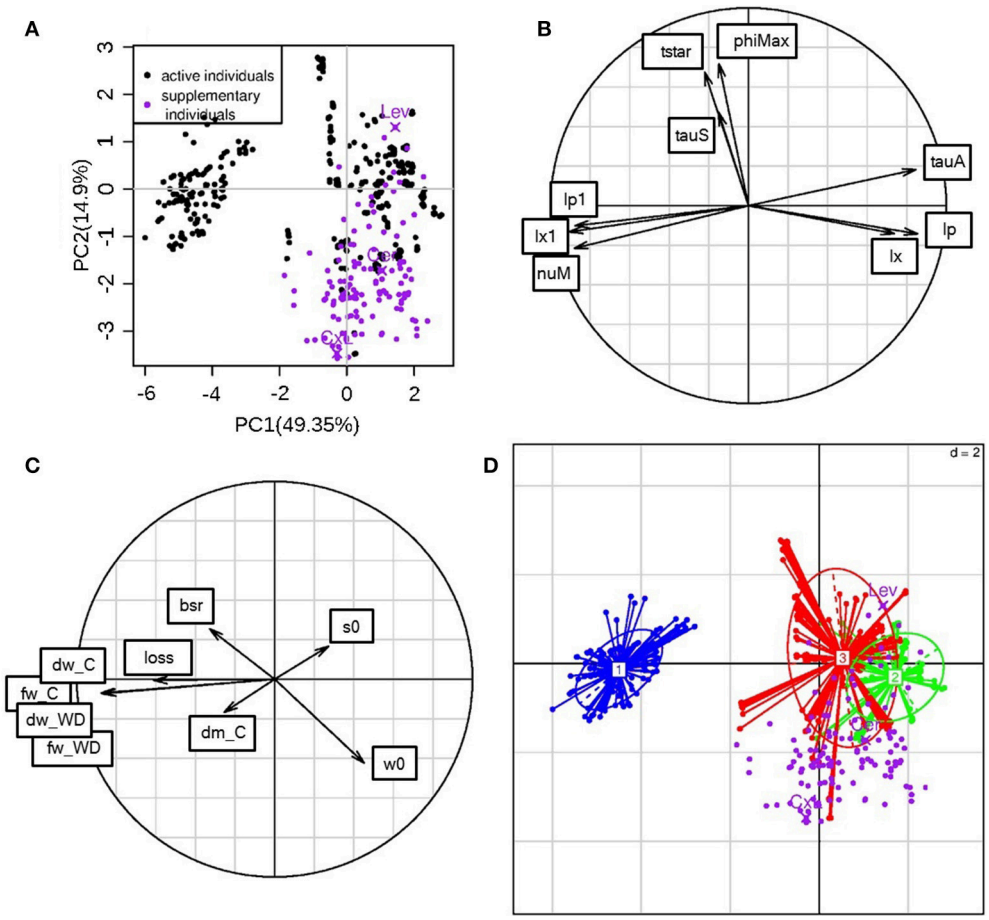

FIGURE 8 | PCA performed on the ideotype parameters. (A): ideotype positions in the first two principal components plane (black dots), and projection as inactive variables of the parameter values calibrated for the RIL population (purple dots); The parental lines (Cervil and Levovil) and F1 hybrid (CxL) are highlighted; the % of variance explained on each component is given in parenthesis. **(B)**: variable coordinates normed to the square root of the eigenvalue represented in the correlation circle. **(C)** Inactive variable coordinates in the correlation circle. *bsr* is the *bssrat* parameter, *s0* and *w0* are the estimated initial dry and fresh weights; *dm_C* states for dry matter content in C condition and *dw_C* for dry weight in C condition. Three more variables were hidden by this last one: *fw_C, fw_WD,* and *dw_WD* representing fresh weight under C and WD, and dry weight under WD, respectively **(D)**: ideotypes divided into fruit grade groups: (1) 100–300 g (blue), (2) 20–80 g (green), (3) 5–15 g (red). Purple dots represent the projections of the RILs.

(60% fresh mass loss and 6% dm content). Pedicel conductivity and fruit composite membrane conductivity were opposed in the ideotype population (**Figure 8**). The model considers three pathways for water and carbon flows: the plant-to-pedicel, the pedicel-to-fruit and the fruit apoplasm-to-cell, which all differ in carbon concentration and water potential. Conductance is mainly axial in the first two pathways (plant-pedicel and pedicel-fruit), whereas it is radial within the fruit. Thus high conductance in the pedicel which promotes water and sugar inflows in combination with high active uptake of sugars could be a successful strategy to produce large fruit-size ideotypes able to maintain, under WD conditions, a fresh weight above 100 g and dm content above 6 % (group 1 on **Figure 8**). These ideotypes also exhibit a low tauA value, indicating that the active uptake decreases slowly during the growth stage. On the contrary, the medium fruit-size ideotypes (group 2) were associated with low pedicel conductance and sugar uptake rate, but high fruit composite membrane conductivity. Such interactions between pedicel and fruit conductivities in relation to the demand for water and carbon, is intriguing and should deserve further attention. As mentioned above, the genetic variability of the conducting tissue geometry in the pedicel and fruit has been hardly described. In an anatomical descriptive study, Rančić et al. (2010) suggested that the low phloem efficiency (defined as the ratio between fruit dry weight and phloem pedicel area) of tomato flacca mutants was responsible for low fruit growth, whereas the phloem area and the functional xylem area were not affected compared to the wild type. In agreement, a modeling approach showed that, under a wide range of conditions, water import in young tomato fruit would be limited by the pedicel resistance (Bussières, 2002) and by phloem conductivity in relation to sap viscosity (Bussiéres et al., 2011). In this respect, QTL observed on chromosome 2, 4, and 8 may be really interesting. Regarding the small fruit-size genotypes, the four RILs, which scattered among

the ideotypes (**Figure 7C**) could probably bring new interesting source of genetic variations for breeding programs, as their fruit fresh mass at maturity is two to three times higher than the fresh mass of Cervil, which is already known to be WD resistant (Albert et al., 2016; Ripoll et al., 2016).

Comparing the RIL population (**Figure 6**) with the ideotype population (**Figure 8**), a main difference states in the orthogonality of nuM and lx/lp or lx1/lp1 in the RIL population, suggesting that fruit growth was limited either by the incoming fluxes (group 5 on **Figure 6**) or by the active transport of sugars (Lev or group 1 on **Figure 6**). Thus, the uptake of carbon was likely the limiting step for fruit growth of large fruit-size genotypes such as Lev, which bears large fruits with low dry matter content in the C condition.

CONCLUSIONS

The fruit model was able to reproduce contrasting behaviors in the RIL population, regarding fresh weight loss and/or dm content increase under WD. Cell expansion, water transport and sugar uptake were all involved in the genetic variability of the fruit response to WD, but pedicel conductivity and active uptake of sugars seemed to be the key-mechanisms. In the future, model improvements should account for WD effects on cell wall extensibility, sugar uptake and exchanges of water between phloem and xylem tissues. Such advances will boost our understanding of the complex interactions between osmotic adjustments, changes in cell wall extensibility and maintenance of cell turgor under WD. The present study also outlined three interesting QTLs that deserve attention in breeding program for adaptation to WD and 4 RILs, which could bring new interesting traits in this regard. Finally, we are aware of the fact that Levovil is the only big fruit size genotype in the studied population; all other RILs ranged between 5 and 60 g FW. Thus, applying our approach to other tomato populations will be valuable. In a longer-term perspective, using a plant-fruit model (Baldazzi et al., 2013) would allow a better assessment of the respective contribution of source and sink capacities to the genetic variability. From a methodological point of view, other algorithms e.g., the Reference-point-based Non-dominated Sorting Genetic Algorithm R-NSGA-II could be used to calibrate the process-based model considering individual errors for each output variables, which could open new perspectives regarding the accurate integration of genetic information into the process-based model. Indeed, here ideotypes were discussed without considering the genetic constraints (epistasis or linkage). For this purpose, we should first integrate the genetic information into the process-based model through the QTL analysis. Then, we shall consider the allelic combinations of the loci involved in the genetic models allowing the computation of the parameter values. In this step, taking into account the genetic constraints (probabilities of two loci to be identical) shall be achieved either through their direct integration into the genetic model or through the optimization algorithm (mathematical formulation of the problem). In the future, such genetic models could be used to test virtual scenarios of fruit adaptation to water stress and identify key-regions on the tomato genome.

AUTHOR CONTRIBUTIONS

NB, MG, GV, and MM conceived and designed the work; BB and NB collected the experimental data; DC, PV, and MM devised the algorithms and performed the simulations; DC, NB, MG, GV, EA, MC, and MM analyzed and interpreted the data; DC, NB, MM, GV, and EA wrote the paper; MG, MC, and VB revised it critically; all authors approved the final version.

FUNDING

INRA provided all experimental and modeling supports as well as permanent manpower.

ACKNOWLEDGMENTS

This project has been supported by the CTPS Project TOMSEC, by the ANR project ADAPTOM (ANR-13-ADAP-0013-01) and by Agropolis Foundation under the reference ID 1202-039 through the "Investissements d'avenir" Programme (Labex Agro: ANR-10-LABX-0001-01). We acknowledge the experimental teams of UR GAFL (Yolande Carretero, Alain Goujon) and PSH.

REFERENCES

Albert, E., Gricourt, J., Bertin, N., Bonnefoi, J., Pateyron, S., Tamby, J. P., et al. (2016). Genotype by watering regime interaction in cultivated tomato: lessons from linkage mapping and gene expression. *Theor. Appl. Genet.* 129, 395–418. doi: 10.1007/s00122-015-2635-5

Baldazzi, V., Pinet, A., Vercambre, G., Bénard, C., Biais, B., and Génard, M. (2013). *In-silico* analysis of water and carbon relations under stress conditions. A multi-scale perspective centered on fruit. *Front. Plant Sci.* 4:495. doi: 10.3389/fpls.2013.00495

Bertin, N., Martre, P., Génard, M., Quilot, B., and Salon, C. (2010). Under what circumstances can process-based simulation models link genotype to phenotype for complex traits? Case-study of fruit and grain quality traits. *J. Exp. Bot.* 61, 955–967. doi: 10.1093/jxb/erp377

Blum, A. (2011). *Plant Breeding for Water-Limited Environments*. New York, NY: Springer.

Bodner, G., Nakhforoosh, A., and Kaul, H.-P. (2015). Management of crop water under drought: a review. *Agron. Sustain. Dev.* 35, 401–442. doi: 10.1007/s13593-015-0283-4

Boote, K. J., Kropff, M. J., and Bindraban, P. S. (2001). Physiology and modelling of traits in crop plants: implications for genetic improvement. *Agric. Syst.* 70, 395–420. doi: 10.1016/S0308-521X(01)00053-1

Broman, K. W., Wu, H., Sen, Ś., and Churchill, G. A. (2003). R/qtl: QTL mapping in experimental crosses. *Bioinformatics*, 19, 889–890. doi: 10.1093/bioinformatics/btg112

Bussières, P. (2002). Water import in the young tomato fruit limited by pedicel resistance and calyx transpiration. *Funct. Plant Biol.* 29, 631–641. doi: 10.1071/PP00144

Bussiéres, P., Bertin, N., Morris, C. E., Vigne, C., Orlando, P., Glaux, C., et al. (2011). High external sucrose concentration inhibits the expansion of detached tomato fruits grown in a novel semi-open device. *In Vitro Cell. Dev. Biol. Plant* 47, 743–751. doi: 10.1007/s11627-011-9378-z

Chapman, S., Cooper, M., Podlich, D., and Hammer, G. (2003). Evaluating plant breeding strategies by simulating gene action and dryland environment effects. *Agron. J.* 95, 99–113. doi: 10.2134/agronj2003.0099

Cosgrove, D. J. (2016). Plant cell wall extensibility: connecting plant cell growth with cell wall structure, mechanics, and the action of wall-modifying enzymes. *J. Exp. Bot.* 67, 463–476. doi: 10.1093/jxb/erv511

Deb, K., Pratap, A., Agarwal, S., and Meyarivan, T. A. M. T. (2002). A fast and elitist multiobjective genetic algorithm: NSGA-II. *IEEE Trans. Evol. Comput.* 6, 182–197. doi: 10.1109/4235.996017

Ding, W., Xu, L., Wei, Y., Wu, F., Zhu, D., Zhang, Y., et al. (2016). Genetic algorithm based approach to optimize phenotypical traits of virtual rice. *J. Theor. Biol.* 403, 59–67. doi: 10.1016/j.jtbi.2016.05.006

Dray, S., and Dufour, A.-B. (2007). The ade4 package: implementing the duality diagram for ecologists. *J. Stat. Softw.* 22, 1–20. doi: 10.18637/jss.v022.i04

Fishman, S., and Génard, M. (1998). A biophysical model of fruit growth: simulation of seasonal and diurnal dynamics of mass. *Plant Cell Environ.* 21, 739–752. doi: 10.1046/j.1365-3040.1998.00322.x

Frary, A., Nesbitt, T. C., Frary, A., Grandillo, S., Van Der Knaap, E., Cong, B., et al. (2000). Fw2. 2: a quantitative trait locus key to the evolution of tomato fruit size. *Science* 289, 85–88. doi: 10.1126/science.289.5476.85

Gong, P., Zhang, J., Li, H., Yang, C., Zhang, C., Zhang, X., et al. (2010). Transcriptional profiles of drought-responsive genes in modulating transcription signal transduction, and biochemical pathways in tomato. *J. Exp. Bot.* 61, 3563–3575. doi: 10.1093/jxb/erq167

Hall, A. J., Minchin, P. E. H., Clearwater, M. J., and Génard, M. (2013). A biophysical model of kiwifruit (*Actinidia deliciosa*) berry development. *J. Exp. Bot.* 64, 5473–5483. doi: 10.1093/jxb/ert317

Labate, J. A., Robertson, L. D., and Baldo, A. M. (2009). Multilocus sequence data reveal extensive departures from equilibrium in domesticated tomato (*Solanum lycopersicum* L.). *Heredity (Edinb).* 103, 257–267. doi: 10.1038/hdy.2009.58

Lander, E. S., and Botstein, D. (1989). Mapping mendelian factors underlying quantitative traits using RFLP linkage maps. *Genetics* 121, 185–199.

Lechaudel, M., Vercambre, G., Lescourret, F., Normand, F., and Génard, M. (2007). An analysis of elastic and plastic fruit growth of mango in response to various assimilate supplies. *Tree Physiol.* 27, 219–230. doi: 10.1093/treephys/27.2.219

Lecomte, L., Saliba-Colombani, V., Gautier, A., Gomez-Jimenez, M., Duffé, P., Buret, M., et al. (2004). Fine mapping of QTLs for the fruit architecture and composition in fresh market tomato, on the distal region of the long arm of chromosome 2. *Mol. Breed.* 13, 1–14. doi: 10.1023/B:MOLB.0000012325.77844.0c

Lescourret, F., and Génard, M. (2005). A virtual peach fruit model simulating changes in fruit quality during the final stage of fruit growth. *Tree Physiol.* 25, 1303–1315. doi: 10.1093/treephys/25.10.1303

Lescourret, F., Génard, M., Habib, R., and Fishman, S. (2001). Variation in surface conductance to water vapor diffusion in peach fruit and its effects on fruit growth assessed by a simulation model. *Tree Physiol.* 21, 735–741. doi: 10.1093/treephys/21.11.735

Letort, V., Mahe, P., Cournède, P. H., de Reffye, P., and Courtois, B. (2008). Quantitative genetics and functional-structural plant growth models: simulation of quantitative trait loci detection for model parameters and application to potential yield optimization. *Ann. Bot.* 101, 1243–1254. doi: 10.1093/aob/mcm197

Liu, H. F., Génard, M., Guichard, S., and Bertin, N. (2007). Model-assisted analysis of tomato fruit growth in relation to carbon and water fluxes. *J. Exp. Bot.* 58, 3567–3580. doi: 10.1093/jxb/erm202

Lu, C., Han, J. L., Hu, F. J., and Qin, T. G. (2012). Mathematical model of wheat stalk lodging-resistance during the later growth period. *Math. Pract. Theory* 42, 46–53. Available online at: http://en.cnki.com.cn/Journal_en/A-A002-SSJS-2012-15.htm

Mazzeo, M. (2008). *Xylem Transport Efficiency and Calcium Accumulation in Fruit of Actinidia deliciosa: Implications for Fruit Quality*. PhD. thesis, University of Basilicata, Potenza.

Osorio, S., Ruan, Y.-L., and Fernie, A. R. (2014). An update on source-to-sink carbon partitioning in tomato. *Front. Plant Sci.* 5:516. doi: 10.3389/fpls.2014.00516

Pascual, L., Albert, E., Sauvage, C., Duangjit, J., Bouchet, J. P., Bitton, F., et al. (2016). Dissecting quantitative trait variation in the resequencing era: complementarity of bi-parental, multi-parental and association panels. *Plant Sci.* 242, 120–130. doi: 10.1016/j.plantsci.2015.06.017

Qi, R., Ma, Y. T., Hu, B. G., De Reffye, P., and Cournede, P. H. (2010). Optimization of source-sink dynamics in plant growth for ideotype breeding: a case study on maize. *Comput. Electron. Agric.* 71, 96–105. doi: 10.1016/j.compag.2009.12.008

Quilot, B., Kervella, J., Génard, M., and Lescourret, F. (2005). Analysing the genetic control of peach fruit quality through an ecophysiological model combined with a QTL approach. *J. Exp. Bot.* 56, 3083–3092. doi: 10.1093/jxb/eri305

Quilot-Turion, B., Ould-Sidi, M.-M., Kadrani, A., Hilgert, N., Génard, M., and Lescourret, F. (2012). Optimization of parameters of the 'Virtual Fruit' model to design peach genotype for sustainable production systems. *Eur. J. Agron.* 42, 34–48. doi: 10.1016/j.eja.2011.11.008

Rančić, D., Quarrie, S. P., and Pećinar, I. (2010). "Anatomy of tomato fruit and fruit pedicel during fruit development," in *Microscopy: Science, Technology, Applications and Education,* eds A. Méndez-Vilas and J. Díaz (Badajoz: Formatex), 851–861.

Rebolledo, M. C., Dingkuhn, M., Courtois, B., Gibon, Y., Clement-Vidal, A., Cruz, D. F., et al. (2015). Phenotypic and genetic dissection of component traits for early vigour in rice using plant growth modelling, sugar content analyses and association mapping. *J. Exp. Bot.* 66, 5555–5566. doi: 10.1093/jxb/erv258

Reymond, M., Muller, B., Leonardi, A., Charcosset, A., and Tardieu, F. (2003). Combining quantitative trait loci analysis and an ecophysiological model to analyze the genetic variability of the responses of maize leaf growth to temperature and water deficit. *Plant Physiol.* 131, 664–675. doi: 10.1104/pp.013839

Ripoll, J., Urban, L., and Bertin, N. (2015). The potential of the MAGIC TOM parental accessions to explore the genetic variability in tomato acclimation to repeated cycles of water deficit and recovery. *Front. Plant Sci.* 6:1172. doi: 10.3389/fpls.2015.01172

Ripoll, J., Urban, L., Brunel, B., and Bertin, N. (2016). Water deficit effects on tomato quality depend on fruit developmental stage and genotype. *J. Plant Physiol.* 190, 26–35. doi: 10.1016/j.jplph.2015.10.006

Ripoll, J., Urban, L., Staudt, M., Lopez-Lauri, F., Bidel, L. P. R., and Bertin, N. (2014). Water shortage and quality of fleshy fruits–making the most of the unavoidable. *J. Exp. Bot.* 65, 4097–4117. doi: 10.1093/jxb/eru197

Rötter, R. P., Tao, F., Höhn, J. G., and Palosuo, T. (2015). Use of crop simulation modelling to aid ideotype design of future cereal cultivars. *J. Exp. Bot.* 66, 3463–3476. doi: 10.1093/jxb/erv098

Ruan, Y.-L., and Patrick, J. W. (1995). The cellular pathway of postphloem sugar transport in developing tomato fruit. *Planta*, 196, 434–444. doi: 10.1007/BF00203641

Saliba-Colombani, V., Causse, M., Langlois, D., Philouze, J., and Buret, M. (2001). Genetic analysis of organoleptic quality in fresh market tomato. 1. Mapping QTLs for physical and chemical traits. *Theor. Appl. Genet.* 102, 259–272. doi: 10.1007/s001220051643

Saltelli, A., Ratto, M., Andres, T., Campolongo, F., Cariboni, J., Galtelli, D., et al. (2008). *Global Sensitivity Analysis: The Primer*. Chichester: John Wiley and sons. doi: 10.1002/9780470725184

Semenov, M. A., Stratonovitch, P., Alghabari, F., and Gooding, M. J. (2014). Adapting wheat in Europe for climate change. *J. Cereal Sci.* 59, 245–256. doi: 10.1016/j.jcs.2014.01.006

Sevanto, S. (2014). Phloem transport and drought. *J. Exp. Bot.* 65, 1751–1759. doi: 10.1093/jxb/ert467

Shackel, K. A., Greve, C., Labavitch, J. M., and Ahmadi, H. (1991). Cell turgor changes associated with ripening in tomato pericarp tissue. *Plant Physiol.* 97, 814–816. doi: 10.1104/pp.97.2.814

Sidi, M.-M. O., Quilot-Turion, B., Kadrani, A., Génard, M., and Lescourret, F. (2014). The Relationship between metaheuristics stopping criteria and performances: cases of NSGA-II and MOPSO-CD for sustainable peach fruit design. *Int. J. Appl. Metaheuristic Comput. (IJAMC)* 5, 44–70. doi: 10.4018/ijamc.2014070104

Tardieu, F. (2003). Virtual plants: modelling as a tool for the genomics of tolerance to water deficit. *Trends Plant Sci.* 8, 9–14. doi: 10.1016/S1360-1385(02)00008-0

Tardieu, F. (2012). Any trait or trait-related allele can confer drought tolerance: just design the right drought scenario. *J. Exp. Bot.* 63, 25–31. doi: 10.1093/jxb/err269

Wallach, D., Makowski, D., Jones, J. W., and Brun, F. (2013). *Working with Dynamic Crop Models: Methods, Tools and Examples for Agriculture and Environment*. London: Academic Press; Elsevier Ltd. doi: 10.1016/B978-0-12-397008-4.00011-3

White, J. W., and Hoogenboom, G. (1996). Simulating effects of genes for physiological traits in a process-oriented crop model. *Agron. J.* 88, 416–422. doi: 10.2134/agronj1996.00021962008800030009x

Xu, L., Zhu, J., Henke, M., Kurth, W., Ding, W., and Buck-Sorlin, G. H. (2012). "Simulating superior genotypes for plant height based on QTLs: towards virtual breeding of rice," in *The 4th International Symposium on Plant Growth Modeling, Simulation, Visualization and Applications (PMA 12),* eds M. Kang, Y. Dumont, and Y. Guo Shanghai, 31.10.-03.11, 2012, IEEE, 447–454.

Conflict of Interest Statement: The authors declare that the research was conducted in the absence of any commercial or financial relationships that could be construed as a potential conflict of interest.

2 Model-assisted analysis of the pedicel-fruit system suggests a fruit sugar uptake regulation and a water saving strategy

Authors

Dario Constantinescu[1], Gilles Vercambre[1], Michel Génard[1]

[1]PSH, INRA - Centre PACA, Domaine Saint Paul - Site Agroparc, 228 route de l'aérodrome, CS 40509, 84 914 Avignon Cedex 9, France

Résumé

Un modèle basé sur la représentation biophysique des flux d'eau et de sucre entre le pédicelle, le xylème et le phloème du fruit, l'apoplasme et le symplasme du fruit a été développé pour identifier les modes de transport sur le système pédicelle-fruit du pêcher au cours du nycthémère. Le modèle a prédit qu'au cours de la nuit, l'eau était principalement importée dans le fruit par le xylème et que les transferts entre le phloème et le xylème du fruit entraînaient une concentration plus élevée dans le fruit que dans le pédicelle. Cela a entraîné un transport de sucre relativement élevé vers l'apoplasme des fruits, ce qui a entraîné une absorption relativement élevée de sucre par le symplasme des fruits malgré de faibles concentrations de sucre dans le pédicelle. Nous avons prédit, à midi, un reflux d'eau du xylème entraîné par un potentiel de pression plus faible dans le xylème que dans l'apoplasme des fruits. De plus, les transferts d'eau du xylème du fruit vers le phloème diminuent la concentration en sucre du phloème du fruit, ce qui entraîne une absorption modérée de sucre par le symplaste du fruit, malgré la forte concentration en sucre du pédicelle. Globalement, les transferts d'eau du xylème vers le phloème ont tamponné les concentrations en sucre du phloème et de l'apoplasme, entraînant une absorption de sucre journalière

régulée. De plus, une possible recirculation de l'eau du xylème du fruit vers l'apoplasme par le phloème du fruit a réduit les pertes en eau à midi.

Abstract

We developed a model based on the biophysical representation of water and sugar flows between pedicel, fruit xylem and phloem, fruit apoplast and symplast to identify diurnal patterns of such transports in the pedicel-fruit system of peach. The model predicted that during the night, water was mainly imported to the fruit through the xylem and fruit phloem-xylem water transfers allowed sugar concentrations in the phloem to be higher in the fruit than in the pedicel. This resulted in a relatively high sugar transport to the fruit apoplast, leading to a relatively high sugar uptake by the fruit symplast despite low sugar concentrations in the pedicel. We predicted, at midday, a xylem backflow of water driven by a lower pressure potential in the xylem than in the fruit apoplast. Moreover, fruit xylem-to-phloem water transfers decreased the fruit phloem sugar concentration, resulting in a moderate sugar uptake by the fruit symplast, despite the high sugar concentration in the pedicel. Globally, the predicted fruit xylem-phloem water transfers buffered the fruit phloem and apoplast sugar concentrations, leading to a diurnally regulated sugar uptake. Additionally, a possible fruit xylem-to-apoplast water recirculation through the fruit phloem reduced water loss at midday.

Introduction

Fruit water inflows are determined by water transports occurring in the pedicel vascular system, and vary with plant water status during the day (Tromp, 1984; Guichard *et al.*, 2005; Matthews and Shakel, 2005; Morandi and Grappadelli, 2009). Fruit loses water through transpiration, which can highly contribute to diurnal fruit contraction (Clearwater *et al.*, 2011; Brüggenwirth *et al.*, 2016). Effluxes from fruit could also consist of water backflows through the xylem, driven by higher pressure potential in the fruit than in the plant xylem (Zhang and Keller, 2017). Backflows were experimentally observed in many species at different fruit growth stages (Lang and Thorpe, 1989; Huguet *et al.*, 1997; Keller *et al.*, 2006; Carlomagno, 2018). Although many studies have been conducted on fruit water flows at both hourly and diurnal scales, measures of fruit water balance are always indirect and can lead to systematic

errors (Fishman *et al.*, 2001). Recently, non-invasive methods such as positron emission tomography (PET) and magnetic resonance imaging (MRI) have been used in many studies to determine fruit and pedicel water relations. These techniques have also been used to assess the xylem contribution to fruit water inflows in the late fruit growth stage and to better understand the decline in xylem functionality in grape and tomato (Windt *et al.*, 2009; Knipfler, *et al.*, 2015; Van de Wal *et al.*, 2017).

Fruit dry matter accumulation mainly results from sugar transport processes. According to Munch's theory, sugars are initially transferred to the fruit through the pedicel phloem by a mass flow driven by higher pressure potential in the plant than in the fruit (Thompson and Holbrook, 2003a). Sugars translocation from the fruit sieve elements into the fruit cells happens via either symplastic or apoplastic pathways. Symplastic transport consists of mass flow through plasmodesmata from the sieve element to the fruit cell cytoplasm. Apoplastic transport comprises the following: first, sugars are transported from the phloem sieve element to the apoplast surrounding the fruit cell through diffusion (Patrick and Offler, 1996) and active transports (Zhang *et al.*, 2004; Lalonde *et al.*, 2003; Lemoine *et al.*, 2013); then, sugars are transferred into the cell cytoplasm through active transport (Ruan and Patrick, 1995; Manning *et al.*, 2001). Sugars transport occurring in the fruit leads to changes in the water flows, since sugars accumulation alters the water potential differences between the plant and the fruit (Zhu *et al.*, 2018). Such large interplay between water and sugar flows was highlighted by Keller *et al.* (2015) who recently proposed a conceptual model of water and sugar movement in a ripening grape berry. According to this model, at late ripening, the water inflow from the fruit phloem to the fruit cell apoplast exceeds transpiration demands and sustains both fruit growth and solute accumulation. This fruit phloem water inflow increases the pressure potential of the apoplast surrounding the fruit cell, which becomes higher than the pedicel xylem pressure potential; so, part of the water incoming from the phloem evaporates by transpiration, part is moved from the apoplast surrounding the fruit cell to the fruit cell cytoplasm to sustain fruit growth, and another part is recirculated to the fruit xylem via the fruit cell surrounding apoplast, this latter having a higher pressure potential than the fruit xylem. The fruit growth model of Fishman and Génard (1998) is a mathematical tool developed to predict fruit growth by simulating the water and sugar flows occurring in the fruit xylem and phloem. In the

extended version proposed by Hall *et al.* (2013) and Hall *et al.* (2017), a pedicel compartment and distinct apoplastic/symplastic pathways were added to the growth model.

The aim of this work is to identify and describe diurnal water flows and sugar transports occurring in the pedicel-fruit system with a simple mathematical tool. We built a biophysical model of water and sugars flows across the pedicel-fruit system at an hourly scale. Our model focused on the pedicel, the fruit vascular system, and the cell apoplast. We mathematically described water and sugar flows using the same paradigm as the already existing fruit growth model, including the pedicel and the distinction between apoplast and symplast proposed by Hall *et al.* (2013) and Hall *et al.* (2017). Subsequently, we estimated the model parameters by model calibration, to predict the diurnal volume variation of a peach fruit in given crop load conditions. The simulations allowed underlining different water and sugar transport patterns in the pedicel-fruit system.

Material and methods

Experimental treatments

The model was calibrated for the late-maturing peach (*Prunus persica* (L.) Batsch) cv. 'Suncrest'/GF 677. The measurements were performed on peach trees grown in the INRA Avignon Centre orchard, which received routine horticultural care. In 1994, the observed fruit-bearing shoots were thinned to 30 leaf-to-fruit and in 1995 to 5 and 30 leaf-to-fruit ratios (heavy crop load and light crop load, respectively). The measurements were performed on fruits at the same growth stage in two different years: from 19 to 30 July 1994, and from 20 to 30 July 1995 - 120-130 DAA (days after anthesis). Fruit diameter diurnal variations were recorded by a linear variable differential transformer (LVDT) gauges set as described in Huguet *et al.* (1985). Table 2.1 reports the number of fruits and the total days when the fruits diameters were monitored. The measured diameters D (mm) were transformed into fresh weight W (g) using an empirical correlation for peach, cv. “Suncrest”: $W\ (g) = 0.003 \times D^{2.58}$ (Huguet *et al.*, 1997). The observations were made on intact (control) fruits and “pedicel-girdled” fruits (the bearing shoot was girdled just before the fruit pedicel to prevent the phloemic flow entering the pedicel). Detached fruits were picked at the beginning of the

measurements period and suspended in the tree canopy at their previous position in order to evaluate the water mass lost by transpiration. We considered that the dry weight was 10% of the average fruit fresh weight measured for a given fruit during the day; this value derived from data collected on Suncrest peaches in the same orchard. Climatic data collected at INRA weather stations located close to the experimental fields were used as model inputs.

Table 2.1. Number of fruits and total days in which the fruits diameters were monitored, for each treatment (fruit charge and year) and each condition (control – intact – or girdled-pedicel)

Treatment	Growing conditions	Number of fruits	Total days of monitoring
30 leaf-to-fruit 1994	Control (intact)	3	31
	Girdled	5	29
	Detached	7	29
30 leaf-to-fruit 1995	Control (intact)	1	9
	Girdled	2	6
	Detached	4	8
5 leaf-to-fruit 1995	Control (intact)	1	8
	Girdled	2	5
	Detached	4	8

Model description and flow equations

The pedicel-fruit system was conceptually described as shown in Fig. 2.1. We ideally considered the fruit as a big cell made of a symplast surrounded by an apoplast and a vascular system connected to the plant by the pedicel. The pedicel was divided into pedicel xylem and phloem (*px* and *pp*, respectively). Water is transported from the pedicel to the fruit vascular system, composed of fruit xylem and phloem (*fx* and *fp*, respectively); sugars are transported from the pedicel phloem to the fruit phloem by mass flow. We assumed that the phloem and xylem water potentials are the same and that local water exchanges could maintain this equilibrium (Thompson and Holbrook, 2003b; Hall and Minchin, 2013). We assumed that sugars are the only osmotically

active solutes. We supposed that solutes concentrations were negligible both in pedicel and fruit xylem so that the xylem pressure potential equals the xylem water potential. The region where the fruit xylem and phloem terminate was represented with a system formed by the fruit cell apoplast (*fa*) connected to the vascular system and surrounding the fruit cell symplast (*fs*) (as in Hall *et al.*, (2017) model). A membrane separates the fruit phloem from the fruit cell apoplast, while we assumed that there was no barrier for solutes between the fruit xylem and the fruit cell apoplast. Water is transported in the fruit cell symplast across a membrane and lost through transpiration by the fruit cell apoplast.

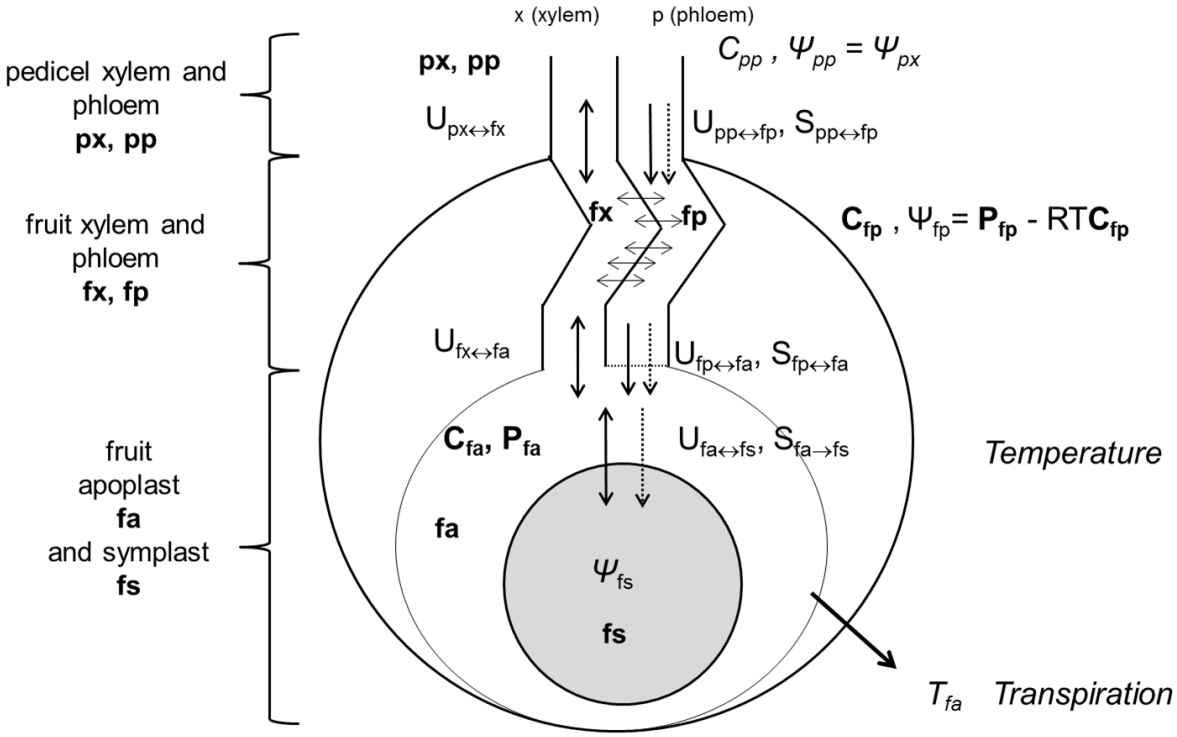

Fig. 2.1 **Pedicel-fruit conceptual model**. Each compartment is represented by a bold letter. We distinguish the pedicel xylem and phloem (px, pp) and the fruit xylem and phloem (fx, fp). Fruit xylem and fruit phloem compose the fruit vascular system. The fruit cell apoplast (fa) surrounds the fruit cell symplast (fs). The model external inputs are represented in italics; the unknown variables of the linear system (Eq 18-21) are represented in bold. Full-line arrows represent water flows. Pointed arrows represent sugar flows. The principal model hypotheses are mathematically expressed: xylem and phloem have the same water potential, and the xylem pressure potential equals the xylem water potential.

The sugars transport from fruit phloem to fruit cell symplast progressively shifts from the symplastic to the apoplastic pathway during fruit development (Damon *et al.*, 1988; Ruan and Patrick, 1995; Brown *et al.*, 1997; Moing *et al.,* 1997*,* Zhang *et al.*, 2006). We assumed that the symplastic transport through plasmodesmata could be neglected during the fruit last growth phase for which we collected experimental data (Zanon *et al.,* 2015). The apoplastic pathway comprises the following steps:

(i) sugars are transported from the fruit phloem to the fruit cell apoplast by diffusion and active uptake. Here, the transported sugar is mainly sucrose;

(ii) sucrose is rapidly converted into hexoses by the acid invertase in the fruit apoplast;

(iii) hexoses are transported into the fruit symplast by active uptake.

We computed the water potential Ψ_w (MPa) of each compartment as the sum of pressure potential Ψ_p (MPa) and osmotic potential Ψ_π (MPa):

$\Psi_w = \Psi_p + \Psi_\pi$ (1)

We computed the osmotic potential Ψ_π as the product of gas constant R (g MPa K^{-1} mol^{-1}), the temperature T (K), and sugar concentration C (mol g^{-1}):

$\Psi_\pi = -R \times T \times C$ (2)

We computed the water flows (g h^{-1}) following the equations used in the previous model of Hall *et al.* (2013). The phloem water flow between pedicel and fruit ($U_{pp\leftrightarrow fp}$), the xylem water flow between pedicel and fruit ($U_{px\leftrightarrow fx}$), and the water flow occurring between fruit xylem and apoplast ($U_{fx\leftrightarrow fa}$) are assumed as directly proportional to the pressure potential difference between compartments. So:

$U_{pp\leftrightarrow fp} = K_{pp\leftrightarrow fp} \times (\Psi_{p,pp} - \Psi_{p,fp})$ (3)

$U_{px\leftrightarrow fx} = K_{px\leftrightarrow fx} \times (\Psi_{p,px} - \Psi_{p,fx})$ (4)

$U_{fx\leftrightarrow fa} = k_{fx\leftrightarrow fa} \times A_f \times (\Psi_{p,fx} - \Psi_{p,fa})$ (5)

$K_{pp\leftrightarrow fp}$ and $K_{px\leftrightarrow fx}$ (g MPa^{-1} h^{-1}) are the conductances of the water flow path between pedicel phloem and fruit phloem, and between pedicel xylem and fruit xylem, respectively, and $k_{fx\leftrightarrow fa}$ (g MPa^{-1} h^{-1} cm^{-2}) is the conductivity of the water flow path between fruit xylem and fruit cell apoplast. We assumed that the conductances of the water paths in the fruit between the fruit xylem and phloem and the fruit cell apoplast

and between the fruit cell apoplast and the fruit cell symplast are proportional to the fruit surface area A_f (cm^2), following the assumption of Fishman and Génard (1998).

The water flows (g h^{-1}) occurring between the fruit phloem and the fruit cell apoplast ($U_{fp\leftrightarrow fa}$) and between the fruit cell apoplast and the fruit cell symplast ($U_{fa\leftrightarrow fs}$) are supposed directly proportional to the difference of water potential between the compartments since we assumed that water flows across membranes in this pathway. So:

$$U_{fp\leftrightarrow fa} = k_{fp\leftrightarrow fa} \times A_f \times (\Psi_{w,fp} - \Psi_{w,fa}) \quad (6)$$

$$U_{fa\leftrightarrow fs} = k_{fa\leftrightarrow fs} \times A_f \times (\Psi_{w,fa} - \Psi_{w,fs}) \quad (7)$$

$k_{fp\leftrightarrow fa}$ and $k_{fa\leftrightarrow fs}$ (g MPa^{-1} h^{-1} cm^{-2}) are the conductivities of the water flows path between fruit phloem and fruit cell apoplast, and between fruit cell apoplast and fruit cell symplast, respectively.

We assumed that the sugar flow $S_{pp\leftrightarrow fp}$ (g h^{-1}) between the pedicel phloem and the fruit is mass flow given as follows:

$$S_{pp\leftrightarrow fp} = M_S \times C_{pp} \times U_{pp\leftrightarrow fp} \quad (8)$$

M_S (g mol^{-1}) is the sucrose molar mass and C_{pp} (mol g^{-1}) is the sucrose concentration in the pedicel phloem. $U_{pp\leftrightarrow fp}$ is computed with equation 3.

We assumed that both diffusion and active uptake drive the sugar transport from the fruit phloem to the fruit cell apoplast and that the main transported sugar is sucrose. We supposed that the diffusion process is driven by the difference between fruit phloem and fruit cell apoplast sucrose concentrations and that the fruit cell apoplast sucrose concentration is negligible compared to that of the fruit phloem. Indeed, Ruan *et al.*, (1996) measured sucrose concentrations in the tomato cell apoplast solution, finding a value of approximately 0.5 mM hence much lower than the fruit phloem sucrose concentrations estimated in our model. The rate of sugar active uptake from the fruit phloem to the fruit cell apoplast was then assumed to be proportional to the fruit phloem sugar concentration, for the sake of simplicity. Moreover, we supposed that both the diffusion and the active transport rates were directly proportional to the surface area of the exchange membrane between fruit phloem and fruit cell apoplast, which was supposed directly proportional to the fruit surface area.

So, we computed the sugar flow $S_{fp\to fa}$ (g h^{-1}) from the fruit phloem to the fruit cell as follows:

$S_{fp\to fa} = M_S \times v_{fp\to fa} \times A_f \times C_{fp}$ (9)

$v_{fp\to fa}$ (g cm^{-2} h^{-1}) is the sugar transport coefficient considering both the diffusion and active uptake, and C_{fp} (mol g^{-1}) is the sucrose concentration in the fruit phloem.

We assumed the sugar flow from the fruit cell apoplast to the fruit cell symplast $S^{in}_{fa\to fs}$ (g h^{-1}) as directly proportional to the fruit cell apoplast sugar concentration C_{fa} (mol g^{-1}) and to the fruit dry weight, as in Fishman and Génard (1998). So:

$S^{in}_{fa\to fs} = M_H \times v^{in}_{fa\to fs} \times DW \times C_{fa}$ (10)

M_H (g mol^{-1}) is the hexoses molar mass, $v^{in}_{fa\to fs}$ (h^{-1}) is the coefficient of sugar transport from the fruit cell apoplast to the symplast, and DW (g) is the fruit dry weight.

Moreover, for the sake of simplicity, we assumed that fruit respiration is a fraction k_{Resp} of the imported sugar, so we could compute the net sugar import $S_{fa\to fs}$ (g h^{-1}) into the symplast as follows:

$S_{fa\to fs} = S^{in}_{fa\to fs} - S^{out}_{fs} = (1 - k_{Resp}) \times S^{in}_{fa\to fs}$ (11)

S^{out}_{fs} (g h^{-1}) is the sugar outflow by respiration.

The sugar net inflow $S_{fa\to fs}$ (g h^{-1}) into the symplast is then expressed as follows:

$S_{fa\to fs} = M_H \times v_{fa\to fs} \times DW \times C_{fa}$ (12)

$v_{fa\to fs}$ is the coefficient of net sugar inflow into the symplast and can be seen as

$v_{fa\to fs} = (1 - k_{Resp}) v^{in}_{fa\to fs}$ (13)

Model formulation

We assumed that, at a given time of day, the system was at steady-state, hence the pedicel xylem and phloem, the fruit xylem and phloem, and the fruit apoplast accumulated no sugar or water. This enabled writing four equations for mass conservation of water and sugars, referring to a given time:

(1) The conservation of water flows through xylem and phloem compartments between the pedicel and the fruit:

$U_{px\leftrightarrow fx} + U_{pp\leftrightarrow fp} = U_{fx\leftrightarrow fa} + U_{fp\leftrightarrow fa}$ (14)

(2) The conservation of water flows through fruit xylem and phloem, the fruit apoplast and the fruit symplast:

$$U_{fx\leftrightarrow fa} + U_{fp\leftrightarrow fa} = U_{fa\leftrightarrow fs} + T_{fa} \quad (15)$$

(3) The conservation of sugars in the phloem between the pedicel and the fruit:

$$S_{pp\leftrightarrow fp} = S_{fp\rightarrow fa} \quad (16)$$

(4) The conservation of sugars in the fruit phloem, the fruit cell apoplast and the fruit cell symplast:

$$S_{fp\rightarrow fa} = S_{fa\rightarrow fs} \quad (17)$$

T_{fa} is the fruit transpiration (g h^{-1}).

Handling the flows expressions presented in this section, we can write the following system:

$$K_{px\leftrightarrow fx}\times(\Psi_{w,pp} - (\boldsymbol{\Psi_{p,fp}} - R\times T\times \boldsymbol{C_{fp}})) + K_{pp\leftrightarrow fp}\times((\Psi_{w,pp} + R\times T\times C_{pp}) - \boldsymbol{\Psi_{p,fp}}) -$$

$$k_{fx\leftrightarrow a}\times A_f\times((\boldsymbol{\Psi_{p,fp}} - R\times T\times \boldsymbol{C_{fp}}) - \boldsymbol{\Psi_{p,fa}}) - k_{fp\leftrightarrow fa}\times A_f\times((\boldsymbol{\Psi^p_{fp}} - R\times T\times \boldsymbol{C_{fp}}) - (\boldsymbol{\Psi_{p,fa}} - R\times T\times \boldsymbol{C_{fa}})) = 0 \quad (18)$$

$$k_{fx\leftrightarrow fa}\times A_f\times((\boldsymbol{\Psi_{p,fp}} - R\times T\times \boldsymbol{C_{fp}}) - \boldsymbol{\Psi_{p,fa}}) + k_{fp\leftrightarrow fa}\times A_f\times((\boldsymbol{\Psi_{p,fp}} - R\times T\times \boldsymbol{C_{fp}}) - (\boldsymbol{\Psi_{p,fa}} - R\times T\times \boldsymbol{C_{fa}})) - k_{fa\leftrightarrow fs}\times A_f\times((\boldsymbol{\Psi_{p,fa}} - R\times T\times \boldsymbol{C_{fa}}) - \Psi_{w,fs}) - T_{fa} = 0 \quad (19)$$

$$M_S\times C_{pp}\times k_{pp\leftrightarrow fp}\times A_f\times((\Psi_{w,pp} + R\times T\times C_{pp}) - \boldsymbol{\Psi_{p,fp}}) - M_S\times v_{fp\rightarrow fa}\times A_f\times \boldsymbol{C_{fp}} = 0 \quad (20)$$

$$M_S\times v_{fp\rightarrow fa}\times A_f\times \boldsymbol{C_{fp}} - M_H\times v_{fa\rightarrow fs}\times DW\times \boldsymbol{C_{fa}} = 0 \quad (21)$$

Equations 18-21 compose a linear system with four unknown variables (represented in bold); we computed the algebraic expressions of the unknown variables in terms of the other variables, i.e. model parameters and inputs, with the symbolic solver Sympy (Meurer *et al.*, 2017). Solutions are shown in supplementary data S2.1. We could then compute water and sugar flows given the parameters and inputs values for each hour of the day. The model source code used here is available upon request, by email, to the corresponding author.

Model inputs

In this work, we consider as model inputs all the variables representing system external conditions, i.e. pedicel water potential, pedicel phloem sugar concentrations, fruit transpiration, fruit symplast water potential, and temperature. The pedicel water

potential and the pedicel phloem sugar concentrations were supposed to vary during the day (Hocking, 1980; Klages *et al.*, 2001). They were set to a constant value in the 18:00-06:00 period. We assumed that both these input variables followed a sinusoidal function (24 h periods) in the 06:00-18:00 period. The pedicel water potential was supposed to decrease until reaching its minimum value at 12:00, while we assumed that the pedicel phloem sugar concentration increased up to its maximum value at 12:00. Then, both variables return to their base value. Table 2.2 resumes the minimum and maximum values used for these inputs in the different treatments and years, and the time of day when the input variables had their extreme values. The values of pedicel phloem water potential were set according to measurements of peach stem water potential conducted by Remorini and Massai (2003). The maximum values of sap sugar concentration were in the lower range given for peach by Jensen *et al.* (2013). The minimum values ranged those given by Fishman and Génard (1998). We supposed that in the heavy crop load condition, sugar concentrations in the pedicel phloem were lower than in the light crop load condition, as hypothesized in Fishman and Génard (1998). Fruit transpiration per fruit surface area estimation was obtained by fitting a sinusoidal curve (24 h period) on the measured data of the detached fruits volume variation (see the Plant materials section for further details). Then, we multiplied it by the surface areas of the fruits considered for the model calibration. Fruit surface areas A_f (cm^2) were computed from fresh weights (g) with the empirical relationship $A_f = 6.049 \times W^{0.601}$ (Fishman and Génard, 1998). We assumed that the symplast water potential was equal to the fruit water potential. Measurements on mango and tomato (Lechaudel, 2004, Johnson *et al.*, 1992) suggested that the fruit water potential is stable throughout the day. However, other measurements showed a slight variability in diurnal fruit water potential (McFayden *et al.*, 1996; Morandi and Grappadelli, 2008). Thus, we assumed that the symplast water potential followed a sinusoidal behavior (24 h period) in the 06:00-18:00 period, reaching its minimum at 12:00. We calibrated the symplast water potential of the 18:00-06:00 period, and hypothesized that the symplast water potential at 12:00 was 1.2-fold the symplast water potential of the18:00-6:00 period, as estimated by Morandi and Grappadelli (2008). Moreover, we assumed that the fruit water potential changed according to treatment, year, and the conditions in which fruits were grown (control or girdled

conditions). The night period refers to the period when the driving variables are constant (18.00-06:00).

Table 2.2: **Input variables of the model.** The times of day (hour) corresponding to the maximum and the minimum values are indicated.

Variable	Treatments	Minimum value	Maximum value
Pedicel phloem sugar concentration (g g^{-1})	30 leaf-to-fruit 1994 and 1995	0.12 (from 18:00 to 06:00)	0.28 (12:00)
	5 leaf-to-fruit 1995	0.08 (from 18:00 to 06:00)	0.24 (12:00)
Pedicel phloem water potential (MPa)	All	-1.3 (12:00)	-0.5 (from 18:00 to 06:00)
Fruit transpiration per area (g cm^{-2} h^{-1})	All	2.74×10^{-4} (05:00)	2.63×10^{-3} (17:00)

Model calibration and analysis of the model variables response to changing inputs

We estimated the model parameters in order to reproduce the average fruit fresh weight variation during a single day. We assumed that the fruits biophysical parameters did not vary along the measurement period. The system of Eq. 18-21 was reduced for describing the girdled pedicel condition, imposing the absence of phloem flows ($U_{pp\leftrightarrow fp}$ = 0 and $U_{fp\leftrightarrow fa}$ = 0). A consequence of the system reduction was that sugar flows were equal to zero. This hypothesis agreed with the measurements made by Génard *et al.* (2003), which showed that in girdled fruits, sugar accumulation immediately ceased.

The simulated fruit fresh weight (W_h, g) at a given hour h was calculated as the water and sugars accumulation in the fruit between a reference time h_0 and h.

$$W_h = W_{ref} + \sum_{i=h_0}^{h} \left(U_{\mathrm{fx}\leftrightarrow\mathrm{fa},i} + U_{\mathrm{fp}\leftrightarrow\mathrm{fa},i} - T_{\mathrm{fa},i} + S_{\mathrm{fa}\rightarrow\mathrm{fs},i}\right) \quad (22)$$

$U_{fx\leftrightarrow fa,i}$, $U_{fp\leftrightarrow fa,i}$, $T_{fa,i}$, $S_{fa\rightarrow fs,i}$ are the water flows between fruit xylem and fruit cell apoplast, the water flow between fruit phloem and fruit cell apoplast, the fruit transpiration, and the net fruit symplast sugar inflow at hour *i*, respectively.

The objective function we minimized is the root mean squared error made in the hourly fruits fresh weight prediction (RMSE (g)).

$$RMSE = \sqrt{\frac{1}{N} \times \sum_{h=1}^{N} \left(W_h - W_{obs,h}\right)^2} \quad (23)$$

N is the number of observed points during the measurement period, and W_h and $W_{obs,h}$ are, respectively, the simulated and the observed values of fruit fresh weight at hour *h*.

We aimed at minimizing the RMSE index for both the control (C) and the girdled (G) condition simulations, for one and two treatments in 1994 and 1995, respectively. For solving this problem, we found the dominant solutions of a multi-objective optimization problem, minimizing both $RMSE_C$ and $RMSE_G$. $RMSE_C$ (resp $RMSE_G$) is the mean RMSEs for fresh weight prediction in control (resp girdled fruit) conditions for the different leaf-to-fruit ratios. We solved the calibration problem with the multi-objective genetic algorithm NSGA II (Deb *et al.*, 2002). Among the dominant solutions, we chose the one corresponding to the minimum mean value between $RMSE_C$ and $RMSE_G$. The parameters we estimated are compiled in Table 2.3.

In order to further verify the goodness of our model predictions, we confronted our predicted xylem and phloem inflows contributions to the total water inflow to those experimentally observed by Morandi *et al.*, (2007) for peach fruits at stage III of growth. Moreover, we confronted our predicted dry mass accumulation to the mean diurnal dry mass accumulation measured by Fishman and Génard (1998) on the same cultivar (cv 'Suncrest') in heavy and light crop load treatments.

In order to assess our results dependence on the model inputs, we analyzed the main model variables outputs response to different levels of pedicel water potential and sugar concentration given as input. We present this analysis results in supplementary material (S2.3).

Table 2.3: Calibrated model parameters and brief descriptions. C: control fruit, G: girdled fruit, 30_94: 30 leaf-to-fruit year 1994, 5_95: 5 leaf-to-fruit year 1995, 30_95: 30 leaf-to-fruit year 1995.

Parameter	Description	Value**	Units
$K_{px\leftrightarrow fx}$	Conductance of the water path between the pedicel xylem and the fruit xylem	9.1×10^{-1}	(g h^{-1} MPa^{-1})
$K_{pp\leftrightarrow fp}$	Conductance of the water path between the pedicel phloem and the fruit phloem	3.3	(g h^{-1} MPa^{-1})
$k_{fx\leftrightarrow fa}$ $K_{fx\leftrightarrow fa}$ *	Conductivity and conductance of the water path between the fruit xylem and the fruit apoplast	1.1×10^{-2} 7.4×10^{-1}	(g h^{-1} MPa^{-1} cm^{-2}) (g h^{-1} MPa^{-1})
$k_{fp\leftrightarrow fa}$ $K_{fp\leftrightarrow fa}$ *	Conductivity and conductance of the water path between the fruit phloem and the fruit apoplast	1.1×10^{-3} 7.6×10^{-2}	(g h^{-1} MPa^{-1} cm^{-2}) (g h^{-1} MPa^{-1})
$k_{fa\leftrightarrow fs}$ $K_{fa\leftrightarrow fs}$*	Conductivity and conductance of the water path between the fruit apoplast and the fruit symplast	9.1×10^{-3} 6.4×10^{-1}	(g h^{-1} MPa^{-1} cm^{-2}) (g h^{-1} MPa^{-1})
$v_{fp\leftrightarrow fa}$	Sugar transport rate between the fruit phloem and the fruit apoplast	5.0×10^{-4}	(g h^{-1} cm^{-2})
$v_{fa\rightarrow fs}$	Fruit symplast sugar uptake rate	3.6×10^{-2}	(h^{-1})
Ψ_{fs}	Fruit symplast water potential (from 18:00 to 06:00)	-1.7 (C30_94) -1.7 (C30_95) -1.3 (C5_95) -0.89 (G30_94) -1.1 (G30_95) -0.91 (G5_95)	(MPa)

*conductances are given at the estimated value for the fruits grown in the 5 leaf-to-fruit treatment and in control conditions in 1995, which we took as a reference for the results.

** We compiled in Table S2.2.1 of the Supplementary Data S2.2 the variability of the parameters estimations among the best solutions found with the genetic algorithm.

Results

Model calibration and diurnal contribution of xylem and phloem flow to the total water inflow

Table 2.3 reports the parameters values estimated through the model calibration. Table S2.2.1 shows their variability among the best solutions obtained in calibration. Figure 2.2 depicts the comparison between the predicted and the average observed diurnal fruit fresh weight variations and the 5th and 95th percentile of the diurnal fruit fresh weight variation. The percentiles were computed on the measurement repetitions resumed in Table 2.1. Globally, our simulations well reproduced the fruit mass diurnal variation observed in girdled conditions and the mass increase observed in control conditions in all treatments. Moreover, they well reproduced the differences between fruits fresh mass behavior among crop load treatments in control conditions. However, the simulated girdled fruits fresh mass in the 5 leaf-to-fruit ratio treatment had a smaller variation than the observed one. In both 1994 and 1995 30 leaf-to-fruit ratio treatments, the simulated diurnal phloem and xylem inflows contributions to the total water inflow were 20% and 80% for phloem and xylem inflow, respectively, while values in the 5 leaf-to-fruit ratio treatment in 1995 were 29% and 71% for phloem and xylem inflow, respectively. These agree with measurements made by Morandi *et al.* (2007) for stage III of peach fruit growth, i.e. 30% and 70% for the phloem and xylem inflows contributions to the total water inflow, respectively. The simulated cumulative diurnal dry mass accumulation of the control fruits was 0.29 g day^{-1} in the 30 leaf-to-fruit ratio treatments for both 1994 and 1995, and 0.12 g day^{-1} in the 5 leaf-to-fruit ratio treatment in 1995. These were similar to the mean diurnal dry mass accumulations measured by Fishman and Génard (1998) on the same cultivar, i.e. about 0.37 g day^{-1} for the light crop load treatment and 0.09 g day^{-1} for the heavy crop load treatment.

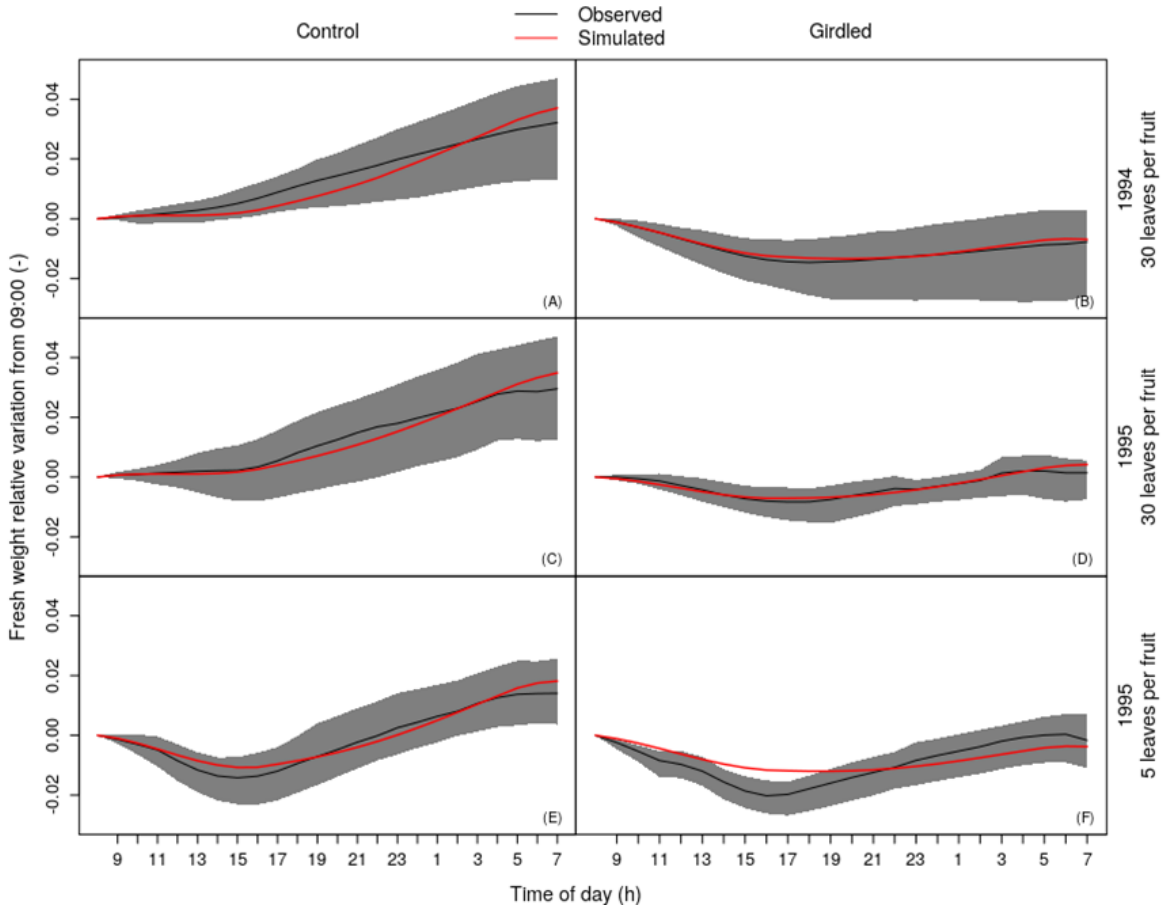

Fig. 2.2 Calibration results. Simulated (red lines) and observed (black lines) relative variation of fruit fresh weight in relation to 09:00 at each hour h of the day. We computed the relative variation as follows: Wrel =(Wh –Wref) / Wref, where Wh is the fruit fresh weight at a given hour h and Wref is the observed fruit fresh weight at 09:00. The black lines represent the mean values of observed fresh weight relative variation at each hour of the day. The grey region is delimited by the 5th and 95th percentile of the observed relative variations at each hour of the day. The percentiles were computed on the measurement repetitions resumed in Table 1. The panels are separated as follows: (A), (C) and (E) represent the fruits grown in the control (intact) condition; (B), (D) and (F) represent the fruits grown in the pedicel-girdled condition (the bearing shoot was girdled just before the fruit pedicel to prevent the phloemic flow from entering the pedicel). The panels are horizontally divided according to different years and fruit-bearing shoots thinning: (A) and (B): 1994, 30 leaf-to-fruit; (C) and (D): 1995, 30 leaf-to-fruit; (E) and (F): 1995, 5 leaf-to-fruit.

The simulated fruit symplast sugar uptake was buffered compared to the variations of the pedicel phloem sugar concentration

We analyzed the simulated water and sugar flows diurnal behavior in the 5 leaf-to-fruit treatment, which we considered the most interesting pattern of water and sugars transports. The input variables of this simulation are presented in the Material and methods section and their values during the day are compiled in Table 2.2. We confronted the diurnal maximum relative variation of the symplast water inflow/outflow and of the sugar uptake with the diurnal maximum relative variation of the input variables related to water and sugar transports, i.e. pedicel phloem water potential and sugar concentration. The diurnal symplast water inflow maximum and minimum values (Fig. 2.3A) were 0.16 g h^{-1}, and -0.13 g h^{-1}, with a diurnal maximum relative variation of 1.8 (computed as $\left|\frac{\max v - \min v}{\max v}\right|$). This value was higher than the maximum diurnal pedicel water potential input relative variation of 1.6 (computed with the same formula) (Fig. 2.3B). Therefore, water potential input variations generated high variations of symplast water inflows and outflows. In order to better highlight this variation, we computed that the simulated symplast water inflow averagely decreased by 0.06 g h^{-1} at every 0.2 MPa decrease of the pedicel water potential input. The minimum sugar uptake value was 0.0035 g h^{-1} and the maximum was 0.0082 g h^{-1} (Fig. 2.3C). The relative variation was 1.4 (computed as $\left|\frac{\max v - \min v}{\min v}\right|$), lower than the variation of the pedicel phloem sugar concentration input, whose value was 2.0 (computed with the same formula). We obtained the same relative variation of 1.4 for both the fruit phloem and the fruit cell apoplast sugar concentrations (Fig. 2.3D). These results suggested that the fruit phloem and the fruit cell apoplast sugar concentrations, and the fruit symplast sugar uptake were buffered in response to the large pedicel phloem sugar concentration variation.

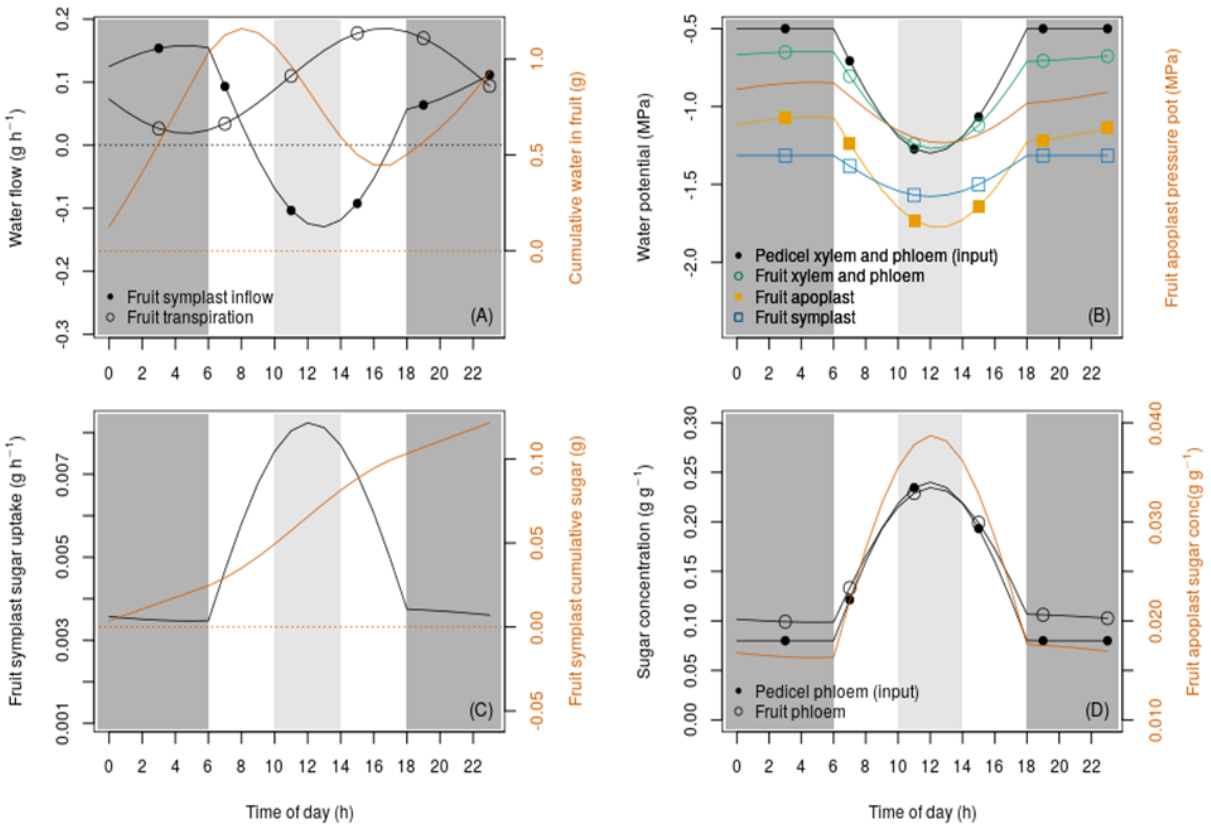

Fig. 2.3. Simulated diurnal behavior of the variables related to fruit sugar transports and water exchanges in the pedicel-fruit system for a fruit grown at a 5 leaf-to-fruit ratio in the control condition. The dark grey region covers the night period (18:00 – 06:00) and the light grey region covers the midday period (10:00 – 14:00). (A) Fruit symplast water inflow from the fruit apoplast (black line, closed circles), fruit transpiration (black line, open circles), and cumulative water in the fruit (orange line). (B) Input pedicel water potential (black line, closed circles), fruit xylem and phloem water potential (green line, open circles), fruit apoplast water potential (yellow line, closed squares), input fruit water potential (blue line, open squares) and fruit apoplast pressure potential (orange line). (C) Fruit symplast sugar uptake (black line) and cumulative sugar stored in the fruit symplast (orange line). (D) Input pedicel sugar concentration (black line, closed circles), fruit phloem sugar concentration (black line, open circles) and fruit apoplast sugar concentration (orange line). Dotted black lines and orange lines are the zero of the variables presented in black and orange, respectively.

In the middle part of the day, we simulated a xylem backflow of water, part of which was recirculated into the phloem permitting the regulation of the symplast sugar uptake

We identified two main patterns of water and sugar flows, occurring during the night (18:00-06:00) and in the midday period (10:00-14:00) (Fig. 2.4).

We predicted that during the night, the fruit symplast imported water from the fruit apoplast (Fig. 2.3A). The main fruit water inflows were xylem flows, which were higher than the phloem flows (Fig. 2.5A and B). However, the phloem inflows were not negligible in relation to the xylem inflows. This higher predicted water flow from pedicel to fruit phloem than from fruit phloem to fruit cell apoplast (Fig. 2.5B) indicated that water was transported from the fruit phloem to the fruit xylem in the fruit vascular system (Fig. 2.5C). In particular, about 20% of the water flow entering the fruit phloem was moved to the fruit xylem.

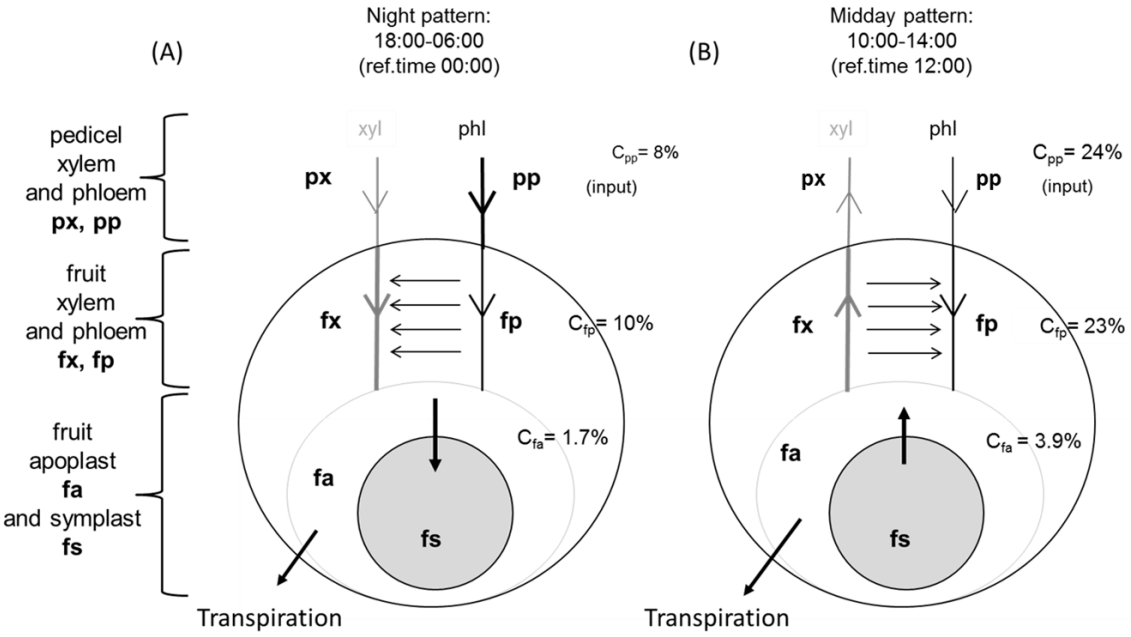

Fig. 2.4. Water flows and sugar concentrations in the night pattern 18:00 – 06:00 (A) and in the midday pattern 10:00 – 14:00 (B). The arrows show flow directions. Grey arrows represent xylem flows; black arrows represent phloem flows. Horizontal arrows represent water exchange between fruit xylem and fruit phloem. Line thicknesses qualitatively represent flow intensities. Reported sugar concentrations are the concentrations that we simulated at the reference times of 00:00 (A) and 12:00 (B).

Transpiration was the only fruit water outflow; which was low from 00:00 to 06:00 and high at 18:00, sharply decreasing from 18:00 to 00:00 (Fig. 2.3A). To sum up, we predicted that water was mainly imported via the pedicel xylem and lost by transpiration during the night; additionally, our simulations showed that part of the water entering the fruit via the phloem was transferred from the fruit phloem to the fruit xylem, leading to higher sugar concentrations in the fruit phloem than in the pedicel phloem during this part of the day (Fig. 2.3D).

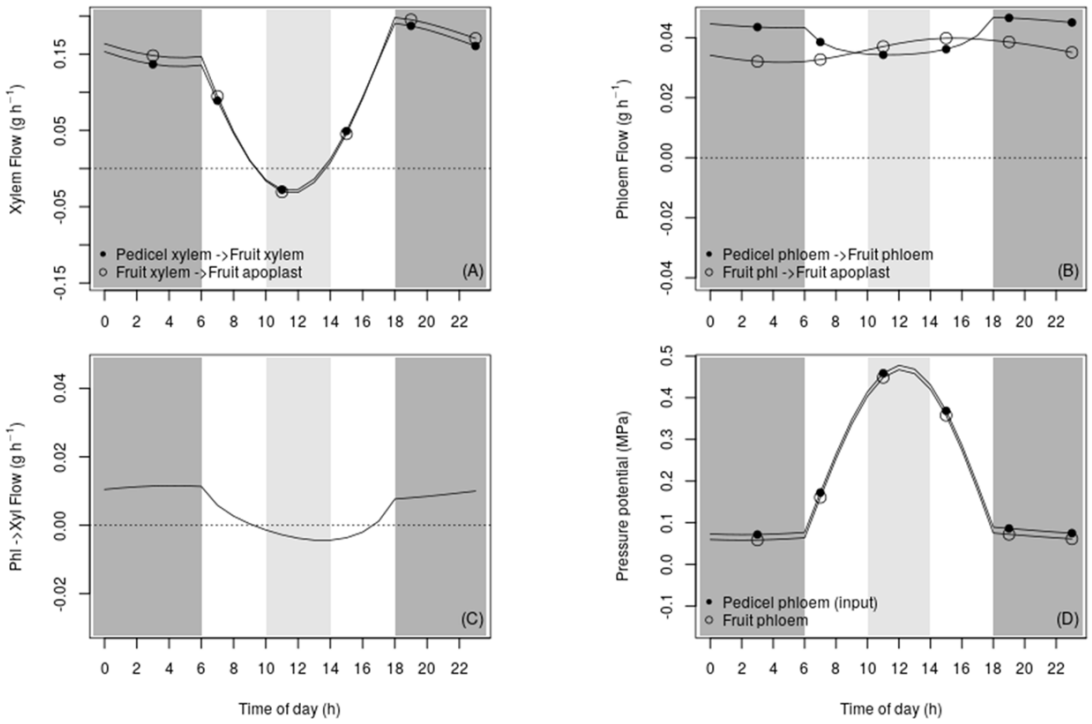

Fig. 2.5. Simulated diurnal behavior of the variables related to the water transports in the xylem and phloem pathways for a fruit grown at a 5 leaf-to-fruit ratio in the control condition. The dark grey region covers the night period (18:00 – 06:00) and the light grey region covers the midday period (10:00 – 14:00). (A) Water flow between the pedicel xylem and the fruit xylem (closed circles) and from the fruit xylem to the fruit apoplast (open circles). (B) Water flow between the pedicel phloem and the fruit phloem (closed circles) and from the fruit phloem to the fruit apoplast (open circles). (C) Water flow between the fruit xylem and the fruit phloem. (D) Input pressure potential in the pedicel phloem (closed circles) and simulated fruit phloem pressure potential (open circles).

Our simulations show that in the midday period water was transferred from the fruit symplast to the fruit apoplast and left the fruit apoplast by transpiration (Fig. 2.3A). Moreover, we obtained a xylem water backflow from the fruit apoplast to the fruit xylem and from the fruit xylem to the pedicel xylem. The backflow intensity was comparable to that of phloem flows (Fig. 2.5A and 2.5B). Simulated phloem flows were both positive even if the intensity of the water flow from the pedicel phloem to the fruit phloem decreased compared to the nighttime value (Fig. 2.5B). Contrary to the night pattern, we predicted a water transfer from fruit xylem to fruit phloem, with the water flow from the pedicel phloem to the fruit phloem being lower than that from the fruit phloem to the fruit apoplast (Fig. 2.5B and 2.5C). To sum up, we predicted a water backflow in the pedicel xylem and in the fruit xylem in the midday period. Moreover, we predicted that part of the water flowing back from the fruit apoplast to the fruit xylem recirculated in a loop, passing from the fruit xylem to the fruit phloem and from the fruit phloem, back to the fruit apoplast. Since water was transferred from the fruit xylem to the fruit phloem, the increase in fruit phloem sugar concentrations was buffered, reaching a slightly lower value than the pedicel phloem sugar concentrations at midday. The slight variation of the fruit cell apoplast sugar concentration led to a regulated sugar uptake in the fruit symplast, generating an almost linear sugar accumulation in the symplast (Fig. 2.3C).

By setting lower sugar concentrations in the pedicel phloem all day long (S2.3), we simulated that water was mainly transferred from fruit phloem to fruit xylem. Conversely, for higher sugar concentration in the pedicel phloem, water was mainly transferred from fruit xylem to fruit phloem (Fig. S2.3.1). Moreover, the sugar accumulation in the fruit symplast was maintained almost linear throughout the days for both the inputs modifications (Fig. S2.3.2).

The simulated water backflow was driven by higher pressure potential in the fruit apoplast than in the pedicel xylem. The simulated non-negligible mass flow of sugars was driven by slightly higher phloem pressure potential in the pedicel than in the fruit.

According to our simulation, the high and comparable xylem flows simulated in the pedicel xylem-fruit xylem pathway and in the fruit xylem-fruit apoplast pathway during the night (Fig. 2.5A) were explained by important pressure potential differences

between the pedicel and the fruit xylem and between the fruit xylem and the fruit apoplast (Fig. 2.3B). In the midday period, the higher fruit apoplast pressure potential than that of the fruit xylem and the higher fruit xylem pressure potential than that of the pedicel xylem explained the non-negligible water backflows simulated during this period (Fig. 2.5A). However, the backflow was lower than the flow of water entering the fruit during the night. Moreover, we estimated relatively high xylem conductances $K_{px\leftrightarrow fx}$ and $K_{fx\leftrightarrow fa}$ (Table 2.3). In the analysis provided in the supplementary material (S2.3), we simulated that the xylem water backflow sensitively increased for decreasing values of pedicel phloem water potential (Fig. S2.3.1). Despite the low-pressure potential difference between the pedicel phloem and the fruit phloem (Fig. 2.5D), the mass flow from the pedicel phloem to the fruit phloem was not negligible (Fig. 2.5B). This flow was associated with a high phloem conductance $K_{pp\leftrightarrow fp}$ (Table 2.3). The water flow from fruit phloem to fruit apoplast was constant during the whole day (Fig. 5B). This flow was guided by the high and constant water potential difference between the fruit phloem and the fruit apoplast (Fig. 2.3A) and relatively low conductance $K_{fp\leftrightarrow fa}$ (Table 2.3).

Discussion

Our simulations suggested that water transfers between the fruit xylem and the fruit phloem buffered the fruit sugar concentrations, regulated the fruit cell sugar uptake and could prevent fruit water loss

Our simulations adequately reproduced the observed average diurnal fresh weight variations of fruits grown in control and pedicel girdled conditions in two different years and subject to two contrasted treatments (heavy and light fruit load). The simulation of the fresh weight diurnal variation of the girdled fruits grown in heavy crop load was less performing. This likely happened because the pedicel water potential diurnal behavior for this treatment was different from the hypothesized, since we supposed that the water potential was the same for all the treatments in our model calibration. The xylem and phloem inflows contributions to the total water inflows in the control condition simulation agreed with the experimental observations by Morandi *et al.* (2007) on peaches at stage III of fruit growth. Moreover, we simulated diurnal dry matter

accumulation values similar to those measured by Fishman and Génard (1998) on the same cultivar for both heavy and light crop load treatments. The analysis of the model variables responses to input diurnal variations in the heavy crop load treatment highlighted that fruit phloem and fruit apoplast sugar concentrations were buffered in relation to the pedicel phloem sugar concentration given as input. Furthermore, we computed a slight variation of the predicted symplast sugar uptake, which suggested that such a buffer effect could be a sugar uptake regulation strategy. The analysis of the predicted diurnal variations of water and sugar transports and of their driving variables enabled the identification of two possible distinct water and sugar flow patterns that could explain this buffer effect and the consequent regulated sugar uptake. In the first pattern, during the night, we predicted a water transfer from fruit phloem to fruit xylem that decreased the fruit phloem pressure potential and maintained a high fruit phloem sugar concentration. These conditions determined a high mass flow passing from the pedicel phloem to the fruit phloem and a high sugar diffusion from the fruit phloem to the fruit apoplast. Consequently, although the pedicel phloem sugar concentration given as input was low, the predicted symplast sugar uptake was relatively high in this part of the day. Interestingly, we estimated a high value of pedicel phloem conductance $K_{pp\leftrightarrow fp}$, which compensated the almost null difference in pressure potential between the pedicel phloem and the fruit phloem. Indeed, we predicted a non-negligible mass flow and thus, a realistic sugar uptake. This result was not surprising since very low differences of turgor pressure (i.e. pressure potential) have been experimentally determined in many herbaceous plants and trees, even though the biological reasons for non-negligible phloem mass flow in conditions of low-pressure potential difference between phloem compartments (and hence, the reasons for high phloem conductance) have not been well understood yet (Turgeon, 2010; Taiz *et al.*, 2015). In the second pattern, occurring in the midday period, we predicted a water backflow from the fruit cell apoplast to the xylem, due to lower pressure potential in the xylem than in the fruit apoplast. In contrast to the night simulations, in the midday period, we predicted a water transfer from the fruit xylem to the fruit phloem. This transfer increased the fruit phloem pressure potential, thus limiting the mass flow, and decreased the fruit phloem sugar concentration, thus reducing the sugar diffusion from the fruit phloem to the fruit apoplast. Therefore, buffered sugar concentrations in the

midday period resulted in a symplast sugar uptake rate that was not much higher in relation to the night period. The predicted sugar uptake was then lower than expected, with a high sugar concentration in the pedicel phloem given as input. In the case of ripening grape berries, Keller *et al.* (2015), hypothesized that the water flowing from the phloem to the fruit apoplast, thus sustaining both fruit growth and solute accumulation, would be recirculated via xylem backflow since it exceeds the low transpiration demands. Moreover, they hypothesized that the backflow would be driven by higher pressure potentials in the fruit apoplast than in the pedicel xylem. In our case, the predicted incoming water from the phloem did not exceed transpiration. However, our simulations showed that water recirculation in the fruit and in the pedicel xylem could be a common phenomenon due to a higher pressure potential in the fruit apoplast than in the pedicel xylem, as also hypothesized by Keller *et al.* (2015). Furthermore, in our simulations, phloem water flows remained low in the midday period, with an absolute value comparable to the xylem water backflow. The relatively high conductance between fruit xylem and fruit apoplast ($K_{fx\leftrightarrow fa}$) suggests that for the peach, fruit xylem conductance could remain high at the late growth stage, contrarily to what happens in fruits where a decrease in xylem conductance occurs near ripening (Lang and Düring, 1991; Dichio *et al.*, 2002). Despite the high predicted water losses in the midday period, the predicted water flow from fruit phloem to fruit apoplast kept the same intensity as in the night period. Such flow intensity was driven by high water potential differences despite the low conductance between the fruit phloem and the fruit apoplast. In the midday period, we predicted a water recirculation from the fruit xylem to the fruit phloem. Together with the xylem backflow, this recirculation could lead to favorable conditions for water flow from the fruit phloem to the fruit apoplast. This could be a strategy to prevent water loss in the midday period.

Our analysis of the model variables to different levels of inputs (S2.3) agreed with what we obtained by the presented simulation. According to our simulations, with lower sugar concentrations in the pedicel phloem all day long, water was mainly transferred from the fruit phloem to the fruit xylem. This transfer would reduce the fruit phloem pressure potential and facilitate the mass flow all day long. With higher concentrations in the pedicel phloem, we simulated that water was mainly transferred from xylem to phloem. This transfer would facilitate the water flow from the fruit phloem to the fruit

apoplast and prevent water loss. Moreover, this analysis allowed confirming that, in our system representation, the xylem water backflow strongly depends on the pedicel water potential variations.

The model we developed is a simple biophysical representation of the pedicel-fruit system. So, some hypotheses should be further discussed. First, we considered that only sucrose is transported in the pedicel phloem. Indeed, most of the peach sap sugar is composed of sucrose and only 35% of sorbitol (Desnoues *et al.*, 2018). Nevertheless, our model probably underestimates the phloem pressure potential because the sorbitol molar mass is nearly half that of sucrose. Secondly, the simulated xylem water backflow from the fruit apoplast to the pedicel xylem across the fruit vascular system would generate a sugar mass flow following the same pathway; these sugars would likely be reloaded by the phloem (Lang and Thorpe, 1989). However, this sugar transport from fruit apoplast to fruit phloem would only have an effect around midday, with a negligible contribution to the cumulative fruit sugar uptake. Thirdly, we supposed that the fruit apoplast sucrose concentration was negligible. Surprisingly, measurements of sucrose concentrations in peach cell apoplast are missing in literature. However, the sugar transport from the fruit phloem to the fruit apoplast is a combination of both diffusion and active uptake. This latter driven only by the fruit phloem sucrose concentration and not by the sucrose concentration in the fruit apoplast. Moreover, the fruit cell apoplast sucrose concentration is most likely much lower than that of the fruit phloem since there is a high activity of the sucrose transformation into hexoses by the acid-invertase. Therefore, considering the apoplast sucrose concentration would probably not bring to different conclusions about the sugars translocation in the whole system. Finally, the parameters used to build our model drive complex physiological processes and are, therefore, difficult to measure experimentally. Lacking literature values for such parameters, we estimated them through model calibration. Techniques like the positron emission tomography (PET) and magnetic resonance imaging (MRI) are promising tools to measure such parameters and hence, improve models of water and sugar flows.

Conclusions and perspectives

In this work, we built a process-based model that allowed describing water transfers and sugar transports occurring in the pedicel-fruit system. We calibrated the model and our simulations well reproduced diurnal fresh weight variations for fruit naturally attached to the plant and for fruit with a girdled pedicel. We predicted that water transfers between the fruit xylem and the fruit phloem could generate a buffer effect on sugar concentrations in the fruit phloem and in the fruit apoplast during the day, which would result in a regulated fruit sugar uptake and in a water recirculation from the fruit phloem to the fruit apoplast in the middle part of the day. This suggested the presence of a sugar uptake regulation and the prevention of water loss driven by the general water exchange pattern between the pedicel-fruit system compartments.

In perspective, our model could be a useful tool to identify water translocation and sugar accumulations strategies in other fruits. Our model could guide the physiological interpretation of the results of non-invasive methods used for analyzing fruit water and sugar translocations, i.e. positron emission tomography (PET) and magnetic resonance imaging (MRI). Our model describes an apoplastic step for sugar transports. In seeds, the apoplast contains high solute concentrations and is a key element in determining nutrient transports from the maternal seed tissues to the filial storage sites (Patrick and Offler, 2001). Our model could also be adapted for further understanding the physiological mechanisms of water and sugar translocation in seeds.

Supplementary data

- S2.1 - Linear system analytical solution
- S2.2 - Parameters variability among best solutions
- S2.3 - Sensitivity to inputs

Acknowledgments

This work was conducted within the project MAGESTAN (PS2A no2016-0244) and was funded by the FranceAgriMer through the “Programme d’investissements d’avenir PIA”. We warmly thank members of the project “MAGESTAN”

3 A mechanistic virtual fruit model describing fruit growth and the main fruit pulp solutes metabolisms well predicts fruit growth and highlights possible osmotic potential regulation mechanisms during fruit development

Résumé

La composition de la pulpe du fruit varie au cours de la saison de la croissance et est principalement déterminée par les sucres solubles, les acides et les minéraux. L'accumulation de ces solutés génère des changements dans le potentiel osmotique du fruit qui affectent le transport de l'eau et de la matière sèche et, ensuite, la croissance du fruit. Les deux processus d'accumulation et de dilution déterminent les changements dans les concentrations de sucres au cours de la croissance du fruit et il a été montré que la dilution joue un rôle non négligeable dans ces changements. Nous avons étudié les interactions entre la croissance des fruits et les variations des concentrations de solutés de pulpe de fruits, en construisant un modèle de fonctionnement des fruits basé sur les processus et décrivant les principales interactions entre l'importation et le métabolisme des solutés et la croissance des fruits. Ce modèle relie les descriptions biophysiques et métaboliques des processus associés à l'élaboration de la masse sèche, masse fraîche, des sucres et d'accumulation d'acides dans la pulpe des fruits. Le modèle a globalement bien prédit les variations saisonnières des concentrations de solutés dans la pulpe de tomate de

trois cohortes de fruits cultivés pour deux traitements de densité. Nos analyses des résultats de simulation du modèle ont suggéré que le potentiel osmotique des fruits calculé comme la somme des contributions estimées de chaque soluté était adéquat pour décrire la croissance du fruit. De plus, nos analyses ont montré qu'au cours de la croissance du fruit, les variations des concentrations du potassium, des acides citrique et malique avaient des contributions non négligeables dans la variation du potentiel osmotique des fruits, particulièrement à la fin de la croissance du fruit. De plus, nous avons estimé une contribution équilibrée de l'accumulation et de la dilution des solutés à cette régulation, avec une contribution importante des acides et minéraux à la fin de la croissance du fruit. Ce modèle intégré de fruit virtuel pourrait être un outil pour analyser l'accumulation de solutés dans la pulpe du fruit et pour prédire comment les processus de croissance du fruit affectent la qualité du fruit à la récolte.

Abstract

The fruit pulp solutes composition varies along fruit growth season and is mainly determined by soluble sugars, acids, and minerals. The accumulation of these solutes generates changes in the fruit osmotic potential that affect water and dry matter transports and, then, influences fruit growth. Both accumulation and dilution processes determine changes in sugars concentrations along fruit growth and dilution has been shown playing a non-negligible role in such changes. We have investigated the interactions between fruit growth and the variations of fruit pulp solutes concentrations, building a process-based model of fruit functioning that describes the main interactions between solutes import, metabolism and fruit growth. This model connects biophysical and metabolic descriptions of the processes of dry mass, fresh mass, sugars, and acids accumulation in the fruit pulp. The model globally well predicted the seasonal variations of tomato fruit pulp solutes concentrations of three cohorts of fruits grown in two shoot density treatments. Our analyses of the model simulation outputs suggested that the fruit osmotic potential computed as the sum of the estimated contributions of each solute was adequate to describe fruit growth. Moreover, our analyses revealed that during fruit growth the variations of potassium, citric acid, and malic acid

concentrations had non-negligible contributions in the fruit osmotic potential regulation, especially at the end of fruit growth. Moreover, we estimated a balanced contribution to this regulation of solutes accumulation and dilution, with an important contribution of acids and minerals at the end of fruit growth. The integrated virtual fruit model could be a tool for analyzing solutes accumulation in the fruit pulp and to predict how the processes of fruit growth affect fruit quality at harvest.

Introduction

The fruit pulp solution composition is mainly determined by soluble sugars, acids, and minerals. The imported sugars that are not used in metabolic and storage processes remain dissolved in the fruit pulp under the form of hexoses and sucrose(Dai *et al.*, 2016). The sugars concentration in the fruit pulp is higher than that of the other solutes along all the fruit growth season. Citric and malic acids are the main acids in the pulp of many fruit species, and their concentration depends on metabolic and transport processes occurring inside the fruit cells (Etienne *et al.*, 2013). Amino acids could have non-negligible concentrations in some fruit species including tomato (Sorrequieta *et al.*, 2010). Among mineral solutes in the fruit pulp, potassium has the higher concentration (Mitchell *et al.*, 1991; Wu *et al.*, 2002; Etienne, Génard, Bancel, *et al.*, 2014).The concentrations of solutes in the fleshy fruit pulp vary along the fruit growth season (Almeida and Huber, 1999; Génard *et al.*, 2003; Albertini *et al.*, 2006; Etienne, Génard, Bancel, *et al.*, 2014), and the solutes accumulation is associated to fruit growth (Bolarin *et al.*, 2001). Indeed, the composition of fruit pulp determines the fruit osmotic potential and, then, affects processes of water and dry matter transport (Johnson, Dixon and Lee, 1992). Dai *et al.* (2016) showed that changes in sugar concentrations in the fruit pulp along fruit growth could be driven by sugar accumulation (import + metabolism) and dilution due to the expanding fruit volume and the water import. Moreover, they showed that dilution has a non-negligible role in determining changes in sugars concentrations. Variations in solutes concentrations due to the combined effects of their accumulation and dilution can then affect the whole fruit

growth. At our knowledge, the interactions between fruit growth and the fruit pulp solutes concentrations variations have not been investigated yet.

In this work, we will present a model of fruit development (i.e. a virtual fruit model) which we will use to describe the main interactions between solutes import and metabolism, and fruit growth already presented.

A biophysical model of fruit growth was proposed by Fishman and Génard (1998). This model was used to highlight many physiological processes concerning the fruit growth of different fruit species such as peach (Quilot *et al.*, 2005), mango (Lechaudel *et al.*, 2007), kiwi (Hall, *et al.*, 2013) and tomato (Liu *et al.*, 2007). Sugars accumulation in the fruit was described with a mathematical model in Génard and Souty (1996). This model describes the repartition of the carbon entering the fruit by the phloem pathway into soluble sugars, starch, and other carbon compounds that result from the biosynthesis of the incoming carbon, including those that are necessary to build the cell walls. In their work, the model was used to simulate the seasonal variation of the sugar composition in peach. A process-based model of the citric acid accumulation in the fruit was proposed by Etienne *et al.* (2015) to describe the observed behavior of the citric acid concentration in dessert banana along the fruit age in both pre and post-harvest. This model provides a simplified description of the TCA cycle following the approach proposed by Lobit *et al.* (2003). Lobit *et al.* (2006) modeled the malic acid accumulation in the vacuole. They linked the mathematical representation of the transport of malic acid across the tonoplast, and the acid-base equilibrium in the vacuole solution determining the vacuolar pH. In this model, the mineral composition of the fruit vacuole is considered as an input, since it is one of the main drivers of the acid-base equilibrium. Etienne *et al.* (2014) showed that the model well predicts the seasonal variations of the dessert banana malic acid concentration in the post-harvest stage.

In this work, we will connect the biophysical model of fruit growth to the mathematical models of the sugar, the citric acid, and the malic acid accumulations, building a unique integrated model of fruit growth and composition. First, we will present the integrated model performances in predicting data of fresh and dry weight, and concentrations of the pulp solutes measured in three cohorts of tomato fruits (*S. lycopersicum*) grown

with two different shoot densities. Secondly, we will use the model to analyze how fruit osmotic potential variations affect the fruit water balance. Then, we will study the contribution of each solute concentration variation on the variation of the fruit osmotic potential during fruit growth. Finally, we will split this contribution into two components: accumulation and dilution. From this information, we will be able to evaluate the respective role of accumulation and dilution of a given solute in determining fruit osmotic potential variations.

Material and methods

Plant material

Data on fruit growth, soluble sugars, acids, and potassium accumulation has been collected in 2018 for two genotyes “Bellastar” and “Sassary”. Tomatoes were grown in a heated greenhouse from march to end of October. In all the experiments, cultural practices (lateral shoots removal, pollination by bumblebee), chemical pest and disease control followed local commercial practices. Tomato plants were grown under two different shoot density (shoots per square meters) treatments: a standard density of 2.5 shoots per square meter and a high density of 3.6 shoots per square meter. Flowering of the tomato trusses was observed at 3 periods (early after the plant transplantation, during the peak production and at the end of the crop cultivation). For each of these periods, flowers were marked to allow the fruits to be identified later and are considered as a cohort. So, for a cohort, all fruits have the same flowering date (12 April, 19 June and 5 September for respectively the 1st, 2nd and 3rd cohort). Each week, at least 20 fruits of each genotype and modality were harvested. Fruits diameters, height, and fresh weight were measured. Half of the fruits were dried in a ventilated oven (75°C for at least 72h) to estimate the dry matter content. The other fruit were plunged in liquid nitrogen and stored at -80°C for biochemical analysis.

Fruit pericarps were frozen immediately in liquid nitrogen, stored at -80°C and freeze-dried. Freeze-dried samples were weighed, powdered and analyzed for glucose, fructose, sucrose, citric acid, malic acid, starch, and mineral content. Soluble carbohydrates and organic acids were determined after extraction with a water–methanol–chloroform mixture as described by Gomez *et al.* (2002). Soluble

carbohydrates were measured using a high-performance liquid chromatography (HPLC) system under the following specific conditions: one guard column (sugar pack, Waters, Milford, MA, USA); one column (sugar pack I, Waters) at 85°C; eluent, 50 mg L−1 EDTA-CaNa2 aqueous solution; flow rate 0.6 mL min−1; detection: refractometer (model 410, Waters). Organic acids were measured using an HPLC system under the following specific conditions: one guard column (Shodex RSpak KC-G, New York, NY, USA); one column (Shodex RSpak KC-811) at 80°C; eluent, 1 mL L−1 aqueous solution of phosphoric acid; flow rate 0.8 mL min−1; detection: UV spectrophotometer (model SPD-10A VP, Shimadzu, Kyoto, Japan) at 210 nm (Wu, Wang and Ching, 2002). Starch was measured using an enzymatic micro-plate assay as described by Gomez *et al.* (2007).

Minerals were measured using a portable X-ray fluorescence spectrometer (P-XRF) as described in Reidinger *et al.* (2012).

Integrated model description

In the next sections, we will first describe how we connected growth, sugar and acid sub-models in an integrated model by highlighting the connections between sub-models. Secondly, we will describe the version of the fruit growth sub-model used in this work. After, we will describe the sub-models of sugar repartition, citric acid accumulation, and malic acid transport and pH, highlighting their connections to the integrated fruit growth model. Finally, we will describe how we computed the fruit osmotic potential, which is the main linking variable between the sub-models

The integrated model

In this work, we will present an integrated virtual fruit model (Fig. 3.1), which is built linking a biophysical fruit growth sub-model and metabolic sub-models. To describe fruit growth model we used the model of Fishman and Génard (1998) in a version which includes the descriptions of the pedicel compartment and the fruit cell wall elasticity (Hall *et al.*, 2013; Lechaudel *et al.*, 2007), as we will more specifically describe in the next section. The fruit growth sub-model predicts the hourly dynamic of fruit dry and fresh weight along the growth season.

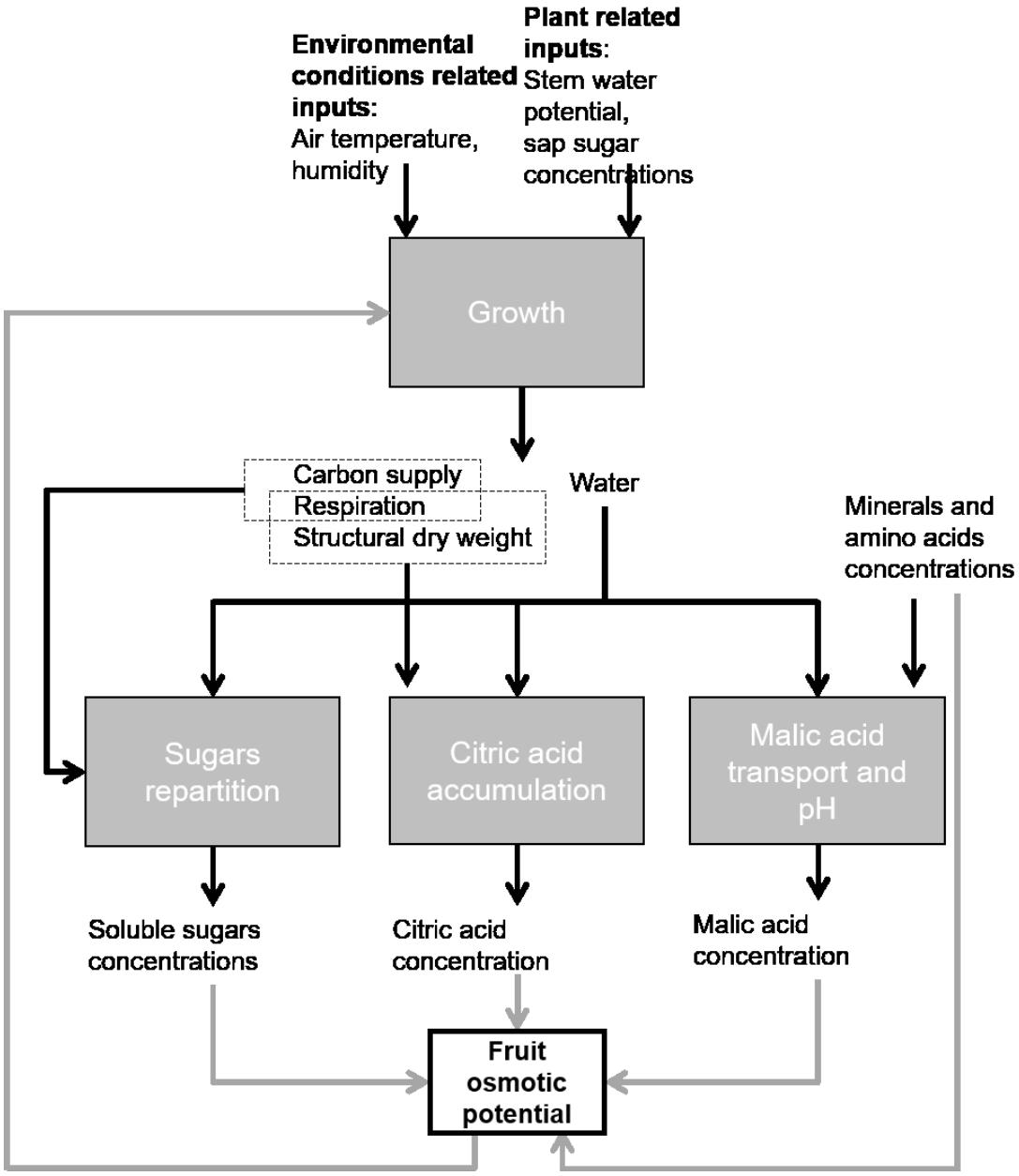

Fig. 3.1. Diagram of the virtual fruit model. The grey-filled rectangles indicate the sub-models that are linked in the integrated model, the black arrows indicate the inputs if they enter the rectangles, the outputs if they exit the rectangles. The grey arrows indicate which variables are used to compute the fruit osmotic potential and that the fruit osmotic potential is used by the growth sub-model.

Three metabolic sub-models will be added to the biophysical fruit growth sub-model: the sub-model of sugars repartition, which starting from the inputs of carbon supply, fruit respiration, and temperature, predicts the repartition of the supplied carbon in

soluble sugars, starch, and other compounds which include those forming the cell walls, and those used for biosynthesis; the sub-model of citric acid accumulation, which predicts the citric acid concentration in the fruit pulp by computing the citric acid outflow from the mitochondrial TCA cycle, with the fruit structural dry weight and the fruit respiration given as inputs; the sub-model of malic acid transport and pH, which predicts the vacuolar pH and the transport of malic acid into the fruit pulp imposing the acid-base equilibrium of the fruit pulp solution and predicting the malic acid transport from the cells cytosol to the cells vacuole, which depends on this equilibrium. The input variables of this model are the temperature and the concentrations of mineral cations and amino acids in the fruit pulp.

The integrated model consists in linking the presented sub-models in a unique system. In this system, we include the contributions of the predicted soluble sugars, citric and malic acids concentrations in the fruit pulp to the fruit osmotic potential, in which we include also the contributions of amino acids and potassium. These are given as input to the integrated model, together with phloem sugar concentration in the plant stem, stem water potential, temperature, and air humidity. Moreover, we use the predictions of fruit respiration and structural dry weight as inputs of the sugar repartition and citric acid accumulation sub-models. These predictions are provided by the model of fruit growth. In the next sections, we will describe each sub-model with further detail.

The sub-model of fruit growth

In the fruit growth sub-model (Fig. 3.2) we ideally consider the fruit as a big cell, connected to the plant vessels by a pedicel. The vascular bundle of the plant and the pedicel are described with a xylem and a phloem compartment that can exchange water. Both xylem and phloem have the same water potential. All along the model description, we will consider that we can compute the water potential Ψ_W (MPa) as the sum of Ψ_P and Ψ_π, which are the pressure and the osmotic potential respectively. So:

$$\Psi_W = \Psi_P + \Psi_\pi \quad (1)$$

Moreover, we compute Ψ_π as the product between the gas constant R (g MPa mol^{-1} K^{-1}), the absolute temperature T_k (K), and the sum of the molar concentrations (c_i, mol g^{-1}) of each osmotically active solute i, computed as the ratio between the

concentration of the i-th solute (C_i, g g^{-1}) and its molar mass (M_i, g mol^{-1}) (Taiz *et al.*, 2015):

$$\Psi_\pi = -R \times T_k \times \sum_i c_i$$

$$\text{with } c_i = \frac{C_i}{M_i} \quad (2)$$

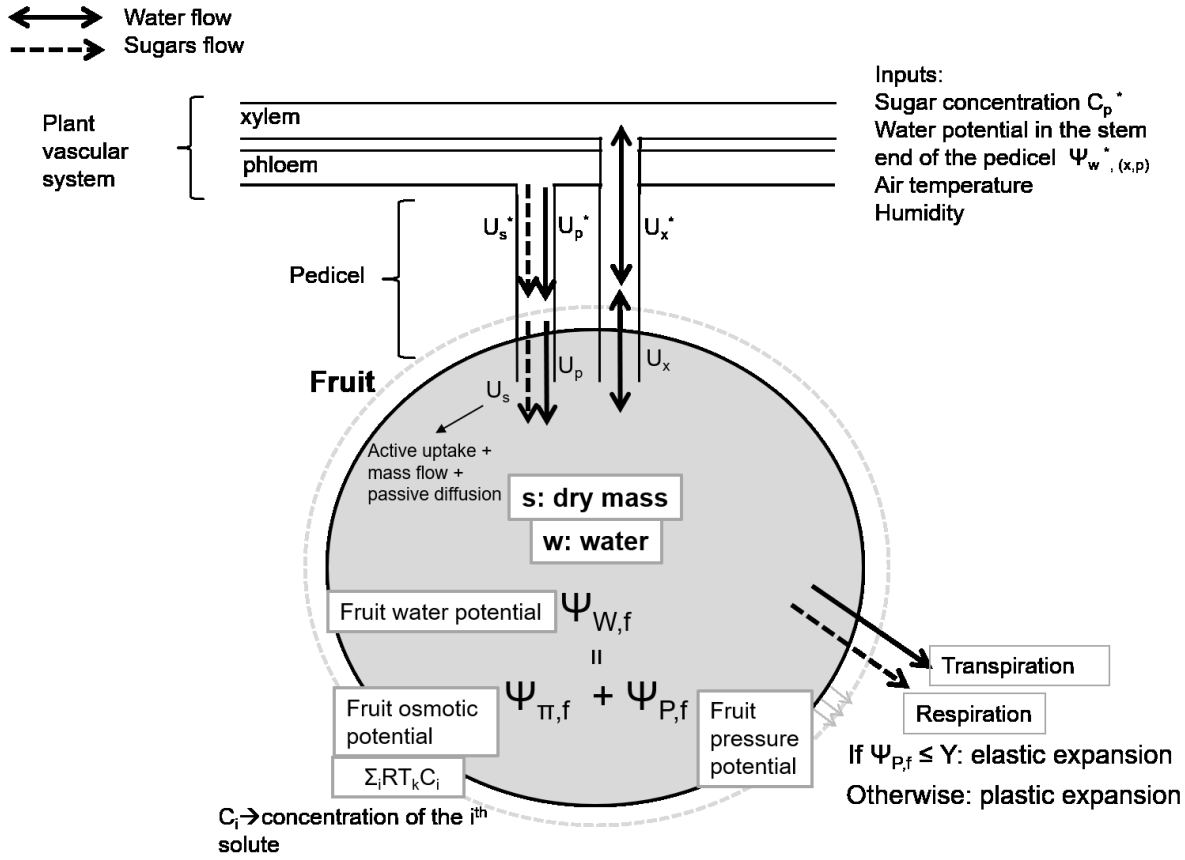

Fig. 3.2 Diagram of the sub-model of fruit growth. The fruit is considered as a big cell connected to the plant through the pedicel. Full arrows represent water flows, dashed arrows represent sugars flows. Variables in bold are the state variables of the model. We briefly indicate how we represent the fruit expansion and the method to compute the fruit osmotic potential in the integrated model.

The model represents the fruit growth rate as the balance of water and dry mass inside the fruit cell. The rate of change of water mass (w, g) is given by the sum of the xylem and phloem water inflows (U_x and U_p, g h^{-1}) minus the water outflow by transpiration (T_f, g h^{-1}), as follows:

$$\frac{dw}{dt} = U_x + U_p + r_w \times R_f - T_f \quad (3)$$

r_w (-) is the proportion of dry mass converted to water during respiration.

The rate of change of dry matter is given by the difference between the sugar inflow U_s (g h^{-1}), and the sugars lost by respiration R_f (g h^{-1}). So, we have:

$$\frac{ds}{dt} = U_s - R_f \quad (4)$$

Following the approach of Hall *et al.* (2013), we consider the presence of the pedicel as an intermediate compartment between the plant stem and the fruit. Therefore, U_x, U_p, and U_s occur between the fruit end of the pedicel and the fruit, and we compute the water and sugar flows U_x^* and U_p^* (g h^{-1}) and the flow of sugar U_s^* (g h^{-1}) occurring between the stem and the fruit end of the pedicel.

The water flows U_x, U_p, U_x^* and U_p^* are computed with the following equations:

$$U_{(x,\,p)} = A_f \times a_{(x,\,p)} \times L_{(x,\,p)} \times [(\Psi_{P^*,(x,\,p)} - \Psi_{P,f}) + \sigma_{(x,\,p)} \times (\Psi_{\pi^*,(x,\,p)} - \Psi_{\pi,f})] \quad (5)$$

$$U_{(x,\,p)^*} = L_{(x,\,p)^*} \times [(\Psi_{P,(x,\,p)} - \Psi_{P^*,(x,\,p)}) + \sigma_{(x,\,p)^*} \times (\Psi_{\pi,(x,\,p)} - \Psi_{\pi^*,(x,\,p)})] \quad (6)$$

x and p (lower-case) refer to xylem and phloem, respectively; f refers to the fruit, variables without the * superscript refer to the fruit end of the pedicel, while variables with the * superscript refer to the stem end of the pedicel, A_f is the fruit surface area (cm^2), $a_{(x,p)}$ (-) is the ratio between the fruit surface area and the membranes surface areas between the fruit end of the pedicel and the fruit along the xylem and the phloem pathways, respectively, $L_{(x,p)}$ (g cm^{-2} MPa^{-1} h^{-1}) are the conductivities of the water paths between the fruit end of the pedicel and the fruit, $L^*_{(x,\,p)}$ (g MPa^{-1} h^{-1}) are the conductances of the water paths between the stem and the fruit ends of the pedicel, Ψ_P and Ψ_π are the pressure and the osmotic potential, respectively. The water potential $\Psi^*_{W,\,(x,\,p)}$ and the sugar concentrations C_p^* at the stem end of the pedicel are given as model inputs. We consider that the solutes contribution to the xylem water potential is negligible (then, $\Psi_{\pi,\,x} = 0$ and $\Psi_{\pi,\,x}{}^* = 0$ which means that in the xylem pathways the water potential equals the pressure potential according to the equation 1) (Liu *et al.*,

2007; Fishman and Génard, 1998). We use the equation 1 combined to the equation 2 to compute the phloem pressure potential $\Psi_{P,p}^{*}$ at the stem end of the pedicel from the model inputs, as follows:

$$\Psi_{P,p}^{*} = \Psi_{W,p}^{*} + R \times T_k \times \frac{C_p^{*}}{M_S} - \Psi_{\pi,p,oth}^{*} \quad (7)$$

where M_S (g mol^{-1}) is the sucrose molar mass, and $\Psi_{\pi,p,oth}^{*}$ (MPa) is the osmotic contribution of solutes other than sugars in determining the pedicel stem end total osmotic potential.

The fruit surface area A_f is computed from the fruit total weight with an empirical relationship: $A_f = Y(s + w)^{\eta}$. The parameter σ and σ^* (varying from 0 to 1) are the solute reflection coefficient. As in Liu *et al.* (2007), we assume that for the phloem flow U_p occurring between the fruit end of the pedicel and the fruit, σ_p varies from 0 to 1 along the tomato fruit growth because the sugar upload progressively shifts from symplastic to apoplastic. We assume that the phloem flow U_p^{*} depends on the difference of pressure potential according to the pressure flow hypothesis of Munch (Hall *et al.*, 2013). Therefore, $\sigma_p^{*} = 0$. For all the xylem flows, $\sigma_x = 1$, as first approximation. We represent the sugar flow U_s occurring between the fruit end of the pedicel and the apoplast as the combination of three mechanisms: active transport, massive flow and passive diffusion. We assume a Michaelis-Menten kinetic for the active uptake, and we include the description of its decline along fruit growth (Fishman and Génard, 1998). The mass flow depends on the reflection coefficient σ_p , which progressively varies from 0 to 1 to represent the shift from symplastic to apoplastic sugar upload as already mentioned.

$$U_s = \frac{s \times C_p \times v_m}{(k_m + C_p) \times \left(1 + \exp\left(\frac{t - t^*}{\tau_a}\right)\right)} + \left(1 - \sigma_p\right) \times C_p \times U_p + A_f \times a_p \times p_s \quad (8)$$

The three terms are the active uptake, the mass flow, and the passive flow components of the total sugar uptake, respectively; C_p (g g^{-1}) is the concentration of sugar at the fruit end of the pedicel, v_m (h^{-1}) is the maximum uptake rate, k_m (-) is the Michaelis' constant, t is the fruit age (h), t^* (h) and τ_a (h^{-1}) are parameters used for computing the intensity of the fruit sugar uptake decline, p_s (g cm^{-2} h^{-1}) is the solute permeability coefficient.

We assume that the sugar flow U_s^* across the pedicel phloem occurs via a mass flow which is proportional to the average between the sugar concentrations (g g^{-1}) C_p^* and C_p at the stem end and the fruit end of the pedicel respectively (Hall *et al.*, 2013):

$$U_s^* = U_p^* \times \frac{C_p^* + C_p}{2} \quad (9)$$

The sucrose concentration in the stem end of the pedicel (C_p^*) and the water potential in the stem end of the pedicel ($\Psi_{W,(p,x)}^*$) are model inputs, the xylem water potential being equal to the xylem pressure potential. The stem phloem pressure potential is computed with the equation 1 setting a value of the osmotic pressure of the tomato stem phloem ($\Psi_{\pi,p,oth}^*$, MPa). We assume the conservation of water and sugar flows between the stem end and the fruit end of the pedicel (i.e. $U_x^* + U_p^* = U_x + U_p$ and $U_s^* = U_s$). Imposing this conservation, we can numerically compute the sugar concentration in the fruit end of the pedicel (C_p^*) (Hall *et al.*, 2013). To compute fruit pressure potential, $\Psi_{P,f}$, we model the fruit expansion as done in Lechaudel *et al.* (2007), who integrated in the fruit model the cell wall expansion model of Ortega (Geitmann and Ortega, 2009). The fruit expansion is seen as a combination of an irreversible expansion and an elastic (i.e reversible) expansion. We then indicate the fruit volume V_f expansion rate (cm^3 h^{-1}) as:

$$\frac{\mathrm{d}V_f}{\mathrm{dt}} = \begin{cases} \frac{1}{e} \times V_f \times \frac{d\Psi_{P,f}}{dt} + V_f \times \Phi \times \left(\Psi_{P,f} - Y\right) \; if \; \Psi_{P,f} > Y \\ \frac{1}{e} \times V_f \times \frac{d\Psi_{P,f}}{dt} \; otherwise \end{cases} \quad (10)$$

where e is the elastic modulus (Mpa), Φ (cm3 MPa^{-1} h^{-1}) is the cell wall extensibility, and Y (MPa) is the threshold pressure under which the fruit expansion is only elastic. In our version of the growth model, we assume that the cell wall extensibility declines along fruit age with a negative exponential law, for taking in account the decreasing activity in tomato epidermis and pericarp of xyloglucan-specific enzymes (Liu *et al.*, 2007). The volume expansion can be also expressed in terms of the water and dry matter balance and of D_w and D_s, i.e. the densities of water and of dry matter:

$$\frac{dV_f}{dt} = \frac{1}{D_w} \times \frac{dw}{dt} + \frac{1}{D_S} \times \frac{ds}{dt} \quad (11)$$

where the water rate of change can be computed with the equation 3, and the second term is considered negligible with respect to the first. From the equations 10

and 11, we can compute the $\Psi_{P,f}$ variation, which we add to the model as a supplementary state variable.

We compute the fruit respiration R_f (g h^{-1}) as sum of the growth and the maintenance respiration (R_g and R_m):

$$R_f = R_g + R_m = q_g \times \frac{ds}{dt} + q_{m,293} \times Q_{10}^{\frac{T-20}{10}} \times s \quad (12)$$

where q_g is the growth respiration coefficient (-), $q_{m,293}$ ($g_{sucrose}$ g_{DM}^{-1} h^{-1}) is the value of the maintenance coefficient at the temperature of 20°C, Q_{10} the factor of change of the maintenance coefficient at each 10°C of temperature rise, T is the temperature (°C).

The sub-model of sugars repartition

We predict soluble sugar composition variations during fruit growth using the model of sugars repartition of Génard and Souty (1996). This model (Fig. 3.3) describes the fruit sugars repartition in the following compartments: soluble sugars, starch, and other compounds that result from the biosynthesis of the raw material provided by the soluble sugars. The model consists in a set of ordinary differential equations describing the instantaneous rate of change of the amount of carbon m_C (g) stored in each compartment, i.e. $m_{C,sol}$, $m_{C,sta}$ and $m_{C,oth}$ for the soluble sugars, starch, and other compounds, respectively. The set represents the balance of carbon mass. The main hypotheses are the following:

1- Carbon supply (S_C, g h^{-1}) to the fruit is mainly in form of sucrose and the carbon losses by respiration (R_C, g h^{-1}), are derived from the soluble sugars.
2- Hexoses are the main soluble sugars, in similar proportion between glucose and fructose
3- Starch is a reserve pool that continuously changes carbon with the soluble sugars compounds during fruit growth. The rates of carbon conversion (h^{-1}) from soluble sugars to starch and from starch to soluble sugars are $k_{sol \rightarrow sta}$ and $k_{sta \rightarrow sol}$ respectively
4- Soluble sugars provide raw material for other compounds biosynthesis, with a rate of carbon conversion $k_{sol \rightarrow oth}$ (h^{-1})

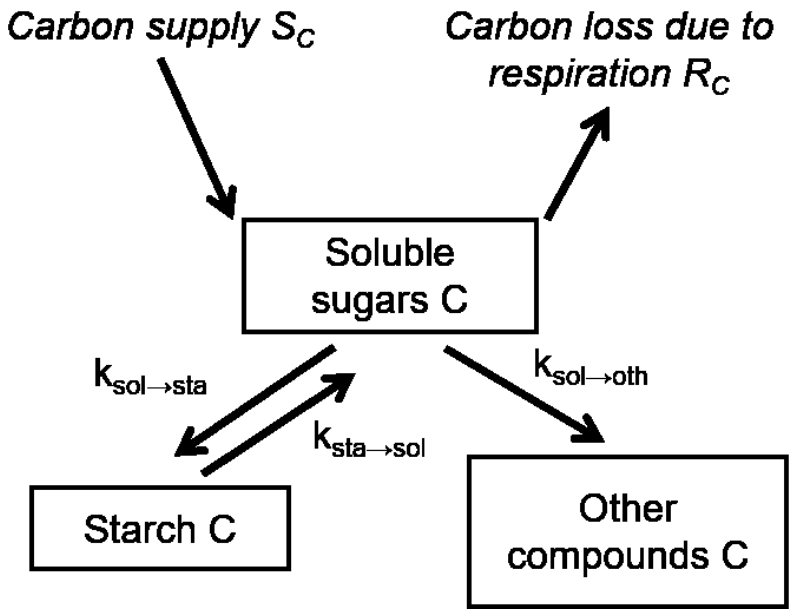

Fig. 3.3 Diagram of the sub-model of sugars repartition. The rectangles indicate the compartments that exchange carbon. The arrows represent the flows of carbon considered in the model. Variables written in italics indicate the model inputs. The carbon loss due to respiration is given as input for the model resolution, even though it is physically an output of the soluble sugars compartment (see the sub-section *The sub-model of sugars repartition* in the Material and methods section for details). For each flow, the variable representing its rate of transfer used in the equations is indicated.

We then define the system as follows:

$$\frac{\mathrm{d}m_{C,sol}}{\mathrm{d}t} = S_C + k_{sta \rightarrow sol} \times m_{C,sta} - (k_{sol \rightarrow sta} + k_{sol \rightarrow oth}) \times m_{C,sol} - R_C \quad (13)$$

$$\frac{\mathrm{d}m_{C,sta}}{\mathrm{d}t} = k_{sol \rightarrow sta} \times m_{C,sol} - k_{sta \rightarrow sol} \times m_{C,sta} \quad (14)$$

$$\frac{\mathrm{d}m_{C,oth}}{\mathrm{d}t} = k_{sol \rightarrow oth} \times m_{C,sol} \quad (15)$$

In our work, we made further hypotheses on the parameters representing the rates of carbon conversion. The rate of conversion from soluble sugars to starch declines during fruit growth. We obtained this result as follows: we fixed a value of $k_{sta \rightarrow sol}$ and we solved the equation 14 with respect to $k_{sol \rightarrow sta}$. We then estimated the hourly values of $\mathrm{d}m_{C,sta}/\mathrm{d}t$ interpolating the temporal series of starch concentrations with a smooth spline (R *smoot.spline* function of the *stat* package) and evaluating its derivative. We

then obtained the temporal behavior of the $k_{sol \rightarrow sta}$ parameter, which was explained by the following relationship:

$$k_{sol \rightarrow sta} = k_{sol \rightarrow sta,0} \times \exp(-k_s \times t) \quad (16)$$

where t denotes time (h), $k_{sol \rightarrow sta,0}$ is the value of the rate if conversion (h^{-1}) at t = 0 and k_s (h^{-1}) determines the rate of the coefficient decrease.

The rate of conversion from soluble sugars to the other components is directly proportional to the relative growth rate (Génard *et al.*, 2003) according to the following equation:

$$k_{sol \rightarrow oth} = k_{sol \rightarrow oth,0} \times \left(\frac{1}{s}\frac{ds}{dt}\right)^{\tau} \quad (17)$$

where $k_{sol \rightarrow oth,0}$ (-) is the rate of conversion at τ=0, and τ (-) is a parameter giving the exponential relationship.

The sugar sub-model output variable $m_{c,sol}$, i.e. the amount of carbon in the soluble sugars compartment is used to compute the soluble sugars concentration C_{sol} (g g^{-1}) in the fruit pulp fresh weight at each time step according to the following equation:

$$C_{sol} = \frac{m_{C,sol}}{s+w} \times \left(\frac{1}{\sigma_{C,hex}}\right) \quad (18)$$

where $\sigma_{C,sol}$ (-) is the fraction of carbon in 1 g of hexoses (i.e. the soluble sugars) ($\sigma_{C,sol}$ = 0.4, Génard and Souty, 1996). In the integrated model, this variable is then used for computing the fruit osmotic potential $\Psi_{\pi,f}$. Moreover, the S_C and R_C terms in the equation 13 are computed from the growth sub-modules variables as follows:

$S_C = U_s \times \sigma_{C,suc}$ (19)

$R_C = R_f \times \sigma_{C,hex}$ (20)

where $\sigma_{C,suc}$ is the fraction of carbon in 1 g of sucrose ($\sigma_{C,suc}$ = 0.421, Génard and Souty, 1996).

The sub-model of citric acid accumulation

We predict citric acid accumulation in the fruit pulp with the model of Etienne *et al.* (2015). This model (Fig. 3.4) describes the TCA cycle, which results in the oxidation of the pyruvate into CO_2 and a reduction of co-enzymes through conversions between organic acids. In this model, we consider only pyruvate, malate and citrate as metabolites. We consider that the fruit is as a big cell (see the fruit growth sub-module)

composed by two compartments: the mitochondrion and the cytosol. We consider that citrate transport from cytosol to vacuole is not thermodynamically limited (Etienne *et al.*, 2014) and that the vacuolar concentration of citric acid is equal to that in the fruit pulp.

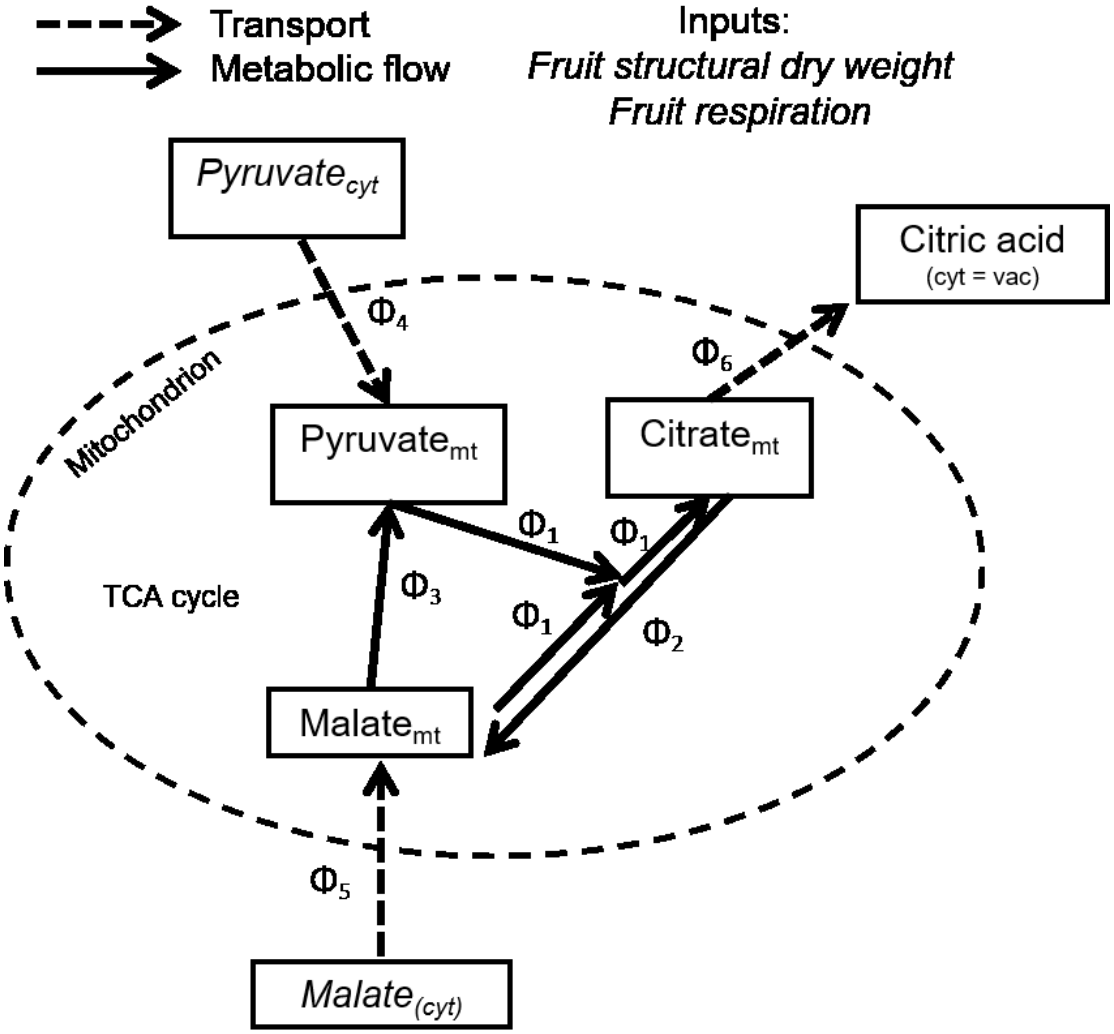

Fig. 3.4. Diagram of the sub-model of citric acid metabolism. The sub-model is a simple representation of the TCA cycle in the fruit cell mitochondrion. The rectangles represent the compartmental variables that we consider in the model for the mitochondrion (*mit*), the cytosol (*cyt*), and the vacuole (*vac*). The full arrows represent the metabolic flows, the dashed arrows represent the transports. Variables written in italics indicate the model inputs. For each flow, the variable used to represent it in the model equations is indicated.

The model is built as a system of synthesis and degradation of metabolites, under the hypothesis that the metabolic fluxes that synthetize a metabolite are equal to those that degrade it, i.e. there is not matter accumulation in the mitochondrial compartment. Indicating the citrate transport occurring from the mitochondrial to the cytosolic compartment with φ_6 (mol h-1), according to the hypotheses already presented, we can express the rate of change of the citric acid amount *Qcit* (mol) with respect to time *t* (h) in the fruit pulp of the TCA cycle as follows:

$$\frac{\mathrm{d}Qcit}{\mathrm{d}t} = \Phi_6 \quad (21)$$

φ_6 is computed solving the following linear system, representing the equilibrium between metabolic fluxes in the mitochondrial TCA cycle:

$$\frac{\mathrm{d}Qpyr_{mt}}{\mathrm{d}t} = \Phi_4 + \Phi_3 - \Phi_1 = 0 \quad (22)$$

$$\frac{\mathrm{d}Qmal_{mt}}{\mathrm{d}t} = \Phi_5 + \Phi_2 - \Phi_3 - \Phi_1 = 0 \quad (23)$$

$$\frac{\mathrm{d}Qcit_{mt}}{\mathrm{d}t} = \Phi_1 - \Phi_2 - \Phi_6 = 0 \quad (24)$$

with

$$R_{CO2} = \Phi_1 + 2\Phi_2 + \Phi_3 \quad (25)$$

where Q_{pyr}, Q_{mal}, and Q_{cit} indicate pyruvate, malate, and citrate quantities (mol) respectively, mt indicates that the metabolite belongs to the mitochondrial compartment, Φ_1, Φ_2, and Φ_3 (mol h^{-1}) are the metabolic fluxes of the TCA cycle (see Fig. 3.4); Φ_4 and Φ_5 (mol h^{-1}) indicate the transport fluxes between the cytosol and the mitochondrion for pyruvate and malate, respectively.

The equation 25 represents the computation of the mass losses by respiration in the TCA cycle.

Metabolic fluxes are described with enzymatic kinetic laws by the following equations:

$$\Phi_1 = k_1 \times cPyr_{mt} \times cMal_{mt} \quad (26)$$

$$\Phi_2 = k_2 \times cCit_{mt} \quad (27)$$

$$\Phi_3 = k_3 \times cMal_{mt} \quad (28)$$

where $cPyr_{mt}$, $cMal_{mt}$ and $cCit_{mt}$ are the molar concentrations (mol L^{-1}) of the mitochondrial pyruvate, malate and citrate, respectively, k_1 (L^2 h-1 mol-1), k_2 and k_3 (L h^{-1}) are the rate constants.

We assume that transports between the mitochondrial and the cytosolic compartments of pyruvate, citrate, and malate are dependent by the species concentrations gradient between the mitochondrial and the cytosolic compartments, for the sake of simplicity. Indicating with *cyt* the cytosolic compartment, we compute transports with the following equations:

$\Phi_4 = K_4 \times (cPyr_{cyt} - cPyr_{mt})$ (29)

$\Phi_5 = K_5 \times (cMal_{cyt} - cMal_{mt})$ (30)

$\Phi_6 = K_6 \times (cCit_{mt} - cCit_{cyt})$ (31)

where K_j (L h^{-1}) are membrane permeability.

Reactions rate constants depend on the enzymes activity and transports depend by transporters activity. Moreover, the number of mitochondria increases during fruit growth, increasing the sum of mitochondria contributions to the fruit pulp citric acid accumulation (Etienne *et al.* 2015). In the citric acid module, this effect is represented by defining the following equations for the reaction rates k_i and the transport rates K_j:

$$k_i = k0_i * \left(\frac{SDW}{SDW_{ref}}\right)^{m_i} \quad i = 1,2,3 \text{ (32)}$$

$$K_j = K0_j * \left(\frac{SDW}{SDW_{ref}}\right)^{m_j} \quad j = 4,5,6 \text{ (33)}$$

where *SDW* (g) is the fruit structural dry weight, SDW_{ref} is a reference value equal to 1 g, $k0_i$ and $K0_j$ are the values of the reaction rates when *SDW* = 1g, $m_{i,j}$ (-) are parameters that determine whether the reaction or transport rate exponentially increases or decreases during fruit development, i.e. which is the dominating effect between mitochondria augmentation and enzymes or transporters activity decline.

Substituting equations from 27 to 30 in the system 22-25 and considering $cPyr_{cyt}$ and $cMal_{cyt}$, $k0_i$, $K0_j$, m_i and m_j as model parameters and *SDW* and R_{CO2} as known model inputs we obtain a linear system composed by four equations and four unknown variables which was numerically solved in Etienne *et al.* (2015) providing an analytic

equation for Φ_6, from which we can compute the vacuolar citric acid amount integrating the equation 21.

In the integrated model, *SDW* and R_{CO2} inputs are computed by the growth sub-model. R_{CO2} (mol h-1) value is converted from the respiration flux R_f (g h^{-1}) following the stoichiometry of fruit cell respiration and using the molar mass of hexoses M_H (g mol^{-1}) as follows:

$$R_{CO2} = 6 \times \frac{R_f}{M_H} \quad (34)$$

The concentration of citric acid in the fruit pulp fresh weight C_{cit} (g g^{-1}) can be derived from the estimated amount of citric acid Q_{cit} (mol) with the following relationship:

$$C_{cit} = M_{cit} \times \frac{Q_{cit}}{w+s} \quad (35)$$

where M_{cit} (g mol^{-1}) is the molar mass of citric acid.

The value of the citric acid concentration C_{cit} computed by the citric acid sub-model is used in the computation of the fruit osmotic potential $\Psi_{\pi,f}$.

The sub-model of malic acid transport and pH

We predict malic acid concentrations in the fruit pulp with the model of Lobit *et al.* (2006) in the version proposed by Etienne *et al.* (2014) adapted to the case of tomato (Fig. 3.5). We assume that the malate concentration in the fruit pulp is determined by its concentration in the fruit cell vacuole. The idea of the malic acid transport model is to estimate the vacuolar concentration of malic acid that assures the thermodynamic equilibrium of the di-anion malate transport from the cell cytosol to the cell vacuole across the tonoplast.

The transport of the di-anion malate occurs passively by facilitated diffusion through specific ion channels and transporters, following the electrochemical potential gradient ΔG_{Mal}^{2-} (J mol^{-1}) of the di-anion across the tonoplast defined by the Nernst equation:

$$\Delta G_{Mal}^{2-} = -2 \times F \times \Delta\Psi + R \times T_k \times \ln\left(\frac{(Mal_{vac}^{2-})}{(Mal_{cyt}^{2-})}\right) \quad (36)$$

where (Mal^{2-}_{vac}) and (Mal^{2-}_{cyt}) are the activities of the di-anion malate in the cytosol and in the vacuole respectively (mol L^{-1}), $\Delta\Psi$ is the electric potential gradient across the tonoplast (V), T_k is the temperature (K), R is the gas constant (J mol^{-1} K^{-1}), and F is the Faraday's constant (C mol^{-1}).

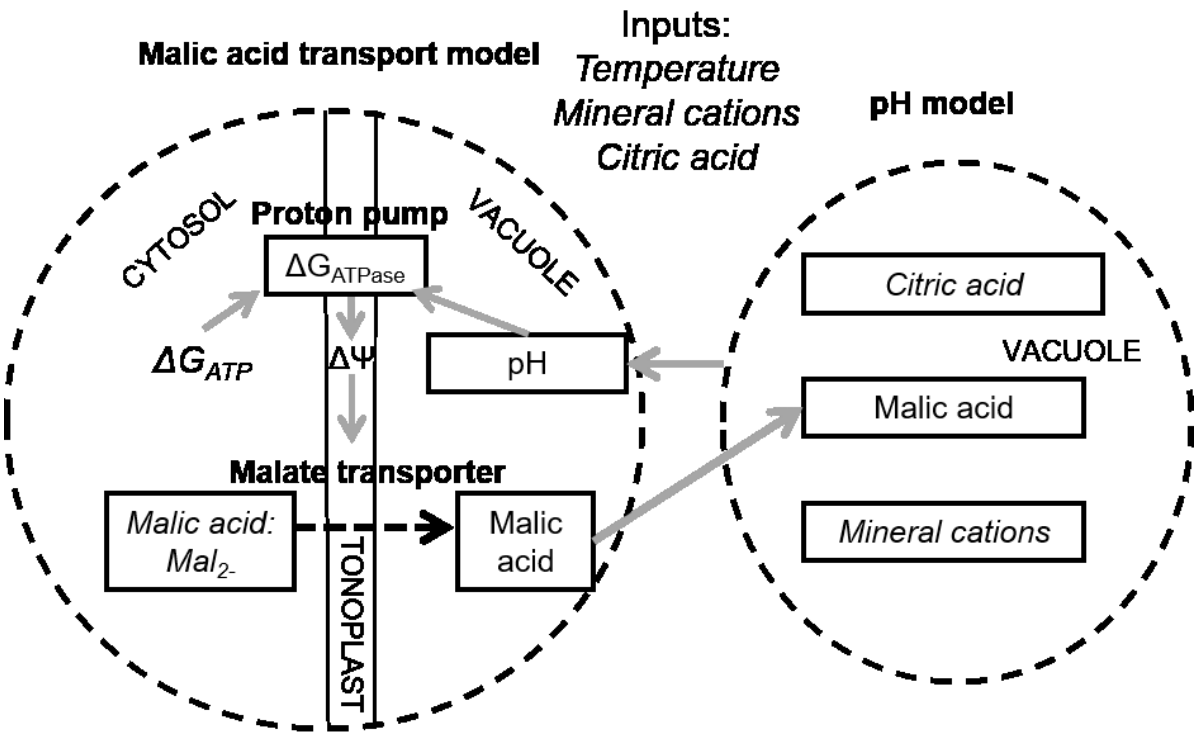

Fig. 3.5. Diagram of the sub-model of malic acid transport and pH. The two connected models of malic acid transport and pH are represented. The dashed arrow indicates the malic acid flow, the grey arrows represent the flow of information. Variables written in italics are the sub-model inputs and parameters. These variables are shown also in the sub-modules diagrams for sake of simplicity.

We consider that (Mal^{2-}_{cyt}) is constant and that the activity of the di-anion malate in the vacuole (Mal^{2-}_{vac}) is proportional to its vacuolar molar concentration $cMal^{2-}_{vac}$ (mol L^{-1}) by mean of the activity coefficient $a_{Mal2-,vac}$ obtaining the following equation:

$$(Mal^{2-}_{vac}) = a_{Mal2-,vac} \times cMal^{2-}_{vac} \quad (37)$$

The vacuolar activity coefficient of the dianion malate is related to the concentration of all the ionic species; we represent its vacuolar concentration $cMal^{2-}_{vac}$ (mol L^{-1}) with the following partial dissociation equation:

$$cMal^{2-}_{vac} = cMal_{vac} \times \left(\frac{K'_1 \times K'_2}{h^2 + h \times K'_1 + K'_1 \times K'_2}\right) \quad (38)$$

where K'_1 and K'_2 are the apparent acidity constants of the vacuolar malate (mol l^{-1}), $cMal_{vac}$ (mol L^{-1}) is the malic acid concentration in the vacuole, h is the vacuolar

concentration of the hydrogen ions computed from the vacuolar pH pH_{vac} as $h = 10^{-pHvac}$.

In plant cells ΔΨ is mainly generated by the tonoplastic proton pumps, which catalyze the active transport of protons into the vacuole. We considered ATPase as the proton pomp which mainly catalyzed this transport. The transport of protons happens only with negative values of the chemiosmotic reaction free energy ΔG_{ATPase} (J mol^{-1}). We compute this variable as follows:

$$\Delta G_{ATPase} = \Delta G_{ATP} + n \times F \times \Delta\Psi - n \times R \times T_k \times \ln(10) \times (pH_{vac} - pH_{cyt}) \quad (39)$$

where ΔG_{ATP} is the free energy of ATP hydrolysis (J mol-1), n is the coupling ratio i.e. the number of protons pumped by hydrolyzed ATP, pH_{vac} and pH_{cyt} are the vacuolar and cytosolic pH respectively.

The coupling ratio n is computed with the following equation where n_0, α and β are adjusting parameters estimated on the data of Davies *et al.* (1994):

$$n = n_0 + \alpha \times (pH_{vac} - 7) + \beta \times 10^{pH_{cyt}-7} \quad (40)$$

We hypothesize that the cytosolic pH is neutral (Lobit *et al.*, 2006). To compute the fruit pulp malic acid concentrations, we define a system representing, at a given time *t* (h), the thermodynamic equilibrium of the malate and protons transports from the cytosol to the vacuole. The equilibrium condition corresponds to $\Delta G_{Mal2-} = 0$ and $\Delta G_{ATPase} = 0$.

Combining the equations 36, 37, and 38, and re-writing the equation 39 we obtain the following formulation of the system:

$$cMal_{vac} = \left(\frac{1}{a_{Mal2-,vac}}\right) \times \left(\frac{h^2 + h \times K_1' + K_1' \times K_2'}{K_1' \times K_2'}\right) \times (Mal_{cit}^{2-}) \times \exp\left(\frac{2 \times F \times \Delta\Psi}{R \times T}\right) \quad (41)$$

$$\Delta\Psi = \left(-\frac{\Delta G_{ATP}}{n \times F}\right) + \left(\frac{R \times T_k}{F}\right) \times \ln(10) \times (pH_{vac} - pH_{cyt}) \quad (42)$$

In this system, we compute $a_{Mal2-,vac}$, K'_1, K'_2, and pH_{vac} using the pH model presented in Etienne *et al.* (2013). The pH model requires as input the concentrations of the main acids and minerals in the fruit pulp. In the case of tomato, we considered citric acid, malic acid, amino acids as the main acids. Moreover, for the sake of simplicity, we consider that the tomato amino acids were almost entirely composed by glutamic acid, according to the measurements made by Colombié *et al.* (2015). We

assumed that the only mineral that participates to the acid-base equilibrium is potassium. Indeed, our measurements show that the estimated magnesium and calcium concentrations account the 10% and the 15% of the total measured mineral molar concentrations.

In the pH model, we consider the vacuolar solution as a concentrated aqueous solution. Moreover, we neglect the ionic associations that can occur in the solution (Lobit *et al.*, 2002). The pH model represents the acid-base equilibrium of the dissociated ionic species. In this version of the pH model, we consider as dissociated anions the citric, the malic, and the glutamic acid. The value of pH is estimated by solving a non-linear system constituted by two equations: one representing the neutrality of the ionic balance (i.e. the algebraic sum of cationic and anionic charges must be null), the other representing the ionic strength as a function of the ionic species activities. This system is then described the following equations:

$$\Sigma_i c_{Anions,i} - \Sigma_i c_{Cations,i} = 0 \quad (43)$$

$$\mu - 0.5 \times \Sigma_i z_i^2 \times c_i = 0 \quad (44)$$

where

$$\Sigma_i c_{Anions,i} = cH_2Cit^- + 2 \times cHCit^{2-} + 3 \times cCit^{3-} + cHMal^- + 2 \times cMal^{2-} + cHGlu^- + 2 \times cGlu^{2-} + cOH^- \quad (45)$$

$$\Sigma_i c_{Cations,i} = cK^+ + h \quad (46)$$

where c_i (mol L^{-1}) is the molar concentration of the species i, cH_2Cit^-, $cHCit^{2-}$, and $cCit^{3-}$ are the molar concentrations of the three dissociated forms of the citric acid (mol L^{-1}), $cHMal^-$ and $cMal^{2-}$ are the molar concentrations of the two dissociated forms of the malic acid, $cHGlu^-$, and $cGlu^{2-}$ are the molar concentrations of the two dissociated forms of the glutamic acid, cK^+ (mol l^{-1}) is the molar concentration of the potassium ions. The molar concentration of the hydrogen cations h (mol l^{-1}) is computed as 10^{-pH} and the hydroxide anions molar concentration cOH^- is computed as $10^{(pH-14)}$.

We can compute the concentrations of the dissociated forms of citric, malic, and glutamic acids as a function of their apparent acidity constants K'_i and of the pH, as we did for the di-anion malate in the 37. For further details, see equations from 7a to 7g in Etienne *et al.* (2013). The apparent acidity constants K'_i of a species i is computed as

$$K'_i = K_{a,i} / a_i \quad (47)$$

where $K_{a,i}$ is the acidity constant of the acid *i* and a_i is its activity.

The activities a_i depend on the ionic strength μ according to the following relationship (Davies, 1962):

$\log_{10}(a_i) = -0.509 \times ((\mu^{½}/(1 + \mu^{½})) - 0.3 \times \mu)$ (48)

Combining the equations for the apparent acidity constants K'_i, the equation 47 and the equation 48 with the non-linear system composed by the equations 43 and 44, we obtain a non-linear system of two equations which we can solve for the unknowns pH_{vac} and μ.

The malic acid transport and pH sub-model consists then solving the system of equations 41 and 42 for $cMal_{vac}$, in which pH_{vac} is estimated by the pH model.

In the integrated model, we use the malic acid module to estimate, at a given hour *h*, the vacuolar malic acid molar concentration $cMal_{vac}$ and the *pH*, considering then the malate transport conditions at a stationary state at each hour *h*. The integrated model must receive as extra inputs the concentrations of amino acids (glutamic acid) and potassium.

Improving the computation of the fruit osmotic potential

In all the works involving the fruit growth model – Hall *et al.*, 2013; Lechaudel *et al.*, 2007; Liu *et al.*, 2007 – the fruit osmotic potential has been computed using the equation 2, adding two contributions to the osmotic potential: the contribution of the soluble sugars, whose concentration was set as a fraction (*ssrat*, -) of the dry mass, and the contribution of the other osmotically active solutes, $\Psi_{\pi 0,(f)}$ (MPa) that is arbitrarily set as a constant value along the growth season. The equation that results from this first approximation is:

$$\Psi_{\pi,f} = -R \times T \times \left(\frac{ssrat \times s}{w}\right) * \left(\frac{1}{M_S}\right) + \Psi_{\pi 0,f} \quad (49)$$

where M_S (g mol^{-1}) is the molar mass of the sugar that is assumed to be dominant into the fruit pulp (e.g. hexoses in tomato).

In the integrated model that we have presented, the sub-models of soluble sugar repartition, citric acid accumulation, and malic acid transport and pH are used to compute the dynamic of the variable $\Psi_{\pi, f.}$ For this computation, we consider the main dissolved compounds in the fruit pulp, which determine the total fruit osmotic potential.

We assume that the main sugars in tomato fruit pulp are hexoses, as considered in the model of tomato fruit growth of Liu *et al.* (2007). We assume that the citric and malic, and amino acids are partially dissociated into the fruit solution, while potassium is completely dissociated. As we already mentioned in the malic acid transport and pH sub-model description, we assume that we can neglect the association between cations and anions in the fruit pulp solution (Lobit *et al.*, 2002); among mineral cations, we consider that calcium and magnesium have a negligible effect on the fruit osmotic potential, as already mentioned. Then, we consider that the fruit osmotic potential is mainly determined by potassium concentration as a first approximation. The partial dissociation of the citric and the malic acid and the presence of the dissociated potassium cations determine the acid-base equilibrium of the fruit pulp solution and, then, the concentration of H^+ cations (Etienne *et al.*, 2013; Lobit *et al.*, 2002). Under these hypotheses, we compute the fruit osmotic potential $\Psi_{\pi,f}$ as the sum of the osmotic contributions of hexoses (*HEX*), citric acid (*CIT*), malic acid (*MAL*), amino acids (*AA*), potassium cations (K^+), and hydrogen cations (H^+), as follows:

$$\Psi_{\pi,f} = -\left(R \times T \times c_{HEX} + R \times T \times c_{CIT} + R \times T \times c_{MAL} + R \times T \times c_{AA} + R \times T \times c_{K^+} + R \times T \times c_{H^+}\right)$$

with $c_i = C_i / M_i$ (50)

where c_i (mol g^{-1}), C_i (g g^{-1}), and M_i (g mol^{-1}) are respectively the molar concentration, the concentration, and the molar mass of the *i*-th compound in the fruit pulp solution. Note that we compute c_{H+} from the pH of the pulp solution using the formulation

$$c_{H+} = 10^{-pH} \times 10^{-3} \quad (51)$$

Hexoses, citric acid and malic acid concentrations, and pH are predicted by the respective sub-models. Amino acids and potassium concentrations are given as input to the integrated model and they serve to compute the acid-base equilibrium in the fruit pulp solution, as we will discuss in the malic acid transport and pH model section. We will refer to the terms $R \times T_k \times c_i$ of the equation 50 as “osmotic contribution of the species *i*”.

Sub-models and integrated model parameterization

We considered that all the parameters were dependent on the variety, while they did not depend on the treatment and on the cohort. To estimate the parameters of the integrated model, we applied the following procedure:

1- We estimated parameters of the sugar, the citric acid, and the malic acid and pH sub-models by giving to each sub-model inputs derived from measured data.
2- We estimated growth sub-module parameters, connecting all the sub-models with their parameters previously estimated.

Some parameters were fixed to literature-based values (Table 3.1), in order to reduce the number of parameters to estimate. We estimated the parameters of the sugar model that represent the conversion rates from one compound to the other, the parameters of the citric acid sub-model that represent the metabolic flows and the transports of pyruvate and malate from the cytosolic to the mitochondrial compartments, the parameter ΔG_{ATP} of the malic acid sub-model, and the parameters of the growth sub-module that had the higher sensitivity scores in sensitivity analyses that were made on the fruit growth model, as detailed in Constantinescu *et al.* (2016). The parameters that we estimated are compiled in Table 3.2 and Table 3.3.

We estimated the parameters of the sub-models using the evolutionary multi-objective algorithm NSGA-II (Deb, 2002). For applying the NSGA-II algorithm, we used the Java package *jMetal*. The algorithm provides a set of pareto-dominant solutions. For every solution, we have then a value of each objective that we aim at minimizing and a value of every parameter. Among the pareto-dominant solutions, we chose the best one following a criterion that depended on the sub-model we were calibrating. In all the calibrations, we aimed at minimizing the prediction root mean squared error (RMSE) defined as:

$$RMSE = \sqrt{\frac{1}{N} \times \sum_{h=1}^{N} (P_h - O_h)^2} \quad (52)$$

where N is the total number of observed values of the variable to predict, P_h and O_h are the predicted and observed values of the variable to predict at the hour h, respectively.

Table 3.1. Literature based parameters of the integrated model.

Sub-model	Parameter	Description	Value	Reference
Growth sub-model	γ	Empirical parameters of the relationship linking fruit surface area Af with the fruit weight *Wf*. $Af = \gamma \times W^{\eta}$ (-)	4.84	Measured data
	η		0.67	
	$\psi_{\pi, p, oth}$ *	Contribution to the stem pedicel end osmotic pressure of solutes other than sugars (MPa)	0.7	Chen *et al.*, unpublished
	k_m	Michaelis-Menten constant (-)	0.08	Liu *et al.*, 2007
	p_s	Membrane permeability for sugar diffusion (g cm^{-2} h^{-1})	3.6×10^{-5}	
	Y	Threshold pressure under which fruit expansion is only elastic (MPa)	0.1	
	ρ	Permeation coefficient of fruit surface to water vapour (for transpiration computation) (g cm^{-2} h^{-1} MPa^{-1})	0.162	
	q_g	Respiration coefficients: growth (-), maintenance coefficient at 20°C ($g_{sucrose}$ g_{DM}^{-1} h^{-1}), factor of change of the maintenance coefficient at each 10°C of temperature rise (-)	0.22	
	$q_{m,293}$		4.2×10^{-4}	
	Q_{10}		1.4	
	r_w	Proportion of dry mass converted to water during respiration (-)	0.56	Hall *et al.*, 2013
	e	Elastic modulus (MPa)	15.3	
Citric acid and malic acid	$cPyr_{cyt}$	Concentration of cytosolic pyruvate (mol L^{-1})	5×10^{-4}	Etienne *et al.*, 2015
	$cMal_{cyt}$ / (Mal_{cyt})	Concentration and activity of the cytosolic malate (mol L^{-1})	1×10^{-3}	Etienne *et al.*, 2015 / Etienne *et al.*, 2014
	pH_{cyt}	Cytosolic pH	7	Etienne *et al.*, 2014
	n_0	Coefficients for the coupling ratio computation (-)	4	
	α		0.3	
	β		-0.12	

Table 3.2. Estimated parameters of the sub-models, for each variety. We computed the 10th and the 90th percentiles of the estimated parameters using as dataset the best solution and the 30 pareto-dominant solutions nearest to the best one. For the malic acid model parameters, we used all the 16 solutions.

Sub-model	Parameter	Description	Variety	10th percentile	90th percentile	Estimated value
Sugar	$k_{sta \rightarrow sol}$	Rate of carbon conversion from starch to soluble sugars (h^{-1})	Bellastar	2.78×10^{-3}	3.77×10^{-3}	3.19×10^{-3}
			Sassary	4.71×10^{-3}	5.45×10^{-3}	5.01×10^{-3}
	$k_{sol \rightarrow sta,0}$	Rate of carbon conversion from soluble sugars to starch when t = 0 (h^{-1})	Bellastar	1.33×10^{-2}	1.69×10^{-2}	1.45×10^{-2}
			Sassary	1.16×10^{-2}	1.31×10^{-2}	1.25×10^{-2}
	k_s	Rate of exponential decrease of the carbon conversion rate from soluble sugars to starch (h^{-1})	Bellastar	4.17×10^{-3}	4.73×10^{-3}	4.29×10^{-3}
			Sassary	3.82×10^{-3}	3.99×10^{-3}	3.98×10^{-3}
	$k_{sol \rightarrow oth,0}$	Rate of carbon conversion from soluble sugars to compounds other than sugars when $\tau = 0$ (-)	Bellastar	3.07	3.63	3.29
			Sassary	9.02	9.42	9.07
	τ	Coefficient of the exponential relationship between the rate $k_{sol \rightarrow oth}$ and the relative growth rate (-)	Bellastar	1.02	1.04	1.03
			Sassary	1.20	1.21	1.21
Citric acid	$k0_1$	Rate of the mitochondrial metabolic flow from pyruvate and malate to citrate if SDW=1g ($L^2\ h^{-1}\ mol^{-1}$)	Bellastar	6.18×10^{-3}	8.10×10^{-2}	5.30×10^{-3}
			Sassary	3.17×10^{-3}	9.74×10^{-2}	9.48×10^{-2}
	$k0_3$	Rate constant of the mitochondrial metabolic flow from malate to pyruvate ($L\ h^{-1}$)	Bellastar	2.49×10^{-2}	4.99×10^{-2}	4.99×10^{-2}
			Sassary	6.20×10^{-3}	7.91×10^{-1}	4.97×10^{-1}
	$K0_4$	Rate of transport from the cytosolic to the mitochondrial pyruvate ($L\ h^{-1}$)	Bellastar	19.2	47.6	47.2
			Sassary	8.92	45.6	17.4
	$K0_5$	Rate of transport from the cytosolic to the mithocondrial malate ($L\ h^{-1}$)	Bellastar	6.08×10^{-4}	6.46×10^{-4}	6.45×10^{-4}
			Sassary	5.25×10^{-4}	7.08×10^{-4}	6.68×10^{-4}
	m_1	Determines whether the rate k_1 increases or decreases during fruit development (-)	Bellastar	-3.89	-2.95×10^{-1}	-3.92
			Sassary	-2.99	-6.55×10^{-1}	-3.00
	m_3	Determines whether the rate k_3 increases or decreases as fruit structural dry weight increases (-)	Bellastar	1.14	6.68	1.15
			Sassary	2.18	5.27	5.25
	m_4	Determines whether the rate k_4 increases or decreases as fruit structural dry weight increases (-)	Bellastar	-4.87×10^{-2}	-9.09×10^{-3}	-4.94×10^{-2}
			Sassary	-4.86×10^{-3}	2.84×10^{-3}	8.24×10^{-4}
	m_5	Determines whether the rate k_5 increases or decreases as fruit structural dry weight increases (-)	Bellastar	5.25×10^{-1}	5.64×10^{-1}	5.61×10^{-1}
			Sassary	2.08×10^{-1}	4.20×10^{-1}	3.62×10^{-1}
Malic acid	ΔG_{ATP}	Free energy variation of the ATP hydrolysis ($J\ mol^{-1}$)	Bellastar	-47300	-47030	-47100
			Sassary	-47800	-47300	-47400

Table 3.3. Estimated parameters of the growth sub-model, for each variety. We computed the 10th and the 90th percentiles of the estimated parameters using as dataset the best solution and the 30 pareto-dominant solutions nearest to the best one.

Sub-model	Parameter	Description	Variety	10th percentile	90th percentile	Estimated value
Growth	L_p^*	Conductance of the water path in the phloem between the stem and the fruit ends of the pedicel (g MPa^{-1})	Bellastar	9.52×10^{-2}	1.00×10^{-1}	1.00×10^{-1}
			Sassary	2.60×10^{-2}	3.23×10^{-2}	3.06×10^{-2}
	$a_p \times L_p$	Conductance of the water path in the phloem the fruit end of the pedicel and the fruit (g MPa^{-1})	Bellastar	2.37×10^{-3}	2.83×10^{-3}	2.37×10^{-3}
			Sassary	5.06×10^{-3}	6.77×10^{-3}	5.26×10^{-3}
	rxp	Ratio between xylem and phloem pathways conductances (-)	Bellastar	1.00×10^{-1}	1.02×10^{-1}	1.00×10^{-1}
			Sassary	2.00×10^{-1}	2.34×10^{-1}	2.05×10^{-1}
	v_m	Maximum sugar uptake rate of the fruit (h^{-1})	Bellastar	2.67×10^{-2}	3.02×10^{-2}	3.02×10^{-2}
			Sassary	2.00×10^{-2}	3.04×10^{-2}	2.03×10^{-2}
	*t**	Parameter used to compute the sugar active uptake. The higher is its value, later the active uptake starts decreasing (h)	Bellastar	107	119	117
			Sassary	81.0	104	93.7
	τ_a	Parameter used to compute the sugar active uptake. The higher is its value, the slower is the active uptake decreasing rate in the growth stage (h)	Bellastar	340	383	340
			Sassary	334	388	369
	Φ_{max}	Maximum cell wall extensibility. Cell wall extensibility is half of Φ_{max} at 10 days after anthesis and then decreases exponentially ($Mpa^{-1}\ h^{-1}$)	Bellastar	1.00	2.63	2.63
			Sassary	2.69×10^{-1}	4.65×10^{-1}	4.77×10^{-1}
	τ_s	Parameter used to compute the reflection coefficient of the composite membrane σ_p (h^{-2}) equation $\sigma_p = 1-\exp(-\tau_s \times t^2)$	Bellastar	8.76×10^{-6}	9.00×10^{-6}	8.95×10^{-6}
			Sassary	2.52×10^{-6}	3.15×10^{-6}	2.63×10^{-6}

To find the best parameterizations and have interpretable results of our calibrations, for each sub-model calibration we reduced the number of RMSE to minimize with the NSGA-II algorithm. For a given sub-model simulation, and for every predicted variable of this simulation, we obtained six RMSEs, one for each treatment-cohort combination that we wanted to minimize. To aggregate them, we used a procedure that depended on the sub-model that we were analyzing (see below). Then, among the pareto-dominant solutions identified through the NSGA-II algorithm, we selected the best one in order to obtain the best fruit osmotic potential estimation.

For the sugar acid sub-model calibration, we minimized the prediction errors of the soluble sugar concentrations and of the starch concentrations prediction. These two prediction errors were computed as the average between the RMSEs of each treatment-cohort combination. Once obtained the pareto-dominant solutions that minimized these two prediction errors, we selected the one that had the lower weighted mean value of the two RMSEs, giving a higher weight (80%) to the soluble sugars prediction errors, since this variable is used in the osmotic potential estimation.

For the citric acid sub-model calibration, we minimized three prediction errors, one for each cohort. Each prediction error was computed as the average between the citric acid concentrations prediction errors of the two treatments. Among the pareto-dominant solutions selected by the NSGA-II algorithm, we chose the one that had the minimum average value between the three prediction errors, each computed on the prediction results of a given cohort.

For the malic acid sub-model calibration, we minimized the average prediction errors of the malic acid concentrations and of pH, computed as the average of the RMSEs for each of the treatment-cohort combination for each of the two variables. Among the pareto-dominant solutions, we selected the one that had the minimum error in the malic acid concentration prediction.

Once we determined the best parameterizations of these three sub-models, we used these parameters in the integrated model to estimate the growth sub-model parameters. In the growth sub-model calibration, we minimized the worst prediction errors of fruit fresh and dry weight, computed as the maximum of the RMSEs of each treatment-cohort combination. Among the pareto-dominant solutions, we selected the

one that had the minimum fresh weight prediction error, since the integrated model dry weight prediction error did not vary a lot among the pareto-dominant solutions.

Sub-models and integrated model inputs

To perform the model calibration with to the procedure described in the last section, we used hourly inputs that were either measured or generated from measured data. The hourly inputs of temperature and humidity were derived from measurements made in the greenhouse by sensors. The hourly inputs of fruit fresh weight, fruit dry weight, fruit structural dry weight, potassium concentrations in the fruit pulp, were estimated with a smooth spline performed on the measured data (R *smoot.spline* function of the *stat* package). We assumed that the hourly phloem sugar concentrations at the stem end of the pedicel had a minimum constant value of 11% from 18:00 to 06:00 and had a sinusoidal behavior (period 24h) from 06:00 to 18:00, with a maximum value of 16% at 13:00. We set approximately the same phloem sugar concentrations value given by Liu *et al.* (2007) for the nighttime, hypothesizing a slight increase during the daytime. We assumed that the xylem and phloem water potential at the stem end of the pedicel had a constant value of -0.2 MPa from 18:00 to 06:00 and that it had a sinusoidal behavior (period 24h) from 06:00 to 18:00, reaching a minimum value of -0.45 MPa since the plants were well-irrigated. We estimated the missing data of amino-acids concentrations for every treatment-cohort combination of each variety supposing that amino-acids entered the fruit from the fruit phloem and that the rate of amino acids accumulation in the fruit pulp was linearly and directly proportional to the rate of dry mass accumulation by mean of a proportion constant α. Moreover, we assumed that the main amino acid accumulating in the fruit pulp was the glutamic acid (according to the measured data in Colombie *et al.*, 2015). For a given treatment-cohort combination of each variety, we estimated the mean dry matter accumulation rate for each date by dividing the difference of fruit dry mass measured in two subsequent dates with respect to the time interval between the two dates. Then, we searched the parameter α that corresponded to the best prediction of the fruit pH by the pH model, using as inputs the measured citric acid, malic acid, and potassium concentrations. The glutamic acid concentration was computed by multiplying α to the estimated dry matter accumulation

rate. We used the R *optimization* function of the *stat* package to perform this computation, minimizing as prediction error the RMSE of the pH prediction at every date of measurement. The obtained value of amino acids concentrations was then used as an input for the malic acid model and pH calibration.

Estimation of solutes dilution, accumulation, and global contributions to the fruit osmotic potential variation

The variation of each solute concentration along the fruit development season determines a variation of the fruit osmotic potential. According to the equation 2, the rate of change (MPa h^{-1}) of osmotic potential can be written as:

$$\frac{d\Psi_\pi}{dt} = \sum_i \left(-R \times T \times \frac{dc_i}{dt}\right) \quad (53)$$

t (h) is the time.

Following the approach of Génard *et al.*, (2003) (Eq 6 of their work), we can develop the expression of the molar concentration c_i derivative, observing that the molar concentration can be expressed as the ratio between the total amount Q_i of the solute *i* (mol) divided by the volume (cm^3) of water V_w in the fruit, i.e. $c_i = Q_i/V_w$. We then obtain the following expression:

$$\frac{d\Psi_\pi}{dt} = \sum_i \left(-R \times T \times \frac{1}{V_w} \times \frac{dQ_i}{dt} + R \times T \times \frac{1}{V_W}\frac{dV_W}{dt} \times c_i\right) \quad (54)$$

where the first and the second term inside the sum can be respectively interpreted as the contribution to the fruit osmotic potential variation of the accumulation and the dilution of a solute i. Indeed, the first and the second terms depend on the variation of the solute amount in the solution and on the solvent water volume variation, respectively. This formula represents the additive effect of accumulation and dilution of each solute on the osmotic potential. Indeed, when the accumulation is higher than the dilution, the osmotic potential decreases (its variation is negative), and vice-versa.

Results

Prediction performances of the linked sub-models and analysis of the fruit water response to varying osmotic potentials

We evaluated the prediction performance of the integrated model by confronting the observed and estimated values during fruit growth of fruit fresh weight and dry weight,

fruit pulp sugars concentrations, carbon stored in compounds other than sugar, fruit pulp citric acid concentrations, malic acid concentrations, and pH. The model was simulated using the parameters estimates obtained by model calibration as described in the Material and methods section. The input variables used for performing our simulations are described in the material and methods section as well. We chose to show the simulations of the “Density 3.6” treatment, since the results were similar among the two densities for both the varieties. The figures reporting fits of the treatment “Density 2.4” are then presented in supplementary material (S4). The integrated model was able to well predict fresh and dry weight for both varieties (Fig. 3.6 and Fig. 3.7 A and B). The third cohort fresh weight and dry weight were well estimated in both varieties. However, in the variety Sassary, the first and the second cohort fresh weights were over-estimated, as well as the dry weight of the first cohort. Globally, the model was able to predict fruit fresh and dry weights observed in the first part of the fruit growth, while was less performing in the prediction of the fruits fresh and dry weight at the final growth stage. Moreover, the different behaviors of the cohort 2 dry weight and fresh weight were well estimated in both varieties (Fig. 3.6 and Fig. 3.7 A and B). The predicted soluble sugars concentrations varied less than the observed ones (Fig. 3.6 and Fig. 3.7 C). Moreover, differences among cohorts were less evident in the soluble sugars concentrations prediction. The starch concentration decline during fruit growth was well predicted in both varieties. The amount of carbon stored in other compounds than sugars was well predicted (Fig. 3.6 and Fig. 3.7 D), as well as the difference in other compounds accumulation among cohorts. However, similarly to the dry weight prediction case, this variable was better predicted in the early fruit growth. Citric acid concentrations in the second cohort of Bellastar variety were well predicted. However, the first and the third cohort citric acids concentrations were underestimated and overestimated, respectively (Fig. 3.6 E). In the case of the Sassary variety, citric acids concentrations were well predicted, unless the final predicted values were lower than the observed ones for the first and the second cohort (Fig. 3.7 E). The observed malic acid concentrations were constant in the first part of the fruit growth for both varieties (Fig. 3.6 and Fig. 3.7 E). The pH predictions were better in the case of Sassary confronted to the case of Bellastar (Fig. 3.6 and Fig. 3.7 F). In the Sassary fruit pulp

pH prediction, the pH decrease of the third cohort was well predicted (Fig. 3.7 F). Moreover, the model predicted the rise of pH of the cohort 2, unless it overestimated the final pH. The first cohort pH was bad predicted by the model in both varieties. Globally, the model fairly well predicted the variation range of all variables, as well as their order of magnitude.

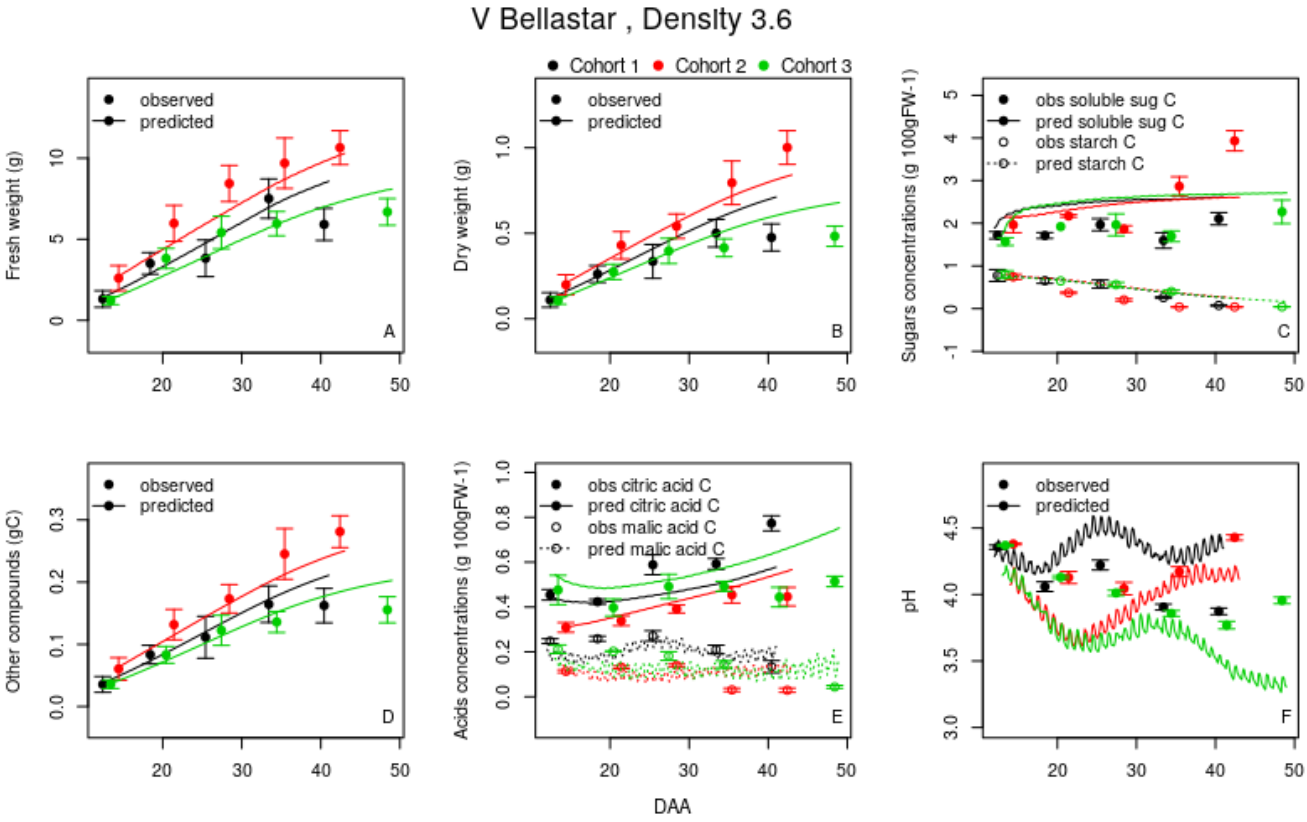

Fig. 3.6. Integrated model simulations performances for the fruits of the variety Bellastar grown in 3.6 shoot density: observed (points) vs predicted (lines) fresh weight (A), dry weight (B), soluble sugar concentrations (C, full points and full lines), starch concentrations (C, empty points and dashed lines), carbon stored in the other compounds (D), citric acid concentrations (E, full points and full lines), malic acid concentrations (E, empty points and dashed lines), and pH (F). Black, red, and green denote the first, the second, and the third cohort, respectively. Bars indicate the standard deviations of measured data.

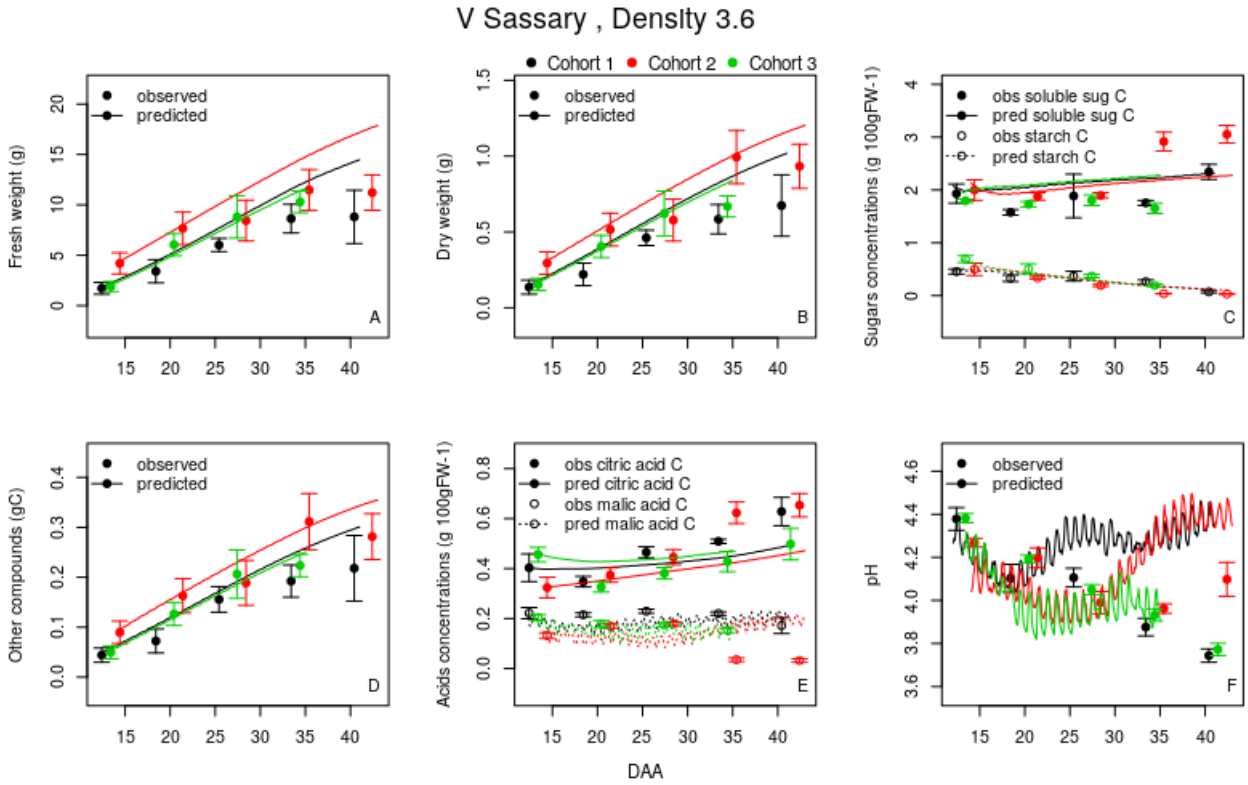

Fig. 3.7 Integrated model simulations performances for the fruits of the variety Sassary grown in 3.6 shoot density: observed (points) vs predicted (lines) fresh weight (A), dry weight (B), soluble sugar concentrations (C, full points and full lines), starch concentrations (C, empty points and dashed lines), carbon stored in the other compounds (D), citric acid concentrations (E, full points and full lines), malic acid concentrations (E, empty points and dashed lines), and pH (F). Black, red, and green denote the first, the second, and the third cohort, respectively. Bars indicate the standard deviations of measured data.

We performed an analysis of the fruit water rate of change variation simulated by the model to given variations of the fruit pulp osmotic potential for the Bellastar fruits grown in the “3.6 Densitiy” treatment. Our results (Fig. 3.8) show that a progressive decrease of osmotic potential generated an almost linear response of the water rate of change, globally determining a higher water net inflow. More specifically, an osmotic potential decrease of 0.1 MPa generated an increase in water inflow of 0.02 g h^{-1}.

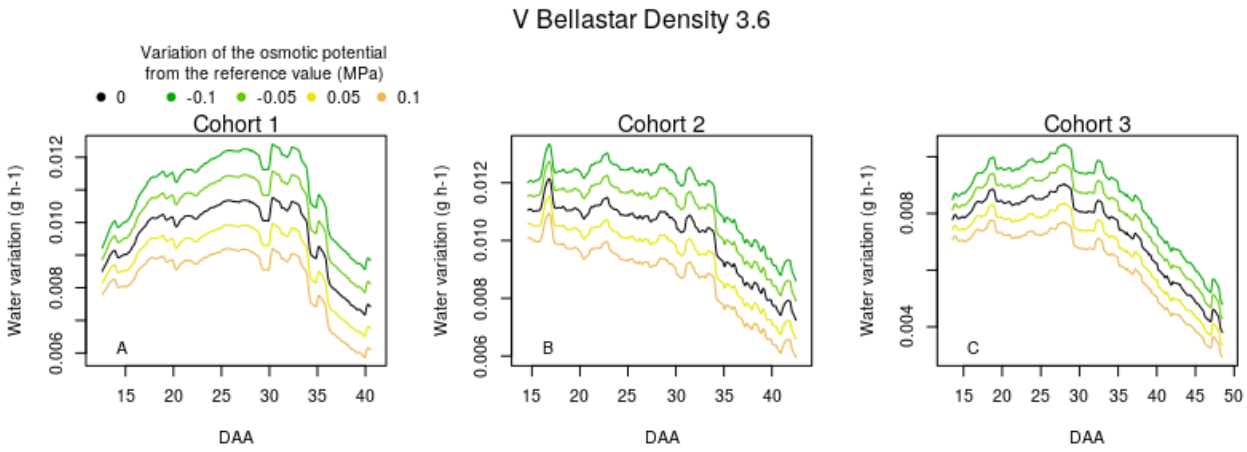

Fig. 3.8. Simulated fruit water rate of change at different fruit osmotic potential inputs. Each color represents a variation of the fruit osmotic potential value with respect to the reference simulation value. The reference simulation was obtained using the estimated parameters belonging to the best solution.

Soluble sugars and potassium concentrations mainly determine the predicted osmotic potential, but the estimated contribution of acids is not negligible.

The contributions of solutes to the whole osmotic potential estimated by the model did not substantially differ among varieties, shoot densities, and cohorts (Fig. 3.9 and Fig. 3.10). Soluble sugars had the principal contribution to the osmotic potential in all the cases, followed by potassium and by citric acid. Malic acid and amino acids contributions are comparable. The total acids contribution had similar values than that of potassium. So, acids contribution was not negligible in determining the fruit osmotic potential. In the first and second cohorts (Fig. 3.9 and Fig. 3.10 A, B, D and E), the contribution of soluble sugars was nearly constant, while potassium contribution changed along fruit growth, driving the osmotic potential variations. Moreover, the ratio between the contributions of acids and potassium changed along the fruit growth in some cases. Indeed, in the third cohorts of both the varieties (Fig. 3.9 and Fig. 3.10 C, F) potassium contribution declined at the end of the growth stage, with an increase of the citric acid contribution. The contribution of potassium increased at the end of the growth stage in the first and second cohorts of both the varieties (Fig. 3.9 and Fig.

3.10 A, B, D and E). The contribution of the H^+ cations was negligible (not shown in figures).

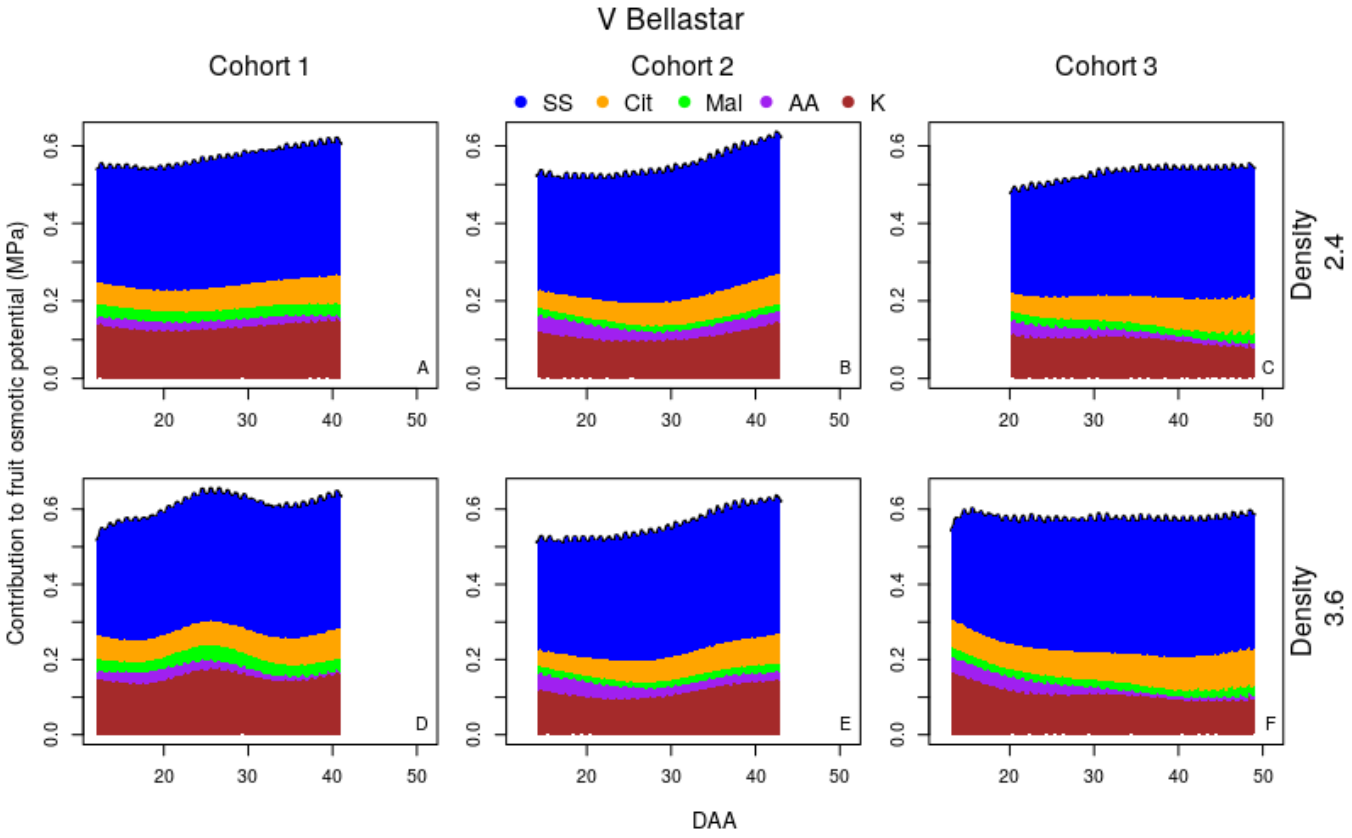

Fig. 3.9. Estimated contributions (absolute value) of solutes concentrations to the osmotic potential (MPa) along fruit growth in the variety Bellastar (DAA = Days after anthesis): the surfaces colors represent the different solutes: (blue) soluble sugars, (orange) citric acid, (green) malic acid, (purple) amino acids, (brown) potassium. A, B, C panels refer to the 2.4 shoot density treatment, D, E, F panels refer to the 3.6 density treatment. Three cohorts are represented: A, D refer to the cohort 1, B and E to the cohort 2, C and F to the cohort 3 (see Materials and methods for further details about cohorts). Details on the computation of this variables are given in the sub-section “Improving the computation of the fruit osmotic potential” of the “Material and methods”.

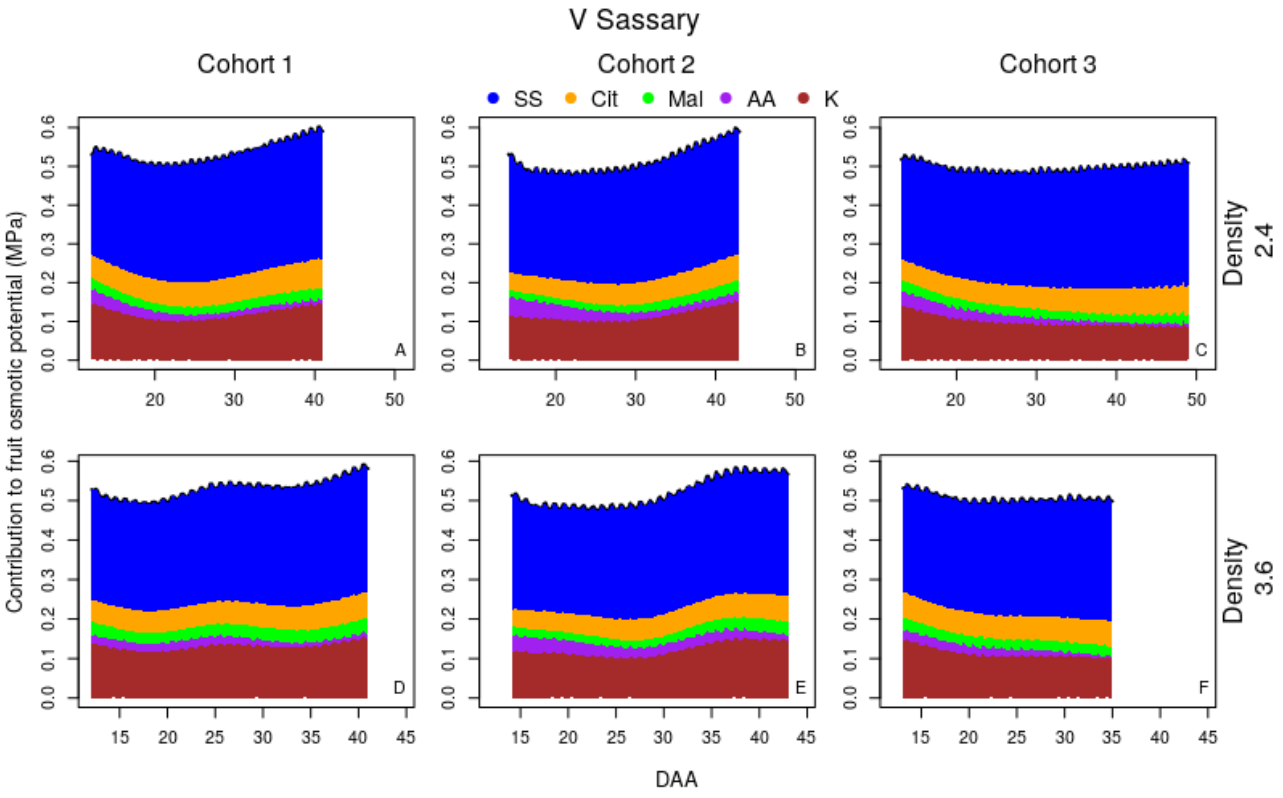

Fig. 3.10. Estimated contributions (absolute value) of solutes concentrations to the osmotic potential (MPa) along fruit growth in the variety Sassary (DAA = Days after anthesis): the surfaces colors represent the different solutes: (blue) soluble sugars, (orange) citric acid, (green) malic acid, (purple) amino acids, (brown) potassium. A, B, C panels refer to the 2.4 shoot density treatment, D, E, F panels refer to the 3.6 density treatment. Three cohorts are represented: A, D refer to the cohort 1, B and E to the cohort 2, C and F to the cohort 3 (see Materials and methods for further details about cohorts). Details on the computation of this variables are given in the sub-section "Improving the computation of the fruit osmotic potential" of the "Material and methods".

The contribution to the fruit osmotic potential variation of the estimated potassium and acids concentrations variations was either higher or comparable to that of soluble sugars concentration variation at the end of the fruit growth season

For all the treatment-cohort combinations of both varieties, the fruit osmotic potential variations progressively shifted from positive to negative, i.e. the fruit osmotic potential mostly increased in the first part of the growth stage and decreased in the second half.

The sum of potassium and acids concentrations variations progressively determined slightly positive to negative variations of the fruit osmotic potential as the fruit developed (Fig. 3.11 and Fig. 3.12). Moreover, the dynamics of the fruit osmotic potential variations due to acids and minerals were similar during fruit growth.

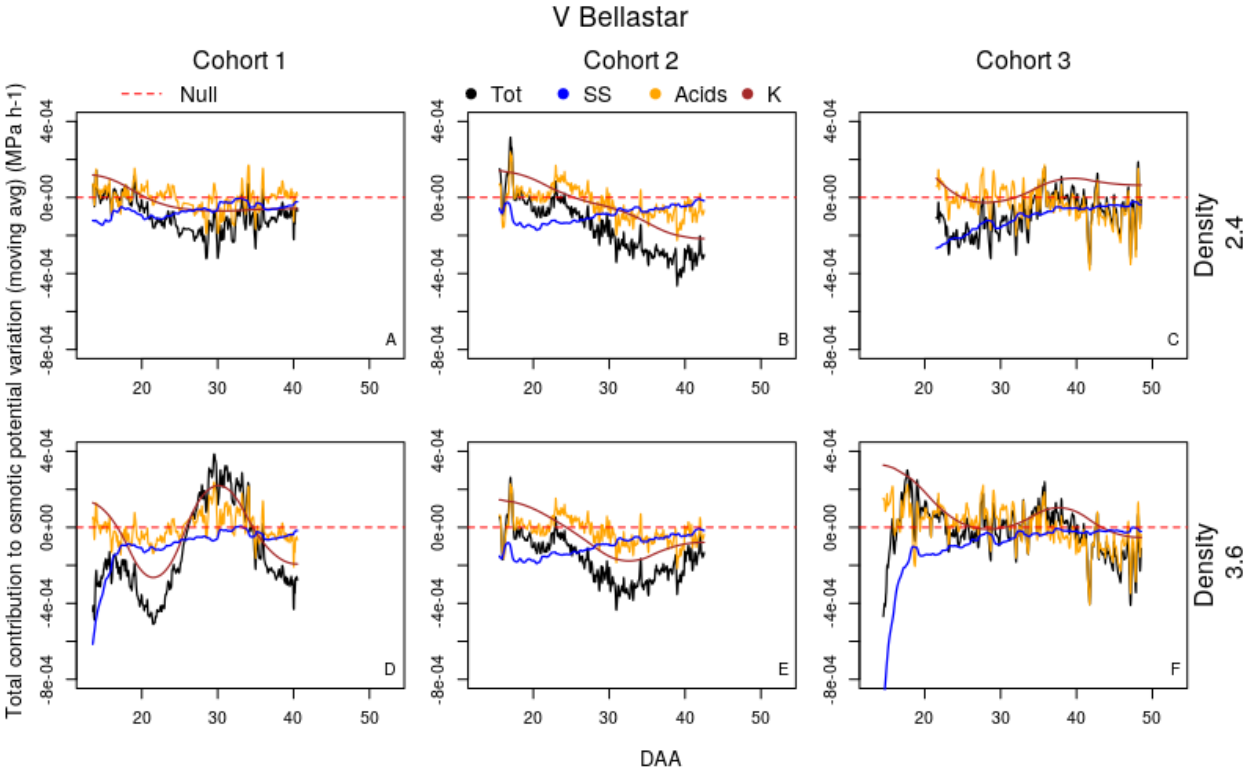

Fig. 3.11. Estimated hourly global contributions to the fruit osmotic potential variation in the variety Bellastar (moving average[a]): black lines represent the global osmotic potential variation, colored lines represent the different solutes: (blue) soluble sugars, (orange) acids, (brown) potassium. The red dashed line corresponds to a null contribution. A, B, C panels refer to the 2.4 shoot density treatment, D, E, F panels refer to the 3.6 density treatment. Three cohorts are represented: A, D refer to the cohort 1, B and E to the cohort 2, C and F to the cohort 3 (see Materials and methods for further details about cohorts). The global contributions to the fruit osmotic potential variation are computed with the equation 53.

[a]the moving average was computed applying the function *ma* of the R package *forecast* (Hyndman and Khandakar, 2008) with the *order* parameter set to 24 h.

Soluble sugars concentrations variations determined a constant fruit osmotic potential decrease during the fruit development. However, at the end of the growth stage, soluble sugars concentrations variations had a weaker effect on fruit osmotic

potential variation confronted to that of the previous part of fruit development. Acids determined fruit osmotic potential variations from slightly positive to slightly negative. Moreover, the contributions of the soluble sugars and acids were comparable at the end of the fruit growth stage.

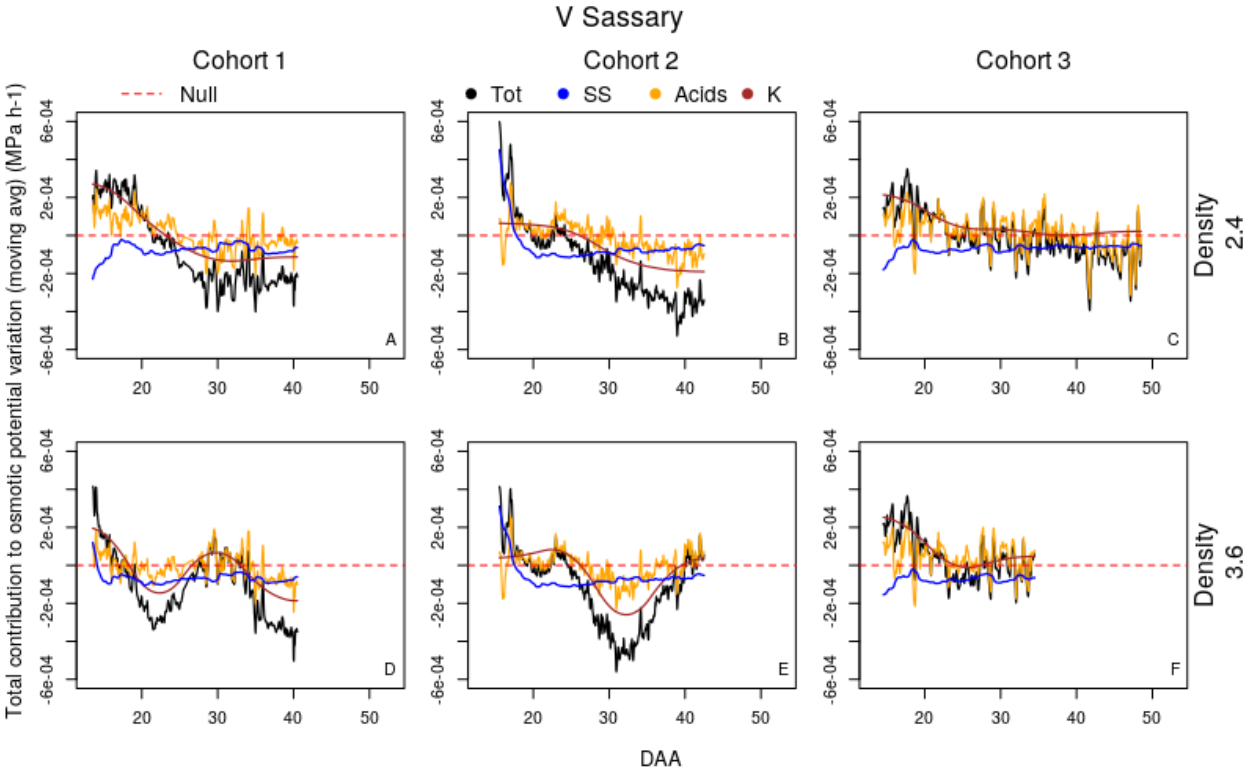

Fig. 3.12. Estimated hourly global contributions to the fruit osmotic potential variation in the variety Sassary (moving average[a]) of the concentration variation solute i (computed according to the equation 53): black lines represent the global osmotic potential variation, colored lines represent the different solutes: (blue) soluble sugars, (orange) acids, (brown) potassium. The red dashed line corresponds to a null contribution. A, B, C panels refer to the 2.4 shoot density treatment, D, E, F panels refer to the 3.6 density treatment. Three cohorts are represented: A, D refer to the cohort 1, B and E to the cohort 2, C and F to the cohort 3 (see Materials and methods for further details about cohorts). The global contributions to the fruit osmotic potential variation are computed with the equation 53.

[a]the moving average was computed applying the function *ma* of the R package *forecast* (Hyndman and Khandakar, 2008)with the *order* parameter set to 24 h.

The estimated contributions of accumulation and dilution processes to the osmotic potential variations are comparable and are mainly driven by soluble sugars with a non-negligible role of acids and potassium.

The estimated global accumulation contributions to the fruit osmotic potential variation were comparable to the global contributions of dilution for all the cohorts and treatments of both the varieties (Fig. 3.13 and Fig. 3.14). The equilibrium between accumulation and dilution was maintained for all the solutes among varieties, treatments and cohorts. Soluble sugars accumulation and dilution contributions were higher than those of other solutes for most of the fruit growth stage and decreased along fruit growth. Both accumulation and dilution of acids and minerals had non-negligible contributions to the fruit osmotic potential variation. Their global contributions were comparable to those of soluble sugars. For both the varieties, sugars accumulation and dilution had a lower contribution on fruit osmotic potential at the beginning of the fruit growth stage in the second cohort and in the third cohort grown at the “Density 2.4” treatment (Fig. 3.13 and Fig. 3.14 B, C, and E). Interestingly, at the end of the fruit growth stage, the contributions of acids and minerals accumulation and dilution had comparable values to those of soluble sugars in both varieties and all the cohort-treatment combinations.

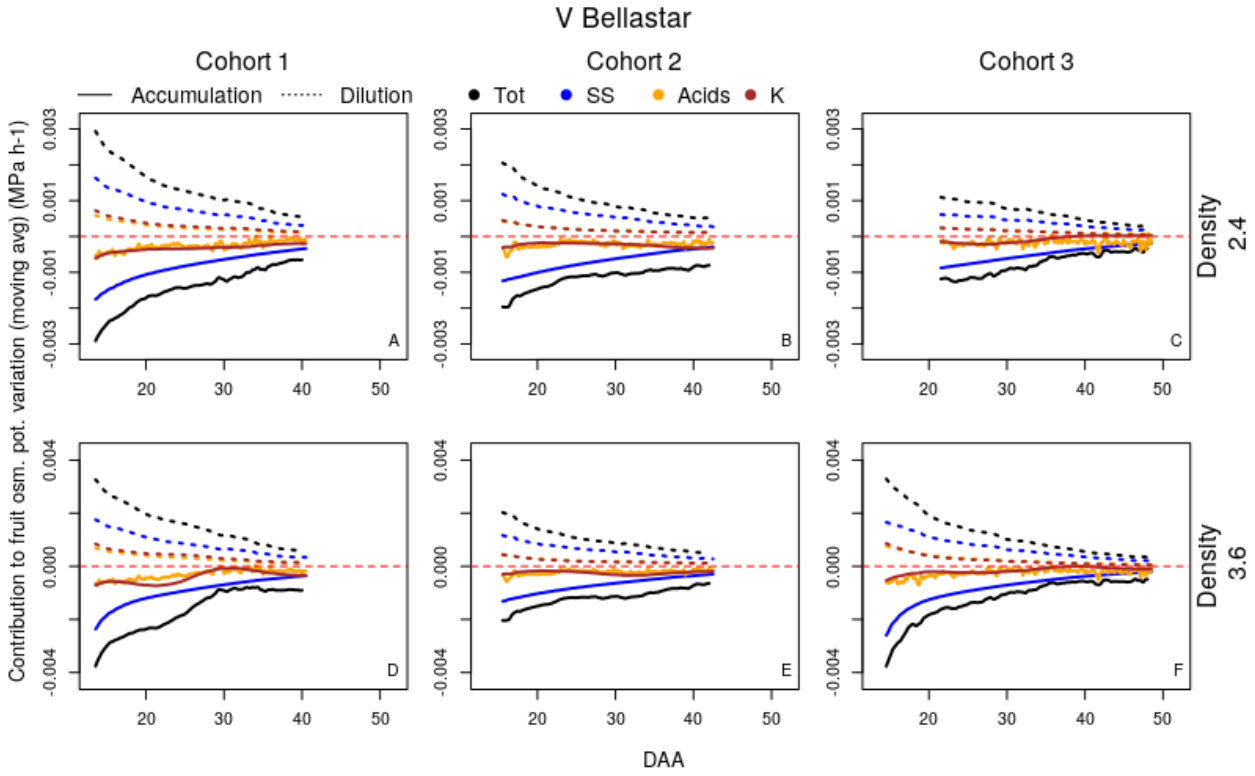

Fig. 3.13 Estimated hourly accumulation (full lines) and dilution (dotted lines) contributions to the fruit osmotic potential variation in the variety Bellastar (moving average[a]). The contribution is lower as it approaches the zero-line (dashed red line) black lines represent the global contributions, colored lines represent the different solutes: (blue) soluble sugars, (orange) acids, (brown) potassium. The pointed orange lines are hidden by the dashed brown ones. A, B, C panels refer to the 2.4 shoot density treatment, D, E, F panels refer to the 3.6 density treatment. Three cohorts are represented: A, D refer to the cohort 1, B and E to the cohort 2, C and F to the cohort 3 (see Materials and methods for further details about cohorts). The contributions to the fruit osmotic potential variation of accumulation and dilution are computed with the equation 54.

[a]the moving average was computed applying the function *ma* of the R package *forecast* (Hyndman and Khandakar, 2008) with the *order* parameter set to 24 h.

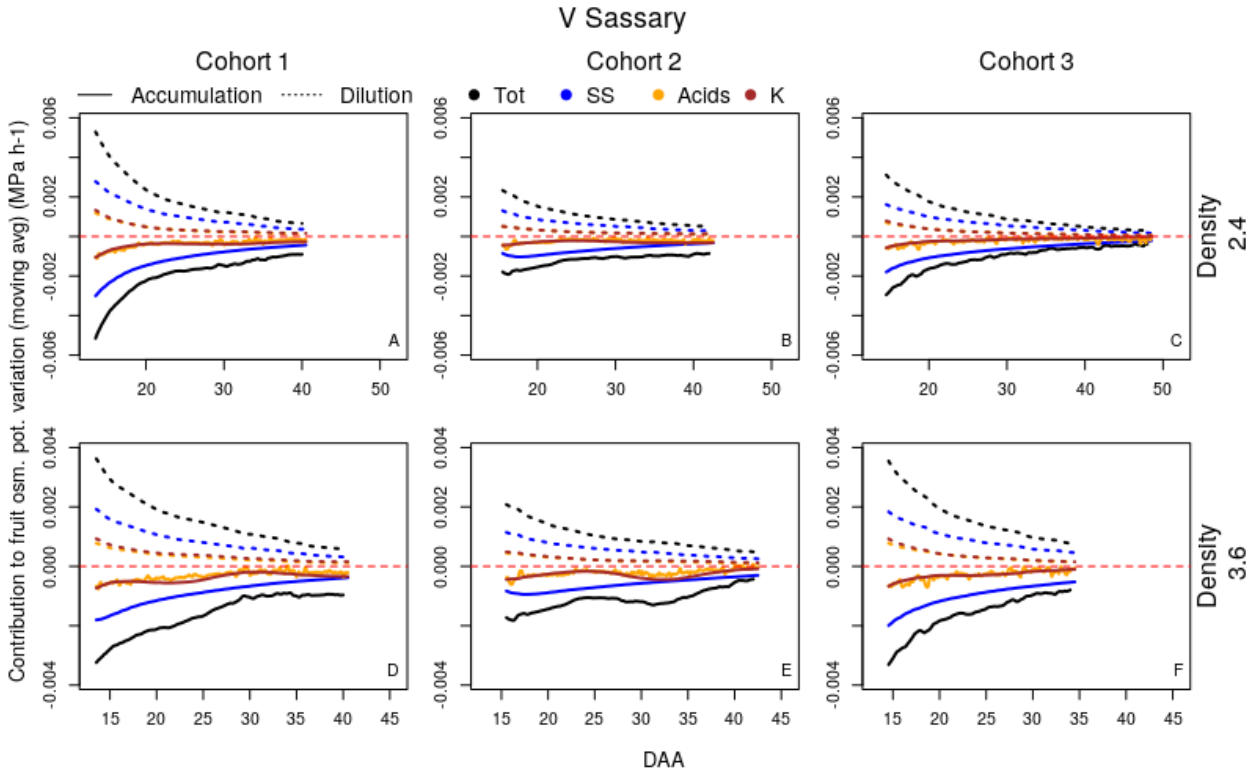

Fig. 3.14: Estimated hourly accumulation (full lines) and dilution (dotted lines) contributions to the fruit osmotic potential variation in the variety Sassary (moving average[a]). The contribution is lower as it approaches the zero-line (dashed red line) black lines represent the global contributions, colored lines represent the different solutes: (blue) soluble sugars, (orange) acids, (brown) potassium. The pointed orange lines are hidden by the dashed brown ones. A, B, C panels refer to the 2.4 shoot density treatment, D, E, F panels refer to the 3.6 density treatment. Three cohorts are represented: A, D refer to the cohort 1, B and E to the cohort 2, C and F to the cohort 3 (see Materials and methods for further details about cohorts). The contributions to the fruit osmotic potential variation of accumulation and dilution are computed with the equation 54.

[a]the moving average was computed applying the function *ma* of the R package *forecast* (Hyndman and Khandakar, 2008) with the *order* parameter set to 24 h.

Discussion

In this work, we developed a virtual fruit model linking sub-models that describe the main biophysical and metabolic processes involving fruit growth and the accumulation of soluble sugars, citric acid and malic acid in the fruit pulp. Our model globally well predicted the concentrations variation ranges of soluble sugars, citric, and malic acid. The model also well reproduced the fruit fresh and dry weight variations during fruit

growth in all the considered cohorts and shoot density treatments. Our analysis of the variations of the fruit water rate of change response to varying fruit osmotic potential suggested that decreasing osmotic potentials determined a not negligible rise of water net import into the fruit. This agreed with the hypothesis that fruit osmotic potential is important for determining fruit water accumulation and, then, fruit growth (Bolarin *et al.*, 2001). The solutes concentrations estimated by the sub-models, together with the given potassium concentrations input, were then adequate to describe fruit growth through the estimation of the total osmotic potential as the sum of their contributions. The inputs that differed among cohorts were the initial values of dry mass, fresh mass, soluble sugars, starch, citric acid concentrations, and the input potassium concentration in the fruit pulp. The model well reproduced differences among cohorts in water and dry weight accumulations. This suggested that potassium concentration seasonal variation was an important discriminating factor in determining the differences of the cohorts growth.

Our analysis of the contributions of each solute to the fruit osmotic potential showed that among solutes, soluble sugars had the higher contribution to the fruit osmotic potential. We expected this result since their predicted concentrations were higher than those of other solutes. Moreover, our results highlighted a non-negligible contribution of potassium in determining the fruit osmotic potential. Indeed, high contribution of potassium to fruit osmotic potential has been measured by Ho *et al* (1987) for the early stages of tomato fruit growth and by Mitchell *et al.*, 1991, along all the tomato growth season. Our analysis of the contributions of solutes concentrations variations to the variations of the fruit osmotic potential further highlighted the role of potassium variations in the fruit growth prediction, having potassium concentrations variations a relatively high contribution to the osmotic potential variation especially during the last fruit growth stage. Not only potassium concentration, but also acids concentrations showed a non-negligible contribution to the osmotic potential variations. Indeed, their contributions followed that of potassium along fruit growth. Our results suggested that the accumulation of malic acid and citric acid could have a not negligible function of osmotic potential regulation at the end of the fruit growth. Indeed, while acids and potassium generally contrasted the sugar contributions to osmotic potential decrease

in the first part of the fruit growth, in the second part of the fruit growth, acids and potassium contributed to osmotic potential decreases and the absolute value of contribution was higher than sugars one.

We found that dilution had a non-negligible effect in determining osmotic potential variations in all solutes. This result further indicates that the distinction between solutes formation and solutes dilution is important in the analysis of metabolic processes (Génard, Baldazzi and Gibon, 2014). Dai *et al.* (2016) estimated that in both cherry tomato and tomato the soluble sugars concentration variations (and, then, osmotic potential variations, which are proportional to this last quantity) were explained by similar contributions of accumulation (import minus metabolism) and dilution. Similarly, we estimated that soluble sugars accumulation and dilution had a comparable role in determining osmotic potential variations in the variety of cherry tomatoes that we analyzed. As in the case of sugars, contributions due to accumulation and dilution on the fruit osmotic potential were similar in the other solutes, suggesting the presence of a balance between the two processes during fruit growth. Moreover, at the end of fruit growth, we computed similar contributions between soluble sugars and the sum of minerals and acids, for both accumulation and dilution. This again suggests that acids could play a role in determining fruit growth regulation.

Conclusions and perspectives

The integrated model of virtual fruit that we presented in this work describes fruit development linking different biophysical and metabolic models. In this work, we presented how this kind of model could be used as a tool for analyzing a physiological aspect of fruit growth. We showed that the model globally well predicted the observed fruit fresh and dry weight behavior during fruit growth, as well as the range of variations of sugars, acids and potassium concentrations. In our study, we estimated the parameters of separate groups of sub-models. However, our model prediction could be improved. Indeed, a calibration on the overall model parameters could improve the model calibration performances. An interesting method to perform this type of calibration has been presented in the work of Mathieu *et al.* (2018). In their work, the authors perform the calibration of a plant development model that has numerous

parameters with a new approach based on a combination of a sensitivity analysis on the calibration loss function and a model selection by Akaike information criterion. They showed that this method could be successful in determining the most important parameters to estimate through the model calibration process.

Among variables determining fruit growth, we focused on the fruit osmotic potential, since it was the main linking variable between sub-models. Fruit osmotic potential is not the only variable that we could analyze in relation to fruit growth. This integrated model could be used as a simulation tool to characterize fruit growth through the analysis of the behavior of many variables concerning solutes metabolism and fruit growth, as was done by Génard *et al.* (2010). We highlighted that potassium and acids concentration variations in cherry tomato fruit pulp could play a non-negligible role in determining fruit osmotic potential variations and, then, fruit growth. This suggests that a model of potassium accumulation, integrated to the model of malic acid transport and pH, would improve the description of fruit growth processes. Also, the integrated virtual fruit model could be used to assess these solutes influence on fruit growth in other fruits. This modeling approach provides details of many important biophysical and metabolic processes involving fruit growth. Fruits solutes determine the fruit composition at harvest and, then, its quality: this integrated model could be used also to analyze how metabolism and water and solutes translocation interact during fruit growth in response to different crop conditions, to design agricultural practices that could improve the fruit quality at harvest and analyze the fruit behavior under determine environmental conditions such as water deficit.

A mechanistic virtual fruit model describing fruit growth and the main fruit pulp solutes metabolisms well predicts fruit growth and highlights possible osmotic potential regulation mechanisms during fruit development

Findings and conclusion

The aim of my thesis was to use and improve a mechanistic fruit model for exploring the genetical variability of tomato, designing water-deficit resistant ideotypes, analyzing the patterns of water and sugar flows in the pedicel-fruit system, and studying the effects on fruit growth of the fruit pulp solutes concentrations that determine fruit quality at harvest.

In the study presented in the first chapter, we performed the calibration of the fruit growth model with the multi-objective evolutionary algorithm NSGA-II to estimate parameters of fruit growth of a population of 117 recombinant inbred lines (RILs). Through a principal component analysis (PCA) made on the obtained parameters, we have highlighted that the three processes associated to the estimated parameters, i.e. cell expansion, water transport, and sugar uptake were strongly discriminant in the RILs population. Conductances to water transports both in the pedicel both in the fruit composite membrane (i.e. the whole water path between the pedicel and the fruit) could be particularly important in determining water deficit resistance. Indeed, high conductances were associated to high dry matter content and high fruit weight. Moreover, sugar active uptake seemed to have an important role. In fact, higher active uptake rate was associated to lower decrease in fresh mass. This is probably linked with osmotic regulations. Moreover, in the work presented in the first chapter, we have shown that the parameter estimates related to different genotypes of the RILs population could be used for determining quantitative trait loci (QTLs). Indeed, we detected QTLs belonging to four chromosomic regions for six of the ten genotypic parameters. We found a significance level below 0.1 for the parameters describing the conductances of the pedicel xylem and phloem, and the conductivity of the phloem of the fruit composite membrane. Interestingly, confronting the results with those obtained by Albert *et al.* (2016), we found a connection between conductivity and firmness, suggesting that this connection may result from the effect of turgor on fruit firmness (Shackel *et al.*, 1991). In the second part of this work, we used the fruit growth model to perform a design of ideotypes, solving an optimization problem to obtain ideal tomato fruits with high dry matter content without excessive growth reduction in water deficit

conditions. The ideotypes were characterized by the model parameters, allowing a physiological interpretation of the results. We were able to obtain large-fruited ideotypes rich in dry matter content (9%) with reasonable fresh mass loss under water deficit (<20%), which were better than the Levovil genotype (6% dry matter content and 60% of fresh mass loss under water deficit). Pedicel conductance and fruit composite membrane conductivity were opposite in the PCA of the ideotype population. Moreover, pedicel conductance was associated to the maximum fruit sugar uptake rate. High conductance in the pedicel that determines water and sugar inflows in combination with the active uptake of sugars could be then a successful strategy to produce large fruit-size ideotypes able to maintain a high fresh weight and satisfying dry matter content. The medium fruit-size ideotypes, on the contrary, were associated to low pedicel conductance and sugar uptake rate, but high fruit composite membrane conductivity. Such interaction between pedicel and fruit conductances is interesting and should be deepened. Indeed, the genetic variability of the conducting tissue geometry in the pedicel and in the fruit has been hardly described. A model approach showed that water import in young tomato fruits would be limited by pedicel resistance (Bussières, 2002) and by phloem conductivity to sap viscosity (Bussière *et al.*, 2011). This agreed with the anatomical results obtained by Rancic *et al.* (2010) in an anatomical descriptive study. In this study, they showed that a low ratio between fruit dry weight and area of the pedicel phloem was responsible for low fruit growth in tomato flacca mutants. Concerning the small fruit-size genotypes, four RILs belonged to the ideal characteristics of the ideotypes were selected. Then, they could bring new interesting source of genetic variations for breeding programs, as their fresh mass is two or three times higher than the fresh mass of the Cervil genotype, which is already known to be WD resistant (Albert *et al.*, 2016; Ripoll *et al.*, 2016). The comparison between the RIL population and the ideotype population revealed that fruit growth was limited either by the incoming fluxes or by the active transport of sugars. Then, uptake of carbon was likely the limiting step for fruit growth of large fruit-size genotypes. Concerning this aspect, the capacity of the plant to provide a carbon supply that would allow high fruit sugar uptake could also be a limiting factor in designing large fruit-size genotypes.

The study of the growth-related parameters variability in the RIL population and the ideotype design allowed highlighting that cell expansion, water transport, and sugar

uptake were involved in the genetic variability of the fruit response to water deficit. Moreover, pedicel conductivity and active uptake of sugars seemed to be the key mechanisms. These mechanisms are likely involved in both fruit osmotic and turgor pressure regulation.

In the study presented in the second chapter, I have built a process-based model of water and sugar transports occurring in the pedicel fruit system during the day, using the same paradigm of the fruit growth model, with a focus on the distinction between the pedicel, the fruit vascular system, the fruit apoplast, and the fruit symplast compartments. This model is simpler than the fruit growth model, since it is a linear system with an analytical solution and a lower number of parameters than the fruit growth model. I obtained simulations of this model that adequately reproduced the diurnal mass variations of intact and pedicel-girdled peach fruits, grown in heavy and light crop load. Analyzing the model variable responses to the input diurnal variations in the heavy crop load treatment, I highlighted that the sugar concentrations in the fruit apoplast were buffered in relation to the stem phloem sugar concentration given as input. Moreover, we simulated a buffer sugar uptake in the fruit symplast, which could be a sugar uptake regulation strategy. Two patterns of water and sugar flows obtained in the simulations could explain this buffer effect and the consequent regulated sugar uptake. The patterns occurred during the night and during the midday periods, respectively. During the night, we predicted a water transfer from the fruit phloem to the fruit xylem. This water transfer decreased the fruit phloem pressure potential, leading to a high phloem flow next to the fruit maintaining a high fruit phloem sugar concentration. Thus, these conditions determined a high mass flow from the pedicel to the fruit phloem and high sugar diffusion from the fruit phloem to the apoplast. This pattern highlighted that during the night, although the sugar concentration of the pedicel phloem given as input to the model was low, the predicted symplast sugar uptake was relatively high. Interestingly, the value of conductance of the water path from the pedicel to the fruit phloem was high and compensated the almost null difference in pressure potential between these two compartments. The associated mass flow allowed realistic sugar uptake by the fruit. The midday pattern that we simulated was characterized by water backflows occurring from the fruit cell apoplast to the pedicel xylem, due to lower pressure potential in the xylem than in the fruit apoplast. Moreover, in contrast from the night simulations, we predicted a water

transfer from the fruit xylem to the fruit phloem. This increased the fruit phloem pressure potential and decreased the fruit phloem sugar concentration. Such a transfer limited then the mass flow and reduced the fruit phloem-to-apoplast sugar diffusion. Therefore, buffered fruit phloem and apoplast sugar concentrations in the midday period resulted in a symplast sugar uptake that was not much higher than that of the night period. Our simulations suggested then that water recirculation in the xylem could be a common phenomenon due to higher pressure potential in the fruit apoplast than in the pedicel xylem, as also hypothesized by Keller *et al.* (2015) for ripe grape berries. In addition to the xylem backflow, we predicted a water recirculation from the fruit xylem to the fruit phloem in the midday period. The simultaneous presence of this recirculation and xylem backflows could lead to favorable conditions for fruit phloem-to-apoplast water flows. This could be then a strategy to prevent water loss in the midday period. In the model calibration, we estimated a relatively high xylem conductance of the water path between fruit and apoplast. This suggested that for peach fruit xylem conductance could remain high at the late growth stage, contrarily to what happens in other fruits in which it decreases near ripening (Lang and During, 1991; Dichio *et al.*, 2002). Moreover, we estimated a fruit phloem-to-apoplast water flow that maintained approximately the same intensity during all day, despite the predicted low conductance between the fruit phloem and the fruit apoplast. This high flow intensity was driven by high water potential differences between these two compartments.

In this chapter, we highlighted that the configuration of conductivities in the fruit pedicel, as well as that of the fruit vascular network, are important in determining patterns of water flow. These patterns could correspond to different strategies of fruit sugar and water accumulation during the day. Similarly, both in the study of the genetic variability of the RIL population both in the procedure of ideotype design, the importance of the connection between conductances and water transports and sugar uptake regulation along the fruit growth season emerged. Therefore, the conductivities role on fruit growth regulation appears to be determinant for fruit water and sugar transports regulation also at daily scale, as well as in the fruit growth season. Moreover, the daily water flow regulation strategies could be identified as a phenotype character in the study of genetic variability, relating them to the resistance to water deficit. Our results obtained in this work suggested that the regulation of water and sugar flows

was associated not only to conductances, but also to the effects of solutes and water translocation on the physical properties of the system compartments, i.e. pressure potential and osmotic potential determining the total water potential. The fluctuations of these variables all day long contribute to the water and sugar translocation regulation.

In the third chapter of this thesis, I have focused on the relationship between fruit osmotic potential and fruit growth. I built a virtual fruit model to evaluate the effect of the fruit pulp solutes composition variation on fruit growth during the fruit growth season. I developed the virtual fruit model linking models describing fruit growth and fruit pulp sugars, citric and malic acid accumulations. The linking key variable between the sub-modules is the fruit osmotic potential, which is computed as the sum of the contributions of the different solutes of the fruit pulp. This integrated model well reproduced fruit fresh and dry weight variations during fruit growth of three different cohorts of cherry tomato, grown in two shoot density treatment. Moreover, the model well predicted the ranges of variation of soluble sugars, citric and malic acid, which are important factors for evaluating the fruit quality at harvest. The model responses to the varying fruit osmotic potential showed a rise of water net import into the fruit for decreasing osmotic potentials. So, the contribution to the fruit osmotic potential of the estimated sugars and acids concentrations, together with those of the potassium concentration given as input, were adequate to describe fruit growth. The model simulations highlighted that potassium concentration variations along fruit growth was an important discriminating factor in determining differences that we observed in the growth of the different cohorts. Among solutes, soluble sugars had the higher contribution to fruit osmotic potential. Moreover, potassium contribution was not negligible, in agreement with measured data (Ho *et al.*, 1987; Mitchell *et al.*, 1991). Considering the contributions of solutes concentrations variations to those of fruit osmotic potential, potassium had a high contribution. This further highlighted the role of potassium concentrations variations on fruit growth, especially in the last fruit growth stage. Moreover, the results suggested that the accumulation of malic and citric acid could have a function on osmotic potential regulation at the end of fruit growth. The analysis on the separated contributions to the fruit osmotic potential of the accumulation and the dilution of the fruit solutes suggested the presence of a balance between these two processes during fruit growth. Moreover, we estimated that acids

and sugars could play a role in determining fruit growth regulation at the end of the fruit growth, for both accumulation and dilution.

Moreover, the fact that solutes dilution plays a non-negligible role in determining the variations of fruit osmotic potential highlighted that water translocation inside the fruit is important for the regulation of the fruit osmotic potential, and next affecting the fruit water net import. The importance of water transfers on the regulation of the osmotic potential that is associated to fruit growth have raised also in the studies presented in the first and the second chapters, suggesting that the interplay between solutes and water transports should be deepened, considering the presence of solutes other than sugars.

Perspectives

The process-based models used in the works that I presented in this thesis could opportunely reproduce different aspects of the fruit growth functioning for different external inputs. However, the models performances should be improved to obtain more realistic reproductions of the fruit growth-related physiological processes. In the study presented in the first chapter, we globally obtained satisfying model predictions both in controlled irrigation and in water deficit conditions for all genotypes. However, the fitting was improved if we considered the two irrigation conditions independently. This suggested that some water deficit effects were poorly taken in account by the model or that some parameters were not independent of the environmental condition. Thus, the physiological processes associated to the estimated parameters should be further investigated in relation to water deficit, to further validate our hypothesis stating that these were independent to the irrigation conditions. The parameters that we used to build the models presented in this thesis drive complex physiological processes of water transport across fruit cells compartments, as well as complex metabolic processes. Then, the experimental measurement of these parameters is difficult. Improving the measurements of these parameters would allow defining more precisely the search space set for the genetic algorithms research of the pareto-dominant solutions of the calibration problem. This would lead to lower incertitude in the estimated values of the model parameters and would improve the QTL detection. Techniques like the positron emission tomography (PET) and the magnetic resonance imaging (MRI) are used to measure pedicel and fruit vascular flows and better

represent water translocations from the plant to the fruit and into the fruit. Moreover, these techniques would allow better conductances estimation (Windt *et al.*, 2009; Knipfler, *et al.*, 2015; Van de Wal *et al.*, 2017). These techniques could help to experimentally estimate water and sugar transport-related parameters. Moreover, combining these techniques with the analysis of model presented in the second chapter would allow having a better knowledge about the water and sugar translocations occurring into the fruit. The sucrose concentration in the phloem sap was used as an input in the models presented in this work. In the calibration step, this input variable had strong effects on model outputs. Giving precise ranges to the variation of phloem sap sugar concentrations is challenging because the measured values belong to wide ranges and the classical methods used to determine them are subjected to high incertitude (Jensen *et al.*, 2013). Moreover, evaluating the effects of different treatments on the phloem sugar concentrations could be advantageous for the model results interpretation. Therefore, an improvement of the phloem sap sugar concentration measurement methods could be a future challenge for improving the modeling of fruit growth processes.

Model prediction performances could be improved also by exploring other strategies of model calibration. The method presented by Mathiew *et al.* (2018) could be applied especially in the case of the calibration of the integrated virtual fruit model that I described in the third chapter. This model calibration technique combines a sensitivity analysis based on the calibration loss function with a model selection through the Akaike information criterion (AIC). This method allows selecting the most important parameters in the model calibration process and could reduce the incertitude of the parameters estimation.

Furthermore, in the analysis of the virtual fruit model made in the third chapter, we highlighted that potassium accumulation was non-negligible in determining fruit growth. This suggests that the virtual fruit model could be improved adding a model of potassium accumulation in the fruit pulp. This model could be integrated to the model of malic acid transport and pH. The integrated fruit model provides the description of the seasonal evolution of fruit pulp solutes accumulations during fruit growth. The result of these accumulations determines changes of fruit quality at harvest. Therefore, the virtual fruit model could be used to analyze the interaction between the water and solutes transports during fruit growth in response to different crop conditions. This

could help growers to design agricultural practices with the objective of obtaining high fruit quality standards at harvest. Such a model could become a useful tool to control irrigation and climate in greenhouses, since it provides hour by hour information about the solutes accumulation in the fruit pulp and predict the solutes concentrations at harvest with given environmental and irrigation conditions. Nevertheless, its performances and robustness should be further evaluated both on data of other fruits both in other agricultural conditions. Finally, the integrated model parameters could be used in QTL analyses to better characterize the genetic variability among genotypes.

Acknowledgments

This thesis was conducted within the project MAGESTAN (PS2A no2016-0244) and was funded by the FranceAgriMer through the “Programme d’investissements d’avenir PIA”. I warmly thank members of the project “MAGESTAN”

References

Albert, E. *et al.* (2016) 'Genotype by watering regime interaction in cultivated tomato: lessons from linkage mapping and gene expression', *Theoretical and Applied Genetics*. doi: 10.1007/s00122-015-2635-5.

Albertini, M. V. *et al.* (2006) 'Changes in organic acids and sugars during early stages of development of acidic and acidless citrus fruit', *Journal of Agricultural and Food Chemistry*. doi: 10.1021/jf061648j.

Almeida, D. P. F. and Huber, D. J. (1999) 'Apoplastic pH and inorganic ion levels in tomato fruit: A potential means for regulation of cell wall metabolism during ripening', *Physiologia Plantarum*. doi: 10.1034/j.1399-3054.1999.105316.x.

Amine, E. K. *et al.* (2003) 'Diet, nutrition and the prevention of chronic diseases', *World Health Organization - Technical Report Series*. doi: 10.1093/ajcn/60.4.644a.

Baldazzi, V. *et al.* (2013) 'In-silico analysis of water and carbon relations under stress conditions. A multi-scale perspective centered on fruit', *Frontiers in Plant Science*. doi: 10.3389/fpls.2013.00495.

Bertin, N. *et al.* (2010) 'Under what circumstances can process-based simulation models link genotype to phenotype for complex traits? Case-study of fruit and grain quality traits', *Journal of Experimental Botany*. doi: 10.1093/jxb/erp377.

Bertin, N., Buret, M. and Gary, C. (2001) 'Insights into the formation of tomato quality during fruit development', *Journal of Horticultural Science and Biotechnology*. Headley Brothers Ltd, 76(6), pp. 786–792. doi: 10.1080/14620316.2001.11511446.

Blum, A. (2011) *Plant breeding for water-limited environments*, *Plant Breeding for Water-Limited Environments*. doi: 10.1007/978-1-4419-7491-4.

Bodner, G., Nakhforoosh, A. and Kaul, H.-P. (2015) 'Management of crop water under drought: a review', *Agronomy for Sustainable Development*, 35(2), pp. 401–442. doi: 10.1007/s13593-015-0283-4.

Bolarin, M. C. *et al.* (2001) 'Relationship between tomato fruit growth and fruit osmotic potential under salinity', *Plant Science*. doi: 10.1016/S0168-9452(01)00360-0.

Boote, K. J., Kropff, M. J. and Bindraban, P. S. (2001) 'Physiology and modelling of

traits in crop plants: Implications for genetic improvement', in *Agricultural Systems*. doi: 10.1016/S0308-521X(01)00053-1.

Broman, K. W. *et al.* (2003) 'R/qtl: QTL mapping in experimental crosses', *Bioinformatics*. doi: 10.1093/bioinformatics/btg112.

Brown, M. M., Hall, J. L. and Ho, L. C. (1997) 'Sugar uptake by protoplasts isolated from tomato fruit tissues during various stages of fruit growth', *Physiologia Plantarum*. doi: 10.1034/j.1399-3054.1997.1010312.x.

Brüggenwirth, M., Winkler, A. and Knoche, M. (2016) 'Xylem, phloem, and transpiration flows in developing sweet cherry fruit', *Trees - Structure and Function*. doi: 10.1007/s00468-016-1415-4.

Bussières, P. (2002) 'Water import in the young tomato fruit limited by pedicel resistance and calyx transpiration', *Functional Plant Biology*. doi: 10.1071/PP00144.

Bussières, P. *et al.* (2011) 'High external sucrose concentration inhibits the expansion of detached tomato fruits grown in a novel semi-open device', *In Vitro Cellular and Developmental Biology - Plant*. doi: 10.1007/s11627-011-9378-z.

Carlomagno, A. *et al.* (2018) 'Pre-harvest berry shrinkage in cv "Shiraz" (Vitis vinifera L.): Understanding sap flow by means of tracing', *Scientia Horticulturae*. Elsevier B.V., 233, pp. 394–406. doi: 10.1016/j.scienta.2018.02.014.

Chapman, S. *et al.* (2003) 'Evaluating plant breeding strategies by simulating gene action and dryland environment effects', in *Agronomy Journal*. doi: 10.2134/agronj2003.0099.

Clearwater, M. J. *et al.* (2012) 'Vascular functioning and the water balance of ripening kiwifruit (Actinidia chinensis) berries', *Journal of Experimental Botany*. doi: 10.1093/jxb/err352.

Colombié, S. *et al.* (2015) 'Modelling central metabolic fluxes by constraint-based optimization reveals metabolic reprogramming of developing Solanum lycopersicum (tomato) fruit', *Plant Journal*. doi: 10.1111/tpj.12685.

Constantinescu, D. *et al.* (2016) 'Model-assisted estimation of the genetic variability in physiological parameters related to tomato fruit growth under contrasted water conditions', *Frontiers in Plant Science*. doi: 10.3389/fpls.2016.01841.

Cosgrove, D. J. (2016) 'Plant cell wall extensibility: Connecting plant cell growth with cell wall structure, mechanics, and the action of wall-modifying enzymes', *Journal of Experimental Botany*. doi: 10.1093/jxb/erv511.

Dai, Z. *et al.* (2016) ‘Inter-species comparative analysis of components of soluble sugar concentration in fleshy fruits’, *Frontiers in Plant Science*, 7(MAY2016). doi: 10.3389/fpls.2016.00649.

Damon, S. *et al.* (1988) ‘Sink Metabolism in Tomato Fruit: II. Phloem Unloading and Sugar Uptake’, *Plant Physiology*. doi: 10.1104/pp.87.3.731.

Davies, J. M., Hunt, I. and Sanders, D. (1994) ‘Vacuolar H+-pumping ATPase variable transport coupling ratio controlled by pH’, *Proceedings of the National Academy of Sciences of the United States of America*. National Academy of Sciences, 91(18), pp. 8547–8551. doi: 10.1073/pnas.91.18.8547.

Deb, K. *et al.* (2002) ‘A fast and elitist multiobjective genetic algorithm: NSGA-II’, *IEEE Transactions on Evolutionary Computation*. doi: 10.1109/4235.996017.

Desnoues, E. *et al.* (2018) ‘A kinetic model of sugar metabolism in peach fruit reveals a functional hypothesis of a markedly low fructose-to-glucose ratio phenotype’, *Plant Journal*. doi: 10.1111/tpj.13890.

Dichio, B., Remorini, D. and Lang, S. (2003) ‘Developmental changes in xylem functionality in kiwifruit fruit: Implications for fruit calcium accumulation’, in *Acta Horticulturae*. doi: 10.17660/ActaHortic.2003.610.25.

Ding, W. *et al.* (2016) ‘Genetic algorithm based approach to optimize phenotypical traits of virtual rice’, *Journal of Theoretical Biology*. doi: 10.1016/j.jtbi.2016.05.006.

Doebley, J. F., Gaut, B. S. and Smith, B. D. (2006) ‘The Molecular Genetics of Crop Domestication’, *Cell*, pp. 1309–1321. doi: 10.1016/j.cell.2006.12.006.

Dray, S. and Dufour, A. B. (2007) ‘The ade4 package: Implementing the duality diagram for ecologists’, *Journal of Statistical Software*. doi: 10.18637/jss.v022.i04.

Etienne, A. *et al.* (2013) ‘What controls fleshy fruit acidity? A review of malate and citrate accumulation in fruit cells’, *Journal of Experimental Botany*. doi: 10.1093/jxb/ert035.

Etienne, A., Génard, M., Bancel, D., *et al.* (2014) ‘Citrate and malate accumulation in banana fruit (Musa sp. AA) is highly affected by genotype and fruit age, but not by cultural practices’, *Scientia Horticulturae*. doi: 10.1016/j.scienta.2014.02.013.

Etienne, A., Génard, M., Lobit, P., *et al.* (2014) ‘Modeling the vacuolar storage of malate shed lights on pre- and post-harvest fruit acidity’, *BMC Plant Biology*. doi: 10.1186/s12870-014-0310-7.

Etienne, A., Génard, M. and Bugaud, C. (2015) ‘A process-based model of TCA

cycle functioning to analyze citrate accumulation in pre- and post-harvest fruits', *PLoS ONE*. doi: 10.1371/journal.pone.0126777.

Fishman, S. and Génard, M. (1998) 'A biophysical model of fruit growth: Simulation of seasonal and diurnal dynamics of mass', *Plant, Cell and Environment*, 21(8), pp. 739–752. doi: 10.1046/j.1365-3040.1998.00322.x.

Fishman, S., Génard, M. and Huguet, J. G. (2001) 'Theoretical analysis of systematic errors introduced by a pedicel-girdling technique used to estimate separately the xylem and phloem flows', *Journal of Theoretical Biology*. doi: 10.1006/jtbi.2001.2442.

Frary, Anne *et al.* (2000) 'fw2.2: A quantitative trait locus key to the evolution of tomato fruit size', *Science*. doi: 10.1126/science.289.5476.85.

Geitmann, A. and Ortega, J. K. E. (2009) 'Mechanics and modeling of plant cell growth', *Trends in Plant Science*. doi: 10.1016/j.tplants.2009.07.006.

Génard, M. *et al.* (2003) 'Changes in fruit sugar concentrations in response to assimilate supply, metabolism and dilution: A modeling approach applied to peach fruit (Prunus persica)', *Tree Physiology*. doi: 10.1093/treephys/23.6.373.

Génard, M. *et al.* (2010) 'Virtual profiling: A new way to analyse phenotypes', *Plant Journal*. doi: 10.1111/j.1365-313X.2010.04152.x.

Génard, M., Baldazzi, V. and Gibon, Y. (2014) 'Metabolic studies in plant organs: Don't forget dilution by growth', *Frontiers in Plant Science*. doi: 10.3389/fpls.2014.00085.

Génard, M. and Souty, M. (1996) 'Modeling the peach sugar contents in relation to fruit growth', *Journal of the American Society for Horticultural Science*. doi: 10.21273/jashs.121.6.1122.

Glazebrook, T. and Kola-Olusanya, A. (2019) *Africa, Food, and Agriculture*, *Encyclopedia of Food and Agricultural Ethics*. doi: 10.1007/978-94-024-1179-9_486.

Gomez, L. *et al.* (2007) 'The microplate reader: An efficient tool for the separate enzymatic analysis of sugars in plant tissues - Validation of a micro-method', *Journal of the Science of Food and Agriculture*. doi: 10.1002/jsfa.2924.

Gomez, L., Rubio, E. and Augé, M. (2002) 'A new procedure for extraction and measurement of soluble sugars in ligneous plants', *Journal of the Science of Food and Agriculture*. doi: 10.1002/jsfa.1046.

Gong, P. *et al.* (2010) 'Transcriptional profiles of drought-responsive genes in

modulating transcription signal transduction, and biochemical pathways in tomato', *Journal of Experimental Botany*. doi: 10.1093/jxb/erq167.

Guichard, S. *et al.* (2001) 'Tomato fruit quality in relation to water and carbon fluxes', *Agronomie, EDP Sciences*, 21(4), pp. 385–392. doi: 10.1051/agro:2001131ï.

Guichard, S. *et al.* (2005) 'Analysis of growth and water relations of tomato fruits in relation to air vapor pressure deficit and plant fruit load', *Journal of Plant Growth Regulation*, 24(3), pp. 201–213. doi: 10.1007/s00344-005-0040-z.

Hall, A. J. *et al.* (2013) 'A biophysical model of kiwifruit (Actinidia deliciosa) berry development', *Journal of Experimental Botany*. doi: 10.1093/jxb/ert317.

Hall, A. J. *et al.* (2017) 'A biophysical model of fruit development with distinct apoplasmic and symplasmic pathways', *Acta Horticulturae*. doi: 10.17660/ActaHortic.2017.1160.53.

Hall, A. J. and Minchin, P. E. H. (2013) 'A closed-form solution for steady-state coupled phloem/xylem flow using the Lambert-W function', *Plant, Cell and Environment*, 36(12), pp. 2150–2162. doi: 10.1111/pce.12125.

Ho, L. C., Grange, R. I. and Picken, A. J. (1987) 'An analysis of the accumulation of water and dry matter in tomato fruit', *Plant, Cell & Environment*. doi: 10.1111/1365-3040.ep11602110.

Hocking, P. J. (1980) 'The Composition of Phloem Exudate and Xylem Sap from Tree Tobacco (Nicotiana glauca Grah.)', *Annals of Botany*. doi: 10.1093/oxfordjournals.aob.a085871.

Huguet, J.-G., Jaussely, B. and Orlando, P. (1985) 'Appréciation de l'état hydrique d'une plante à partir des variations micrométriques de la dimension des fruits ou des tiges au cours de la journée', *Agronomie*. doi: 10.1051/agro:19850809.

Huguet, J. G. *et al.* (1998) 'Xylemic, phloemic and transpiration flows to and from a peach', *Acta Horticulturae*, 465, pp. 345–353. doi: 10.17660/actahortic.1998.465.43.

Hyndman, R. J. and Khandakar, Y. (2008) 'Automatic time series forecasting: The forecast package for R', *Journal of Statistical Software*. doi: 10.18637/jss.v027.i03.

Jensen, K. H., Savage, J. A. and Holbrook, N. M. (2013) 'Optimal concentration for sugar transport in plants', *Journal of the Royal Society Interface*. doi: 10.1098/rsif.2013.0055.

Johnson, R. W., Dixon, M. A. and Lee, D. R. (1992) 'Water relations of the tomato during fruit growth', *Plant, Cell & Environment*. doi: 10.1111/j.1365-

3040.1992.tb01027.x.

Jones, J. W. *et al.* (2017) 'Brief history of agricultural systems modeling', *Agricultural Systems*. Elsevier Ltd, 155, pp. 240–254. doi: 10.1016/j.agsy.2016.05.014.

Keller, M. *et al.* (2015) 'Sugar demand of ripening grape berries leads to recycling of surplus phloem water via the xylem', *Plant, Cell and Environment*. doi: 10.1111/pce.12465.

Keller, M., Smith, J. P. and Bondada, B. R. (2006) 'Ripening grape berries remain hydraulically connected to the shoot', *Journal of Experimental Botany*, 57(11), pp. 2577–2587. doi: 10.1093/jxb/erl020.

Klages, K. *et al.* (2001) 'Diurnal changes in non-structural carbohydrates in leaves, phloem exudate and fruit in "Braeburn" apple', *Australian Journal of Plant Physiology*. doi: 10.1071/pp00077.

Knipfer, T. *et al.* (2015) 'Water transport properties of the grape pedicel during fruit development: Insights into xylem anatomy and function using microtomography', *Plant Physiology*. American Society of Plant Biologists, 168(4), pp. 1590–1602. doi: 10.1104/pp.15.00031.

Labate, J. A., Robertson, L. D. and Baldo, A. M. (2009) 'Multilocus sequence data reveal extensive departures from equilibrium in domesticated tomato (Solanum lycopersicum L.)', *Heredity*. doi: 10.1038/hdy.2009.58.

Lalonde, S. *et al.* (2003) 'Phloem loading and unloading of sugars and amino acids', *Plant, Cell and Environment*, pp. 37–56. doi: 10.1046/j.1365-3040.2003.00847.x.

Lander, E. S. and Botstein, S. (1989) 'Mapping mendelian factors underlying quantitative traits using RFLP linkage maps', *Genetics*.

Lang, A. and Düring, H. (1991) 'Partitioning control by water potential gradient: Evidence for compartmentation breakdown in grape berries', *Journal of Experimental Botany*. doi: 10.1093/jxb/42.9.1117.

Lang, A. and Thorpe, M. R. (1989) 'Xylem, phloem and transpiration flows in a grape: Application of a technique for measuring the volume of attached fruits to high resolution using archimedes' principle', *Journal of Experimental Botany*, 40(10), pp. 1069–1078. doi: 10.1093/jxb/40.10.1069.

Lechaudel, M. (2004) *Croissance et qualité organoleptique de la mangue (Mangifera Indica) : analyse expérimentale et modélisation de l ' effet de la disponibilité hydrique et carbonée*. INA Paris - Grignon.

Lechaudel, M. *et al.* (2007) ‘An analysis of elastic and plastic fruit growth of mango in response to various assimilate supplies’, *Tree Physiology*. doi: 10.1093/treephys/27.2.219.

Lecomte, L. *et al.* (2004) ‘Fine mapping of QTLs of chromosome 2 affecting the fruit architecture and composition of tomato’, *Molecular Breeding*. doi: 10.1023/B:MOLB.0000012325.77844.0c.

Lee, D. R. (1989) ‘Vasculature of the abscission zone of tomato fruit: implications for transport’, *Canadian Journal of Botany*. Canadian Science Publishing, 67(6), pp. 1898–1902. doi: 10.1139/b89-241.

Lemoine, R. *et al.* (2013) ‘Source-to-sink transport of sugar and regulation by environmental factors’, *Frontiers in Plant Science*. Frontiers Research Foundation. doi: 10.3389/fpls.2013.00272.

Lescourret, F. and Génard, M. (2005) ‘A virtual peach fruit model simulating changes in fruit quality during the final stage of fruit growth’, *Tree Physiology*. doi: 10.1093/treephys/25.10.1303.

Letort, V. *et al.* (2008) ‘Quantitative genetics and functional-structural plant growth models: Simulation of quantitative trait loci detection for model parameters and application to potential yield optimization’, *Annals of Botany*. doi: 10.1093/aob/mcm197.

Liu, H. F. *et al.* (2007) ‘Model-assisted analysis of tomato fruit growth in relation to carbon and water fluxes’, *Journal of Experimental Botany*. doi: 10.1093/jxb/erm202.

Lobit, P. *et al.* (2002) ‘Theoretical analysis of relationships between composition, pH, and titratable acidity of peach fruit’, *Journal of Plant Nutrition*. doi: 10.1081/PLN-120015538.

Lobit, P. *et al.* (2003) ‘Modelling citrate metabolism in fruits: Responses to growth and temperature’, *Journal of Experimental Botany*. doi: 10.1093/jxb/erg264.

Lobit, P. *et al.* (2006) ‘Modelling malic acid accumulation in fruits: Relationships with organic acids, potassium, and temperature’, *Journal of Experimental Botany*. doi: 10.1093/jxb/erj128.

Malundo, T. M. M., Shewfelt, R. L. and Scott, J. W. (1995) ‘Flavor quality of fresh tomato (Lycopersicon esculentum Mill.) as affected by sugar and acid levels’, *Postharvest Biology and Technology*, 6(1–2), pp. 103–110. doi: 10.1016/0925-5214(94)00052-T.

Manning, K. *et al.* (2001) ‘Functional characterization of two ripening-related sucrose transporters from grape berries’, *Annals of Botany*, 87(1), pp. 125–129. doi: 10.1006/anbo.2000.1316.

Mathieu, A. *et al.* (2018) ‘A new methodology based on sensitivity analysis to simplify the recalibration of functional-structural plant models in new conditions’, *Annals of Botany*. doi: 10.1093/aob/mcy080.

Matthews, M. A. and Shackel, K. A. (2005) ‘Growth and Water Transport in Fleshy Fruit’, in *Vascular Transport in Plants*. doi: 10.1016/B978-012088457-5/50011-3.

Mazzeo, M. (2008) ‘Xylem transport efficiency and calcium accumulation in fruit of Actinidia deliciosa: implications for fruit quality’, *Italy: University of Basilicata*, p. Phd thesis.

McFadyen, L. M., Button, R. J. and Barlow, E. W. R. (1996) ‘Effects of crop load on fruit water relations and fruit growth in peach’, *Journal of Horticultural Science and Biotechnology*, 71(3), pp. 469–480. doi: 10.1080/14620316.1996.11515428.

Meurer, A. *et al.* (2017) ‘SymPy: symbolic computing in Python’, *peerj.com*. Available at: https://peerj.com/articles/cs-103/?utm_source=TrendMD&utm_campaign=PeerJ_TrendMD_1&utm_medium=TrendMD (Accessed: 11 November 2019).

Mitchell, J. P. *et al.* (1991) ‘Tomato Fruit Yields and Quality under Water Deficit and Salinity’, *Journal of the American Society for Horticultural Science*. doi: 10.21273/jashs.116.2.215.

Moing, A. *et al.* (1997) ‘Phloem loading in peach: Symplastic or apoplastic?’, *Physiologia Plantarum*, 101(3), pp. 489–496. doi: 10.1034/j.1399-3054.1997.1010306.x.

Morandi, B. and Corelli Grappadelli, L. (2009) ‘Source and sink limitations in vascular flows in peach fruit’, *The Journal of Horticultural Science and Biotechnology*. Informa UK Limited, 84(6), pp. 150–156. doi: 10.1080/14620316.2009.11512613.

Morandi, B., Rieger, M. and Grappadelli, L. C. (2007) ‘Vascular flows and transpiration affect peach (Prunus persica Batsch.) fruit daily growth’, *Journal of Experimental Botany*. doi: 10.1093/jxb/erm248.

Nardozza, S. *et al.* (2011) ‘Dry matter content and fruit size affect flavour and texture of novel Actinidia deliciosa genotypes’, *Journal of the Science of Food and Agriculture*, 91(4), pp. 742–748. doi: 10.1002/jsfa.4245.

Osorio, S., Ruan, Y. L. and Fernie, A. R. (2014) ‘An update on source-to-sink carbon partitioning in tomato’, *Frontiers in Plant Science*. doi: 10.3389/fpls.2014.00516.

Pascual, L. *et al.* (2016) ‘Dissecting quantitative trait variation in the resequencing era: Complementarity of bi-parental, multi-parental and association panels’, *Plant Science*. doi: 10.1016/j.plantsci.2015.06.017.

Patrick, J. W. and Offler, C. E. (1996) ‘Post-sieve element transport of photoassimilates in sink regions’, *Journal of Experimental Botany*. Oxford University Press, 47(Special_Issue), pp. 1165–1177. doi: 10.1093/jxb/47.special_issue.1165.

Patrick, J. W. and Offler, C. E. (2001) ‘Compartmentation of transport and transfer events in developing seeds’, in *Journal of Experimental Botany*. doi: 10.1093/jxb/52.356.551.

Qi, R. *et al.* (2010) ‘Optimization of source-sink dynamics in plant growth for ideotype breeding: A case study on maize’, *Computers and Electronics in Agriculture*. doi: 10.1016/j.compag.2009.12.008.

Quilot-Turion, B. *et al.* (2012) ‘Optimization of parameters of the “Virtual Fruit” model to design peach genotype for sustainable production systems’, *European Journal of Agronomy*. doi: 10.1016/j.eja.2011.11.008.

Quilot, B. *et al.* (2005) ‘Analysing the genetic control of peach fruit quality through an ecophysiological model combined with a QTL approach’, *Journal of Experimental Botany*. doi: 10.1093/jxb/eri305.

Rančić, D., Quarrie, S. P. and Pećinar, I. (2010) ‘Anatomy of tomato fruit and fruit pedicel during fruit development’, *Microscopy: Science, Technology, Applications and Education*.

Rebolledo, M. C. *et al.* (2015) ‘Phenotypic and genetic dissection of component traits for early vigour in rice using plant growth modelling, sugar content analyses and association mapping’, *Journal of Experimental Botany*. doi: 10.1093/jxb/erv258.

Reidinger, S., Ramsey, M. H. and Hartley, S. E. (2012) ‘Rapid and accurate analyses of silicon and phosphorus in plants using a portable X-ray fluorescence spectrometer’, *New Phytologist*. doi: 10.1111/j.1469-8137.2012.04179.x.

Remorini, D. and Massai, R. (2003) ‘Comparison of water status indicators for young peach trees’, *Irrigation Science*. doi: 10.1007/s00271-003-0068-4.

Reymond, M. *et al.* (2003) ‘Combining quantitative trait loci analysis and an ecophysiological model to analyze the genetic variability of the responses of maize leaf

growth to temperature and water deficit', *Plant Physiology*. doi: 10.1104/pp.013839.

Ripoll, J. *et al.* (2014) 'Water shortage and quality of fleshy fruits-making the most of the unavoidable', *Journal of Experimental Botany*. Oxford University Press, pp. 4097–4117. doi: 10.1093/jxb/eru197.

Ripoll, J. *et al.* (2016) 'Water deficit effects on tomato quality depend on fruit developmental stage and genotype', *Journal of Plant Physiology*. doi: 10.1016/j.jplph.2015.10.006.

Ripoll, J., Urban, L. and Bertin, N. (2016) 'The potential of the MAGIC TOM parental accessions to explore the genetic variability in Tomato acclimation to repeated cycles of water deficit and recovery', *Frontiers in Plant Science*. doi: 10.3389/fpls.2015.01172.

Rötter, R. P. *et al.* (2015) 'Use of crop simulation modelling to aid ideotype design of future cereal cultivars', *Journal of Experimental Botany*. doi: 10.1093/jxb/erv098.

Ruan, Y. L. and Patrick, J. W. (1995) 'The cellular pathway of postphloem sugar transport in developing tomato fruit', *Planta: An International Journal of Plant Biology*. doi: 10.1007/BF00203641.

Saliba-Colombani, V. *et al.* (2001) 'Genetic analysis of organoleptic quality in fresh market tomato. 1. Mapping QTLs for physical and chemical traits', *Theoretical and Applied Genetics*, 102(2–3), pp. 259–272. doi: 10.1007/s001220051643.

Saltelli, A. *et al.* (2008) *Global Sensitivity Analysis. The Primer*, *Global Sensitivity Analysis. The Primer*. doi: 10.1002/9780470725184.

Semenov, M. A. *et al.* (2014) 'Adapting wheat in Europe for climate change', *Journal of Cereal Science*. doi: 10.1016/j.jcs.2014.01.006.

Shackel, K. A. *et al.* (1991) 'Cell turgor changes associated with ripening in tomato pericarp tissue', *Plant Physiology*. doi: 10.1104/pp.97.2.814.

Sidi, M.-M. O. *et al.* (2014) 'The Relationship between Metaheuristics Stopping Criteria and Performances', *International Journal of Applied Metaheuristic Computing*. doi: 10.4018/ijamc.2014070104.

Slavin, J. L. and Lloyd, B. (2012) 'Health Benefits of Fruits and Vegetables', *Advances in Nutrition*, 3(4), pp. 506–516. doi: 10.3945/an.112.002154.

Sorrequieta, A. *et al.* (2010) 'Free amino acid production during tomato fruit ripening: A focus on L-glutamate', *Amino Acids*. doi: 10.1007/s00726-009-0373-1.

Taiz, L. and Zeiger, E. (2015) *Plant Physiology (Sixth Edition)*, *Sinauer Associates*.

Tardieu, F. (2003) 'Virtual plants: Modelling as a tool for the genomics of tolerance

to water deficit', *Trends in Plant Science*. doi: 10.1016/S1360-1385(02)00008-0.

Tardieu, F. (2012) 'Any trait or trait-related allele can confer drought tolerance: Just design the right drought scenario', *Journal of Experimental Botany*. doi: 10.1093/jxb/err269.

Thompson, M. V. and Holbrook, N. M. (2003a) 'Application of a single-solute non-steady-state phloem model to the study of long-distance assimilate transport', *Journal of Theoretical Biology*. Academic Press, 220(4), pp. 419–455. doi: 10.1006/jtbi.2003.3115.

Thompson, M. V. and Holbrook, N. M. (2003b) 'Scaling phloem transport: Water potential equilibrium and osmoregulatory flow', *Plant, Cell and Environment*. doi: 10.1046/j.1365-3040.2003.01080.x.

Tilman, D. *et al.* (2011) 'Global food demand and the sustainable intensification of agriculture', *Proceedings of the National Academy of Sciences of the United States of America*, 108(50), pp. 20260–20264. doi: 10.1073/pnas.1116437108.

Tromp, J. (1984) 'Diurnal fruit shrinkage in apple as affected by leaf water potential and vapour pressure deficit of the air', *Scientia Horticulturae*. doi: 10.1016/0304-4238(84)90086-4.

Turgeon, R. (2010) 'The puzzle of phloem pressure', *Plant Physiology*. doi: 10.1104/pp.110.161679.

Van de Wal, B. A. E. *et al.* (2017) 'Heat girdling does not affect xylem integrity: an in vivo magnetic resonance imaging study in the tomato peduncle', *New Phytologist*. doi: 10.1111/nph.14610.

Wallach, D. *et al.* (2014) *Working with Dynamic Crop Models: Methods, Tools and Examples for Agriculture and Environment: Second Edition*, *Working with Dynamic Crop Models: Methods, Tools and Examples for Agriculture and Environment: Second Edition*. doi: 10.1016/C2011-0-06987-9.

White, J. W. and Hoogenboom, G. (1996) 'Simulating effects of genes for physiological traits in a process- oriented crop model', *Agronomy Journal*. doi: 10.2134/agronj1996.00021962008800030009x.

Windt, C. W., Gerkema, E. and van As, H. (2009) 'Most water in the tomato truss is imported through the xylem, not the phloem: A nuclear magnetic resonance flow imaging study', *Plant Physiology*. doi: 10.1104/pp.109.141044.

Wu, B. H. *et al.* (2002) 'Influence of assimilate and water supply on seasonal

variation of acids in peach (cv Suncrest)', *Journal of the Science of Food and Agriculture*. doi: 10.1002/jsfa.1267.

Wu, Y. X., Wang, X. and Ching, C. B. (2002) 'Computational fluid dynamics simulation of the adsorption separation of three components in high performance liquid chromatography', *Chromatographia*. doi: 10.1007/BF02492274.

Xu, L. *et al.* (2012) 'Simulating superior genotypes for plant height based on QTLs: Towards virtual breeding of rice', in *Proceedings - 2012 IEEE 4th International Symposium on Plant Growth Modeling, Simulation, Visualization and Applications, PMA 2012*, pp. 447–454. doi: 10.1109/PMA.2012.6524871.

Zanon, L. *et al.* (2015) 'Sucrose transport and phloem unloading in peach fruit: Potential role of two transporters localized in different cell types', *Physiologia Plantarum*. doi: 10.1111/ppl.12304.

Zhang, L. Y. *et al.* (2004) 'Evidence for apoplasmic phloem unloading in developing apple fruit', *Plant Physiology*, 135(1), pp. 574–586. doi: 10.1104/pp.103.036632.

Zhang, X. Y. *et al.* (2006) 'A shift of phloem unloading from symplasmic to apoplasmic pathway is involved in developmental onset of ripening in grape berry', *Plant Physiology*. doi: 10.1104/pp.106.081430.

Zhang, Y. and Keller, M. (2017) 'Discharge of surplus phloem water may be required for normal grape ripening', *Journal of Experimental Botany*, 68(3), pp. 585–595. doi: 10.1093/jxb/erw476.

Zhu, J. *et al.* (2019) 'Modelling grape growth in relation to whole-plant carbon and water fluxes', *Journal of Experimental Botany*. doi: 10.1093/jxb/ery367.

ANNEXES – SUPPLEMENTARY MATERIAL

S2.1 – Linear system analytical solution

In this document, we provide the analytical solution of the system of equations presented in the section "*Model description and flow equations"* in the main text of this paper (Eq. 18-21). The equations of the system are the following (Eq. S1.1-S1.4). The unknown variables are marked in bold:

$K_{px\leftrightarrow fx}\times(\Psi_{w,pp}-(\mathbf{\Psi_{p,fp}}-R\times T\times\mathbf{C_{fp}}))+K_{pp\leftrightarrow fp}\times((\Psi_{w,pp}+R\times T\times C_{pp})-\mathbf{\Psi_{p,fp}})+$

$-k_{fx\leftrightarrow fa}\times A_f\times((\mathbf{\Psi_{p,fp}}-R\times T\times\mathbf{C_{fp}})-\mathbf{\Psi_{p,fa}})-k_{fp\leftrightarrow fa}\times A_f\times((\mathbf{\Psi_{p,fp}}-R\times T\times\mathbf{C_{fp}})-(\mathbf{\Psi_{p,fa}}-R\times T\times\mathbf{C_{fa}}))=0$ (S1.1)

$k_{fx\leftrightarrow fa}\times A_f\times((\mathbf{\Psi_{p,fp}}-R\times T\times\mathbf{C_{fp}})-\mathbf{\Psi_{p,fa}})+k_{fp\leftrightarrow fa}\times A_f\times((\mathbf{\Psi_{p,fp}}-R\times T\times\mathbf{C_{fp}})-(\mathbf{\Psi_{p,fa}}-R\times T\times\mathbf{C_{fa}}))+$

$-k_{fa\leftrightarrow fs}\times A_f\times((\mathbf{\Psi_{p,fa}}-R\times T\times\mathbf{C_{fa}})-\Psi_{fs})-T_{fa}=0$ (S1.2)

$M_S\times C_{pp}\times k_{pp\leftrightarrow fp}\times A_f\times((\mathbf{\Psi_{p}},_p+R\times T\times C_{pp})-\mathbf{\Psi_{p,fp}})-M_S\times v_{fp\rightarrow fa}\times A_f\times\mathbf{C_{fp}}=0$ (S1.3)

$M_S\times v_{fp\rightarrow fa}\times A_f\times\mathbf{C_{fp}}-M_H\times v_{fa\rightarrow fs}\times DW\times\mathbf{C_{fa}}=0$ (S1.4)

The system analytical solutions are:

$\mathbf{\Psi_{p,fp}}=(-DW\times M_H\times A_f\times v_{fp\rightarrow fa}\times v_{fa\rightarrow fs}\times(k_{fp\leftrightarrow fa}+k_{fx\leftrightarrow fa})\times(A_f\times k_{fa\leftrightarrow fs}\times\Psi_{fs}-T_{fa})-$
$DW\times M_H\times A_f\times v_{fp\rightarrow fa}\times v_{fa\rightarrow fs}\times(k_{fa\leftrightarrow fs}+k_{fp\leftrightarrow fa}+k_{fx\leftrightarrow fa})\times(R\times T\times C_{pp}\times K_{pp\leftrightarrow fp}+K_{pp\leftrightarrow fp}\times\Psi_{w,pp}+$
$K_{px\leftrightarrow fx}\times\Psi_{w,pp})+R\times T\times C_{pp}\times K_{pp\leftrightarrow fp}\times(R\times T\times C_{pp}+\Psi_{w,pp})\times(DW\times M_H\times A_f\times v_{fa\rightarrow fs}\times(k_{fp\leftrightarrow fa}+k_{fx\leftrightarrow fa})^2-$
$DW\times M_H\times v_{fa\rightarrow fs}\times(k_{fa\leftrightarrow fs}+k_{fp\leftrightarrow fa}+k_{fx\leftrightarrow fa})\times(A_f\times k_{fp\leftrightarrow fa}+A_f\times k_{fx\leftrightarrow fa}+K_{px\leftrightarrow fx})+$
$M_S\times A_f^2\times k_{fp\leftrightarrow fa}\times v_{fp\rightarrow fa}\times(k_{fa\leftrightarrow fs}+k_{fp\leftrightarrow fa}+k_{fx\leftrightarrow fa})-M_S\times A_f^2\times v_{fp\rightarrow fa}\times(k_{fa\leftrightarrow fs}+k_{fp\leftrightarrow fa})\times(k_{fp\leftrightarrow fa}+$
$k_{fx\leftrightarrow fa})))/(DW\times M_H\times R\times A_f\times T\times C_{pp}\times K_{pp\leftrightarrow fp}\times v_{fa\rightarrow fs}\times(k_{fp\leftrightarrow fa}+k_{fx\leftrightarrow fa})^2-$
$DW\times M_H\times R\times T\times C_{pp}\times K_{pp\leftrightarrow fp}\times v_{fa\rightarrow fs}\times(k_{fa\leftrightarrow fs}+k_{fp\leftrightarrow fa}+k_{fx\leftrightarrow fa})\times(A_f\times k_{fp\leftrightarrow fa}+A_f\times k_{fx\leftrightarrow fa}+K_{px\leftrightarrow fx})+$
$DW\times M_H\times A_f^2\times v_{fp\rightarrow fa}\times v_{fa\rightarrow fs}\times(k_{fp\leftrightarrow fa}+k_{fx\leftrightarrow fa})^2-DW\times M_H\times A_f\times v_{fp\rightarrow fa}\times v_{fa\rightarrow fs}\times(k_{fa\leftrightarrow fs}+k_{fp\leftrightarrow fa}+$
$k_{fx\leftrightarrow fa})\times(A_f\times k_{fp\leftrightarrow fa}+A_f\times k_{fx\leftrightarrow fa}+K_{pp\leftrightarrow fp}+K_{px\leftrightarrow fx})+M_S\times R\times A_f^2\times T\times C_{pp}\times K_{pp\leftrightarrow fp}\times k_{fp\leftrightarrow fa}\times v_{fp\rightarrow fa}\times(k_{fa\leftrightarrow fs}+$
$k_{fp\leftrightarrow fa}+k_{fx\leftrightarrow fa})-M_S\times R\times A_f^2\times T\times C_{pp}\times K_{pp\leftrightarrow fp}\times v_{fp\rightarrow fa}\times(k_{fa\leftrightarrow fs}+k_{fp\leftrightarrow fa})\times(k_{fp\leftrightarrow fa}+k_{fx\leftrightarrow fa}))$ (S1.5)

$\mathbf{C_{fp}}=DW\times M_H\times C_{pp}\times K_{pp\leftrightarrow fp}\times v_{fa\rightarrow fs}\times((k_{fp\leftrightarrow fa}+k_{fx\leftrightarrow fa})\times(A_f\times k_{fa\leftrightarrow fs}\times\Psi_{fs}-T_{fa})+(A_f\times(k_{fp\leftrightarrow fa}+k_{fx\leftrightarrow fa})^2-$
$(k_{fa\leftrightarrow fs}+k_{fp\leftrightarrow fa}+k_{fx\leftrightarrow fa})\times(A_f\times k_{fp\leftrightarrow fa}+A_f\times k_{fx\leftrightarrow fa}+K_{pp\leftrightarrow fp}+K_{px\leftrightarrow fx}))\times(R\times T\times C_{pp}+\Psi_{w,pp})+(k_{fa\leftrightarrow fs}+$
$k_{fp\leftrightarrow fa}+k_{fx\leftrightarrow fa})\times(R\times T\times C_{pp}\times K_{pp\leftrightarrow fp}+K_{pp\leftrightarrow fp}\times\Psi_{w,pp}+$
$K_{px\leftrightarrow fx}\times\Psi_{w,pp}))/(DW\times M_H\times R\times A_f\times T\times C_{pp}\times K_{pp\leftrightarrow fp}\times v_{fa\rightarrow fs}\times(k_{fp\leftrightarrow fa}+k_{fx\leftrightarrow fa})^2-$
$DW\times M_H\times R\times T\times C_{pp}\times K_{pp\leftrightarrow fp}\times v_{fa\rightarrow fs}\times(k_{fa\leftrightarrow fs}+k_{fp\leftrightarrow fa}+k_{fx\leftrightarrow fa})\times(A_f\times k_{fp\leftrightarrow fa}+A_f\times k_{fx\leftrightarrow fa}+K_{px\leftrightarrow fx})+$
$DW\times M_H\times A_f^2\times v_{fp\rightarrow fa}\times v_{fa\rightarrow fs}\times(k_{fp\leftrightarrow fa}+k_{fx\leftrightarrow fa})^2-DW\times M_H\times A_f\times v_{fp\rightarrow fa}\times v_{fa\rightarrow fs}\times(k_{fa\leftrightarrow fs}+k_{fp\leftrightarrow fa}+$

$k_{fx\leftrightarrow fa})\times(A_f\times k_{fp\leftrightarrow fa} + A_f\times k_{fx\leftrightarrow fa} + K_{pp\leftrightarrow fp} + K_{px\leftrightarrow fx}) + M_S\times R\times A_f^2\times T\times C_{pp}\times K_{pp\leftrightarrow fp}\times k_{fp\leftrightarrow fa}\times v_{fp\rightarrow fa}\times(k_{fa\leftrightarrow fs} + k_{fp\leftrightarrow fa} + k_{fx\leftrightarrow fa}) - M_S\times R\times A_f^2\times T\times C_{pp}\times K_{pp\leftrightarrow fp}\times v_{fp\rightarrow fa}\times(k_{fa\leftrightarrow fs} + k_{fp\leftrightarrow fa})\times(k_{fp\leftrightarrow fa} + k_{fx\leftrightarrow fa}))$ (S1.6)

$\boldsymbol{\Psi_{p,fa}} = -(R\times A_f\times T\times C_{pp}\times K_{pp\leftrightarrow fp}\times(R\times T\times C_{pp} + \Psi_{w,pp})\times(DW\times M_H\times v_{fa\rightarrow fs}\times(k_{fp\leftrightarrow fa} + k_{fx\leftrightarrow fa})\times(A_f\times k_{fp\leftrightarrow fa} + A_f\times k_{fx\leftrightarrow fa} + K_{pp\leftrightarrow fp} + K_{px\leftrightarrow fx}) - DW\times M_H\times v_{fa\rightarrow fs}\times(k_{fp\leftrightarrow fa} + k_{fx\leftrightarrow fa})\times(A_f\times k_{fp\leftrightarrow fa} + A_f\times k_{fx\leftrightarrow fa} + K_{pp\leftrightarrow fp} + K_{px\leftrightarrow fx}) - M_S\times A_f^2\times k_{fp\leftrightarrow fa}\times v_{fp\rightarrow fa}\times(k_{fp\leftrightarrow fa} + k_{fx\leftrightarrow fa}) + M_S\times A_f\times v_{fp\rightarrow fa}\times(k_{fa\leftrightarrow fs} + k_{fp\leftrightarrow fa})\times(A_f\times k_{fp\leftrightarrow fa} + A_f\times k_{fx\leftrightarrow fa} + K_{pp\leftrightarrow fp} + K_{px\leftrightarrow fx})) + A_f\times(R\times T\times C_{pp}\times K_{pp\leftrightarrow fp} + K_{pp\leftrightarrow fp}\times\Psi_{w,pp} + K_{px\leftrightarrow fx}\times\Psi_{w,pp})\times(DW\times M_H\times R\times T\times C_{pp}\times K_{pp\leftrightarrow fp}\times v_{fa\rightarrow fs}\times(k_{fp\leftrightarrow fa} + k_{fx\leftrightarrow fa}) + DW\times M_H\times A_f\times v_{fp\rightarrow fa}\times v_{fa\rightarrow fs}\times(k_{fp\leftrightarrow fa} + k_{fx\leftrightarrow fa}) - M_S\times R\times A_f\times T\times C_{pp}\times K_{pp\leftrightarrow fp}\times v_{fp\rightarrow fa}\times(k_{fa\leftrightarrow fs} + k_{fp\leftrightarrow fa})) + (A_f\times k_{fa\leftrightarrow fs}\times\Psi_{fs} - T_{fa})\times(DW\times M_H\times R\times T\times C_{pp}\times K_{pp\leftrightarrow fp}\times v_{fa\rightarrow fs}\times(A_f\times k_{fp\leftrightarrow fa} + A_f\times k_{fx\leftrightarrow fa} + K_{px\leftrightarrow fx}) + DW\times M_H\times A_f\times v_{fp\rightarrow fa}\times v_{fa\rightarrow fs}\times(A_f\times k_{fp\leftrightarrow fa} + A_f\times k_{fx\leftrightarrow fa} + K_{pp\leftrightarrow fp} + K_{px\leftrightarrow fx}) - M_S\times R\times A_f^2\times T\times C_{pp}\times K_{pp\leftrightarrow fp}\times k_{fp\leftrightarrow fa}\times v_{fp\rightarrow fa}))/(A_f\times(DW\times M_H\times R\times A_f\times T\times C_{pp}\times K_{pp\leftrightarrow fp}\times v_{fa\rightarrow fs}\times(k_{fp\leftrightarrow fa} + k_{fx\leftrightarrow fa})^2 - DW\times M_H\times R\times T\times C_{pp}\times K_{pp\leftrightarrow fp}\times v_{fa\rightarrow fs}\times(k_{fa\leftrightarrow fs} + k_{fp\leftrightarrow fa} + k_{fx\leftrightarrow fa})\times(A_f\times k_{fp\leftrightarrow fa} + A_f\times k_{fx\leftrightarrow fa} + K_{px\leftrightarrow fx}) + DW\times M_H\times A_f$ (S1.7)

$\boldsymbol{C_{fa}} = M_S\times A_f\times C_{pp}\times K_{pp\leftrightarrow fp}\times v_{fp\rightarrow fa}\times((k_{fp\leftrightarrow fa} + k_{fx\leftrightarrow fa})\times(A_f\times k_{fa\leftrightarrow fs}\times\Psi_{fs} - T_{fa}) + (A_f\times(k_{fp\leftrightarrow fa} + k_{fx\leftrightarrow fa})^2 - (k_{fa\leftrightarrow fs} + k_{fp\leftrightarrow fa} + k_{fx\leftrightarrow fa})\times(A_f\times k_{fp\leftrightarrow fa} + A_f\times k_{fx\leftrightarrow fa} + K_{pp\leftrightarrow fp} + K_{px\leftrightarrow fx}))\times(R\times T\times C_{pp} + \Psi_{w,pp}) + (k_{fa\leftrightarrow fs} + k_{fp\leftrightarrow fa} + k_{fx\leftrightarrow fa})\times(R\times T\times C_{pp}\times K_{pp\leftrightarrow fp} + K_{pp\leftrightarrow fp}\times\Psi_{w,pp} + K_{px\leftrightarrow fx}\times\Psi_{w,pp}))/(DW\times M_H\times R\times A_f\times T\times C_{pp}\times K_{pp\leftrightarrow fp}\times v_{fa\rightarrow fs}\times(k_{fp\leftrightarrow fa} + k_{fx\leftrightarrow fa})^2 - DW\times M_H\times R\times T\times C_{pp}\times K_{pp\leftrightarrow fp}\times v_{fa\rightarrow fs}\times(k_{fa\leftrightarrow fs} + k_{fp\leftrightarrow fa} + k_{fx\leftrightarrow fa})\times(A_f\times k_{fp\leftrightarrow fa} + A_f\times k_{fx\leftrightarrow fa} + K_{px\leftrightarrow fx}) + DW\times M_H\times A_f^2\times v_{fp\rightarrow fa}\times v_{fa\rightarrow fs}\times(k_{fp\leftrightarrow fa} + k_{fx\leftrightarrow fa})^2 - DW\times M_H\times A_f\times v_{fp\rightarrow fa}\times v_{fa\rightarrow fs}\times(k_{fa\leftrightarrow fs} + k_{fp\leftrightarrow fa} + k_{fx\leftrightarrow fa})\times(A_f\times k_{fp\leftrightarrow fa} + A_f\times k_{fx\leftrightarrow fa} + K_{pp\leftrightarrow fp} + K_{px\leftrightarrow fx}) + M_S\times R\times A_f^2\times T\times C_{pp}\times K_{pp\leftrightarrow fp}\times k_{fp\leftrightarrow fa}\times v_{fp\rightarrow fa}\times(k_{fa\leftrightarrow fs} + k_{fp\leftrightarrow fa} + k_{fx\leftrightarrow fa}) - M_S\times R\times A_f^2\times T\times C_{pp}\times K_{pp\leftrightarrow fp}\times v_{fp\rightarrow fa}\times(k_{fa\leftrightarrow fs} + k_{fp\leftrightarrow fa})\times(k_{fp\leftrightarrow fa} + k_{fx\leftrightarrow fa}))$ (S1.8)

S2.2 – Parameters variability among best solutions

Table S2.2.1: Calibrated model parameters and brief descriptions. C: control fruit, G: girdled fruit, 30_94: 30 leaves-to-fruit year 1994, 5_95: 5 leaves-to-fruit year 1995, 30_95 : 30 leaves-to-fruit year 1995; in the fourth column: 10^{th} and 90^{th} percentile of each parameter, computed on the sample composed by the best solutions among all the solutions found by the genetic algorithm. A solution belonged to the best ones if both the $RMSE_C$ and $RMSE_G$ of this solution were up to 5 percent higher than the minimum $RMSE_C$ and $RMSE_G$

Parameter	Description	Value	10^{th} – 90^{th} percentile in the best solutions	Units
$K_{px\leftrightarrow fx}$	Conductance of the water path between the pedicel xylem and the fruit xylem	9.1×10^{-1}	6.8×10^{-1} – 9.1×10^{-1}	(g h^{-1} MPa^{-1})
$K_{pp\leftrightarrow fp}$	Conductance of the water path between the pedicel phloem and the fruit phloem	3.3	1.6 – 3.5	(g h^{-1} MPa^{-1})
$k_{fx\leftrightarrow fa}$ $K_{fx\leftrightarrow fa}$ *	Conductivity and conductance of the water path between the fruit xylem and the fruit apoplast	1.1×10^{-2} 7.4×10^{-1}	6.2×10^{-3} – 1.8×10^{-2} 4.4×10^{-1} – 1.3	(g h^{-1} MPa^{-1} cm^{-2}) (g h^{-1} MPa^{-1})
$k_{fp\leftrightarrow fa}$ $K_{fp\leftrightarrow fa}$ *	Conductivity and conductance of the water path between fruit phloem and the fruit apoplast	1.1×10^{-3} 7.6×10^{-2}	1.1×10^{-3} – 2.3×10^{-3} 7.6×10^{-2} – 1.6×10^{-1}	(g h^{-1} MPa^{-1} cm^{-2}) (g h^{-1} MPa^{-1})
$K_{fa\leftrightarrow fs}$ $K_{fa\leftrightarrow fs}$*	Conductivity and conductance of the water path between the fruit apoplast and the fruit symplast	9.1×10^{-3} 6.4×10^{-1}	8×10^{-3} – 2.3×10^{-2} 5.6×10^{-1} – 1.6	(g h^{-1} MPa^{-1} cm^{-2}) (g h^{-1} MPa^{-1})
$v_{fp\rightarrow fa}$	Sugar transport rate between the fruit phloem and the fruit apoplast	5.0×10^{-4}	4.6×10^{-4} – 6.6×10^{-4}	(g h^{-1} cm^{-2})
$v_{fa\rightarrow fs}$	Fruit symplast sugar uptake rate	3.6×10^{-2}	3.6×10^{-2} – 8.7×10^{-2}	(h^{-1})
$\Psi_{w,fs}$	Fruit symplast water potential (from 18:00 to 06:00)	-1.7 (C30_94)	-1.8 – -1.4	(MPa)
		-1.7 (C30_95)	-1.8 – -1.4	
		-1.3 (C5_95)	-1.3 – -1.1	
		-0.89 (G30_94)	-1.0 – -0.86	
		-1.1 (G30_95)	-1.2 – -1.0	
		-0.91 (G5_95)	-1.0 – -0.87	

* conductances are given at the estimated value for the fruits grown at the 5 leaves-to-fruit treatment and at control conditions in 1995, which we took as a reference for the results.

S2.3 – Sensitivity to inputs

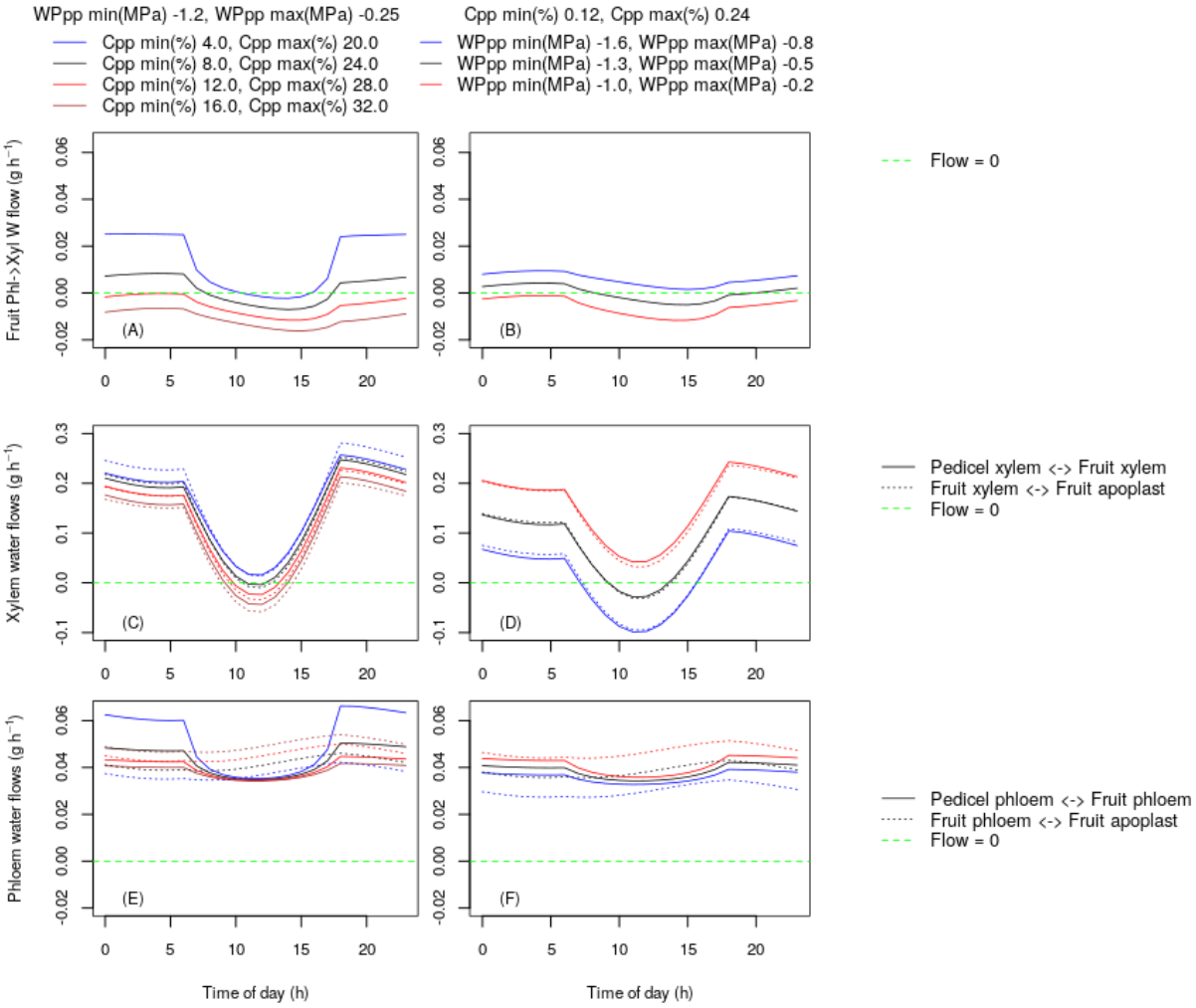

Figure S2.3.1: Response of the predicted diurnal water flows to different levels of pedicel phloem sugar concentration and pedicel phloem water potential given as input. (A, B): simulated diurnal behavior of the water flow from the fruit phloem to the fruit xylem; (C, D): simulated behavior of the diurnal water flows from the pedicel xylem to the fruit xylem (solid lines) and from the fruit xylem to the fruit apoplast (dotted lines); (E,F) simulated behavior of the diurnal water flows from the pedicel phloem to the fruit phloem (solid lines) and from the fruit phloem to the fruit apoplast (dotted lines). (A, C, E): the pedicel phloem sugar concentration input was set at different levels (low, blue lines; medium, black lines; high, red lines; very high, brown lines), while the pedicel phloem water potential input was set to a fixed diurnal variation; (B, D, F): the pedicel phloem water potential was set at different levels (low – more negative – blue lines; medium, black lines; high – less negative – red lines), while the pedicel phloem sugar concentration was set to a fixed diurnal variation. The dashed green lines correspond to the null values of water flows.

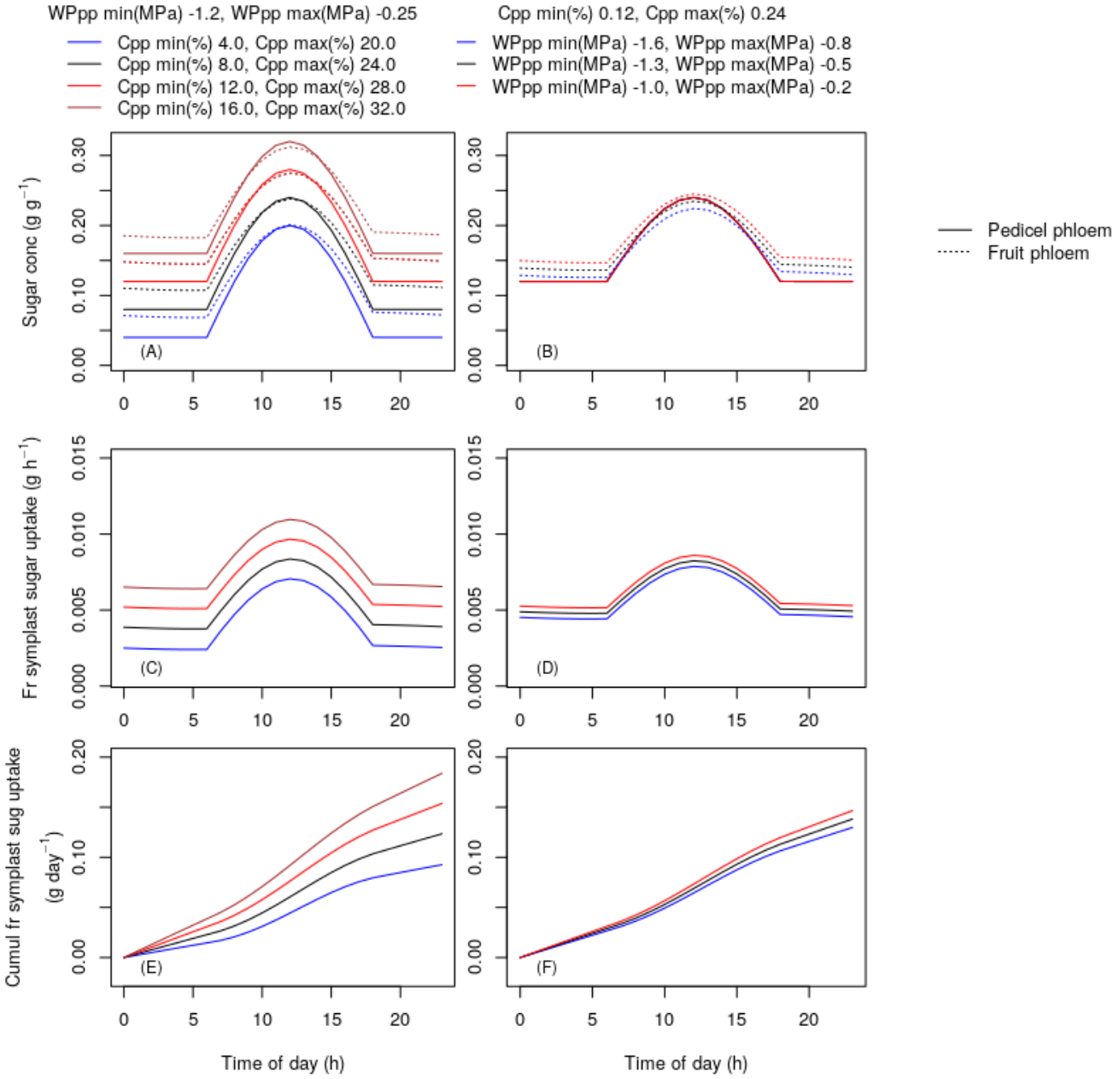

Figure S2.3.2: Response of the predicted diurnal sugar concentrations and sugar uptake to different levels of pedicel phloem sugar concentration and pedicel phloem water potential given as input. (A, B): simulated diurnal behavior of the pedicel phloem sugar concentrations (input, solid line) and the fruit phloem sugar concentrations (dotted lines). (C, D): simulated behavior of the diurnal fruit symplast sugar uptake. (E, F): simulated behavior of the cumulative fruit symplast sugar uptake. (A, C, E): the pedicel phloem sugar concentration input was set at different levels (low, blue lines; medium, black lines; high, red lines; very high, brown lines), while the pedicel phloem water potential input was set to a fixed diurnal variation; (B, D, F): the pedicel phloem water potential was set at different levels (low – more negative – blue lines; medium, black lines; high – less negative – red lines), while the pedicel phloem sugar concentration was set to a fixed diurnal variation.

S3.1 – Supplementary figures for the 2.4 density treatment

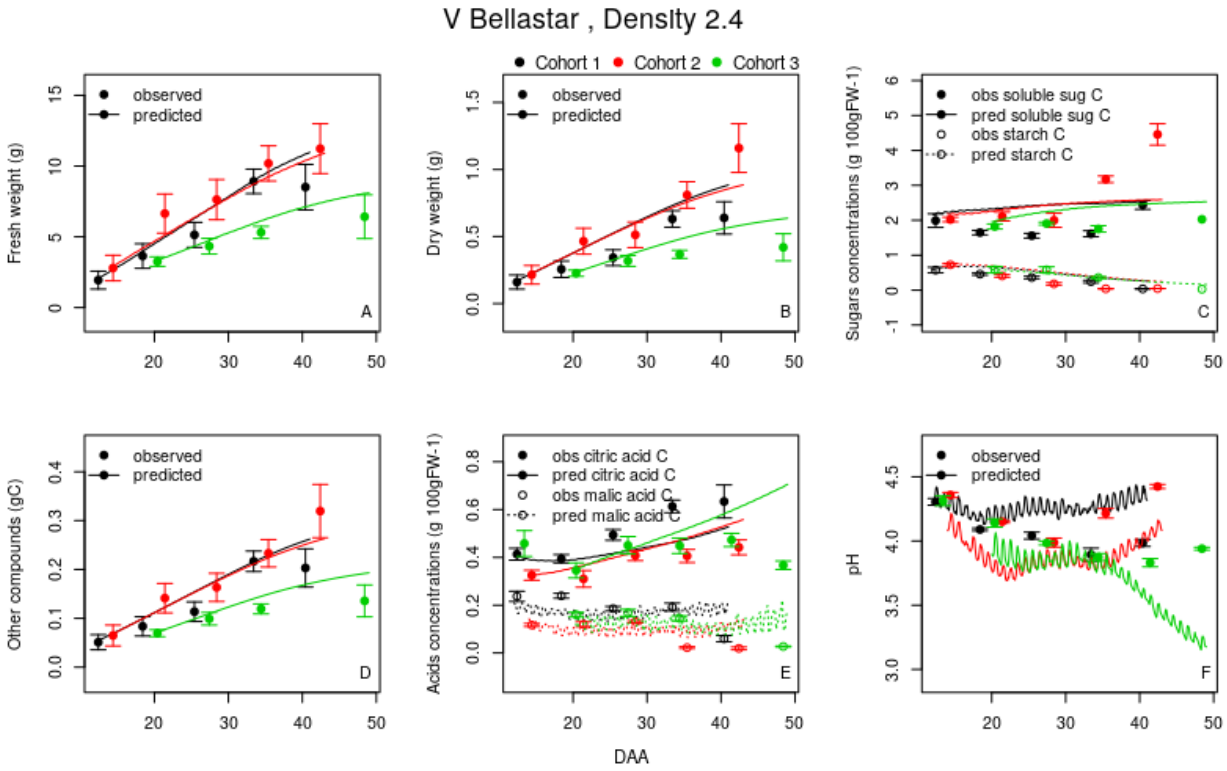

Fig. S3.1.1 Integrated model simulations performances for the fruits of the variety Bellastar grown in 2.4 shoot density: observed (points) vs predicted (lines) fresh weight (A), dry weight (B), soluble sugar concentrations (C, full points and full lines), starch concentrations (C, empty points and dashed lines), carbon stored in the other compounds (D), citric acid concentrations (E, full points and full lines), malic acid concentrations (E, empty points and dashed lines), and pH (F). Black, red, and green denote the first, the second, and the third cohort, respectively. Bars indicate the standard deviations of measured data.

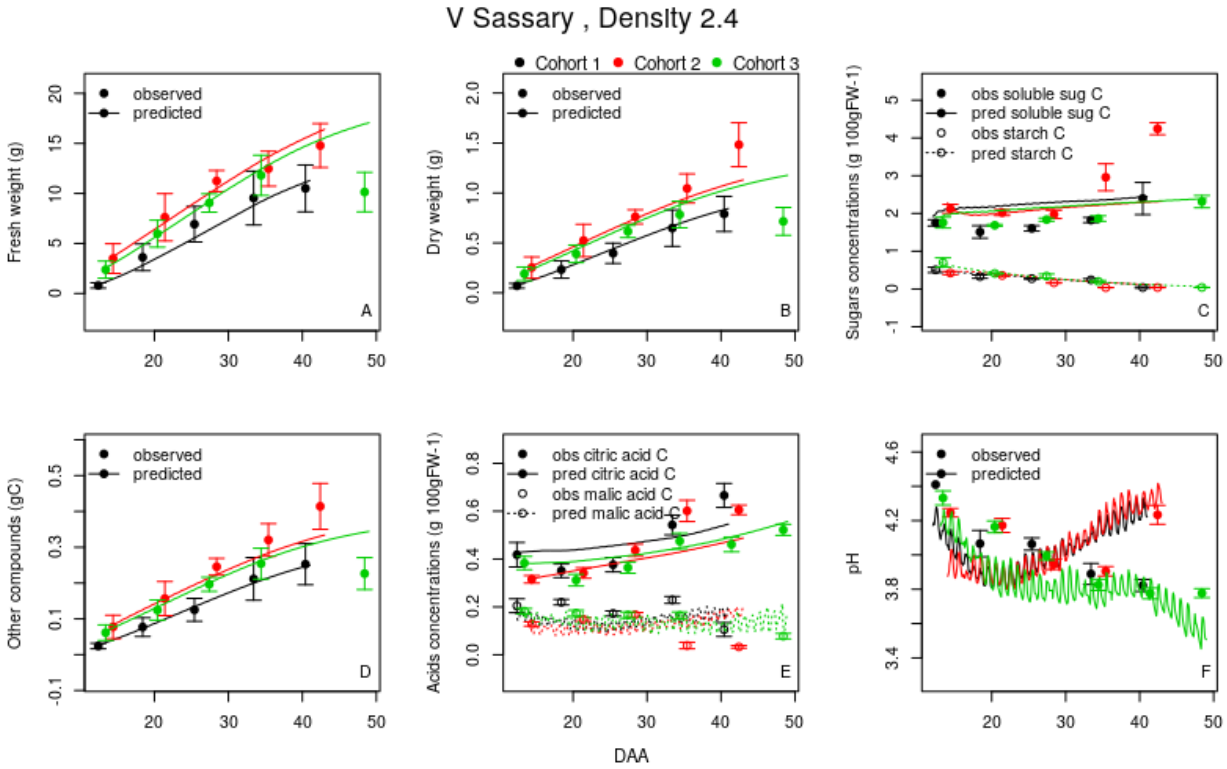

Fig. S3.1.2. Integrated model simulations performances for the fruits of the variety Sassary grown in 2.4 shoot density: observed (points) vs predicted (lines) fresh weight (A), dry weight (B), soluble sugar concentrations (C, full points and full lines), starch concentrations (C, empty points and dashed lines), carbon stored in the other compounds (D), citric acid concentrations (E, full points and full lines), malic acid concentrations (E, empty points and dashed lines), and pH (F). Black, red, and green denote the first, the second, and the third cohort, respectively. Bars indicate the standard deviations of measured data.